Functions and regulation of synaptopodin-2 isoforms under mechanical stress in muscle cells

Dissertation

zur

Erlangung des Doktorgrades (Dr. rer. nat.)

der

Mathematisch-Naturwissenschaftlichen Fakultät

der

Rheinischen Friedrich-Wilhelms-Universität Bonn

vorgelegt von

Keerthika Lohanadan

aus

Rheine

Bonn, Februar 2023

Angefertigt mit Genehmigung der Mathematisch-Naturwissenschaftlichen Fakultät
der Rheinischen Friedrich-Wilhelms-Universität Bonn

Gutachter: Herr Prof. Dr. Dieter O. Fürst
Gutachter: Herr PD Dr. Gregor Kirfel

Tag der Promotion: 27.04.2023
Erscheinungsjahr: 2023

Die vorliegende Arbeit wurde von Februar 2019 bis Februar 2023 in der Arbeitsgruppe molekulare Zellbiologie am Institut für Zellbiologie der Rheinischen Friedrich-Wilhelms-Universität Bonn unter Anleitung von Prof. Dr. Dieter O. Fürst erstellt.

Hiermit versichere ich, dass ich die vorliegende Dissertation, abgesehen von den ausdrücklich bezeichneten Hilfsmitteln, persönlich, selbstständig und unter Offenlegung der erhaltenen Hilfen angefertigt habe.
Diese Arbeit hat bisher noch keiner anderen Prüfungskommission zur Begutachtung vorgelegen.

Keerthika Lohanadan

Publications

Parts of this work have already been published:

Lohanadan K, Molt S, Dierck F, van der Ven PFM, Frey N, Höhfeld J, Fürst DO. Isoform-specific functions of synaptopodin-2 variants in cytoskeleton stabilization and autophagy regulation in muscle under mechanical stress. (2021) *Experimental Cell Research*, 408:112865. doi: 10.1016/j.yexcr.2021.112865.

Mao Y, Schneider R, van der Ven PFM, Assent M, Lohanadan K, Klämbt V, Buerger F, Kitzler TM, Deutsch K, Nakayama M, Majmundar AJ, Mann N, Hermle T, Onuchic-Whitford AC, Zhou W, Margam NN, Duncan R, Marquez J, Khokha M, Fathy HM, Kari JA, El Desoky S, Eid LA, Awad HS, Al-Saffar M, Mane S, Lifton RP, Fürst DO, Shril S, Hildebrandt F. Recessive Mutations in *SYNPO2* as a Candidate of Monogenic Nephrotic Syndrome. (2020) *Kidney Int Rep.*, 6:472-483. doi: 10.1016/j.ekir.2020.10.040.

Other Publications:

Reimann L, Schwäble AN, Fricke AL, Mühlhäuser WWD, Leber Y, Lohanadan K, Puchinger MG, Schäuble S, Faessler E, Wiese H, Reichenbach C, Knapp B, Peikert CD, Drepper F, Hahn U, Kreutz C, van der Ven PFM, Radziwill G, Djinović-Carugo K, Fürst DO, Warscheid B. Phosphoproteomics identifies dual-site phosphorylation in an extended basophilic motif regulating FILIP1-mediated degradation of filamin-C. (2020) *Commun Biol.*, 3:253. doi: 10.1038/s42003-020-0982-5.

Umer N, Arévalo L, Phadke S, Lohanadan K, Kirfel G, Sons D, Sofia D, Witke W, Schorle H. Loss of Profilin3 Impairs Spermiogenesis by Affecting Acrosome Biogenesis, Autophagy, Manchette Development and Mitochondrial Organization. (2021) *Front Cell Dev Biol.*, 9:749559. doi: 10.3389/fcell.2021.749559.

Umer N, Phadke S, Shakeri F, Arévalo L, Lohanadan K, Kirfel G, Sylvester M, Buness A, Schorle H. PFN4 is required for manchette development and acrosome biogenesis during mouse spermiogenesis. (2022) *Development*, 149:200499. doi: 10.1242/dev.200499.

Contributions to Conferences

The role of podin proteins in mechanical stress protection in muscle. *Presentation, Annual Meeting of DFG Research group, Mechanical Stress protection (FOR2743), Oberkochen (2019).*

Function and regulation of podin proteins under mechanical stress in muscle. *Presentation, Annual Meeting of DFG Research group, Mechanical Stress protection (FOR2743), virtual Meeting (2021).*

Isoform-specific functions of synaptopodin-2 variants in cytoskeleton stabilization and autophagy regulation in muscle under mechanical stress. *Presentation, European Muscle Conference, Prague (2022).* Young Investigator Award

Abstract

Synpo2 isoforms are adapter proteins in myofibrillar Z-disc of striated muscle engaged in the homeostasis of the actin-crosslinking protein filamin C under mechanical stress. They interact with the co-chaperone BAG3, which is involved in CASA-mediated degradation of unfolded and damaged protein. In this study isoform-specific functions of Synpo2b, containing a PDZ-domain and Synpo2e lacking this domain, were analyzed. Under mechanical stress Synpo2e was less stably associated with Z-discs than Synpo2b and in part transferred to myofibrillar lesions. Synpo2e was also shown to recruit BAG3 to Z-discs and lesions via interactions of its proline-rich motif with the WW domain of the co-chaperon. This study provides evidence for a role of myofibrillar lesions as a quality control compartment essential for repair of damaged myofibrils with Synpo2 as a key proteostasis factor crucial for the maintenance of the contractile apparatus.

Based on phosphoproteome data pointing to a possible role of (de)phosphorylation in regulating Synpo2, phosphomimetic mutants were generated. A cluster of three phosphosites in the H2 region of Synpo2 revealed a regulatory function in its interactions with filamin C and α-actinin. The mutant mimicking the phosphorylated state of the triple phosphosite bound less strongly to both proteins. The less stable interaction with the actin cytoskeleton led to increased lesion formation, and considerable recruitment of Synpo2b to these structures. Hence, the triple phosphosite has a strong impact on the activity and localization of Synpo2b under mechanical stress. Fluorescence recovery after photobleaching (FRAP) experiments demonstrated increased stability of constitutively dephosphorylated Synpo2b affecting the turnover rate of the protein, thus confirming an influence of this phosphosite on its dynamics. In FRAP experiments constitutively dephosphorylated Synpo2e showed a higher affinity of Synpo2e for Z-discs, whereas the turnover of the protein remained unchanged and was independent of the phosphorylation state. Taken together, it is evident that these clustered phosphorylation sites have strong regulatory roles for the localization, mobility, dynamics, and protein-protein interactions of both investigated Synpo2 isoforms.

LC3B builds a scaffold to recruit numerous proteins on the surface of autophagosomes and interacts via its LIR specific peptide motif. Database analyses identified a LIR motif in the Synpo2 H1 region, which also contains a phosphosite in its core sequence. A peptide array using LIR phosphosite peptides showed a phosphorylation-dependent interaction of Synpo2

with LC3B. In contrast, bimolecular fluorescence complementation assays using LIR phosphosite mutants revealed no phosphorylation-dependent interaction of LC3B and Synpo2. Synpo2e, which is usually localized in Z-discs and lesions, is at least in part associated with vesicular structures in the constitutively phosphorylated state of the LIR motif. These results suggest that the localization and function of this isoform may be affected by LIR motif phosphorylation. FRAP experiments with Synpo2b variants showed a significantly reduced half-life of the dephosphorylation mimicking mutant compared to both the wildtype and the phosphorylation mimicking mutant. Hence it is evident that the LIR phosphosite has a regulatory role for the localization, mobility, dynamics, and the interactions with LC3B of both investigated Synpo2 isoforms.

Kurzfassung

Die verschiedenen Isoformen von Synpo2 fungieren als Adapterproteine in der myofibrillären Z-Scheibe quergestreifter Muskelzellen und sind unter mechanischer Belastung an der Homöostase des Aktin-vernetzenden Proteins Filamin C beteiligt. Sie interagieren mit dem Co-Chaperon BAG3, welches im CASA-vermittelten Abbau ungefalteter und beschädigter Proteine involviert ist. In dieser Studie wurden die Isoform-spezifischen Funktionen von Synpo2b, dass eine PDZ-Domäne enthält, und Synpo2e, dem diese Domäne fehlt, analysiert. Unter mechanischer Belastung zeigte Synpo2e eine weniger stabile Assoziation mit Z-Schreiben als Synpo2b und wurde vermehrt zu myofibrillären Läsionen rekrutiert.

In dieser Arbeit konnte zudem gezeigt werden, dass durch die Interaktion des prolinreichen Motivs von Synpo2e und der WW-Domäne des co-Chaperons BAG3, dieses zu Z-Scheiben und Läsionen rekrutiert wird. Diese Studie liefert Beweise für eine Rolle der myofibrillären Läsionen als Kompartiment der Protein-Qualitätkontrolle, das für die Reparatur beschädigter Myofibrillen, mit Synpo2 als wichtigen Proteostase Faktor, entscheidend für die Aufrechterhaltung des kontraktilen Apparats ist.

Basierend auf phosphoproteomischen Daten, die auf eine mögliche Rolle der (De)Phosphorylierung bei der Regulation von Synpo2 hinweisen, wurden phosphomimetische Mutanten von diesem generiert. Ein Cluster aus drei Phosphorylierungsstellen in der H2-Region von Synpo2, die an mehreren Proteininteraktionen beteiligt sind, zeigte eine regulatorische Funktion in der Interaktion mit Filamin C und α-Actinin. Die Mutante, die den phosphorylierten Zustand der dreifachen Phosphorylierungsstellen nachahmt, zeigte eine verringerte Bindungsaffinität zu beiden Proteinen und eine weniger stabile Wechselwirkung mit dem Aktin-Zytoskelett, was zu einer verstärkten Bildung von Läsionen und einer Rekrutierung von Synpo2b zu diesen Strukturen führte. Somit hat die Dreifach-Phosphorylierungsstelle einen deutlichen Einfluss auf die Aktivität und Lokalisation von Synpo2b unter mechanischer Belastung. *Fluorescence Recovery after Photobleaching* (FRAP) Experimente zeigten eine erhöhte Stabilität des konstitutiv dephosphorylierten Synpo2b, welche die *Turnover*-Rate des Proteins beeinflusst. Dies bestätigt den Einfluss dieser Phosphorylierungsstellen auf die Dynamik von Synpo2b. In FRAP-Experimenten zeigte das konstitutiv dephosphorylierte Synpo2e eine höhere Affinität zu Z-Scheiben, während die *Turnover*-Rate des Proteins unverändert blieb und unabhängig vom Phosphorylierungszustand war. Zusammengefasst ist es offensichtlich, dass diese geclusterten Phosphorylierungsstellen

eine starke regulatorische Rolle für die Lokalisierung, Mobilität, Dynamik und Protein-Protein-Interaktion beider untersuchter Synpo2-Isoformen spielen.

Das Protein LC3B bildet ein Gerüst zu Rekrutierung zahlreicher unterschiedlicher Proteine auf der Oberfläche von Autophagosomen und interagiert mit den meisten Bindugspartnern über sein LIR-spezifisches Pepidmotiv. Eine Datenbankanalyse identifizierte ein LIR-Motiv auch in der Synpo2-H1-Region, die eine Phosphorylierungsstelle in ihrer Kernsequenz enthält.

Ein *Peptid-Array* mit verschiedenen Peptiden, welche die LIR-Phosphorylierungsstelle enthielten, zeigte eine phosphorylierungsabhängige Interaktion von Synpo2 mit LC3B. Im Gegensatz dazu zeigten jedoch bimolekulare Fluoreszenzkomplementations Experimente unter Verwendung von Mutanten der LIR Phosphorylierungsstelle keine Phosphorylierungsabhängigkeit für diese Interaktion in der Zelle. Darüber hinaus wurde im konstitutiv phosphorylierten Zustand des LIR-Motivs Synpo2e, das normalerweise in Z-Scheiben und Läsionen lokalisiert ist, teilweise in Assoziation mit vesikulären Strukturen gefunden. Diese Ergebnisse legen nahe, dass die Lokalisierung und Funktion dieser Isoform durch die Phosphorylierung des LIR-Motivs beeinflusst werden könnte. FRAP-Experimente mit Synpo2b-Varianten zeigten eine signifikant verkürzte Halbwertszeit der konstitutiv dephosphorylierten Mutante, im Vergleich sowohl zum Wildtypen als auch zur konstitutiv phosphorylierten Mutante. Daher ist es offensichtlich, dass die LIR-Phosphorylierungsstelle eine regulatorische Rolle für die Lokalisierung, Mobilität, Dynamik und die Wechselwirkungen mit LC3B beider untersuchter Synpo2-Isoformen spielt.

Contents

1.0 Introduction

1.1 The Muscular System

A huge variety of essential processes in higher animals, such as the rhythmic pumping activity of the heart, are based on the function of a highly specialized contractive tissue, the musculature. Musculature-mediated processes include the voluntary movement such as locomotion and the involuntary movements which are essential for the maintenance of many important functions of the body, such as protein homeostasis and mechanical stress protection upon cellular damage through for example mechanical or oxidative stress. The structure of the muscle depends on its specific function and differs significantly between the smooth muscles and the striated muscles.

1.2 Striated muscle

The skeletal and the heart muscles are categorized as striated muscles due to their characteristic cross-striation already visible in light microscopy with becoming notably clearer in electron microscopy. This cross-striation is caused by the regular assembly of the contractile elements called sarcomeres, which are arranged in an alternating pattern of anisotropic A-bands composed of microfilaments and the isotropic I-Band. In the middle of the I-Band the Z-discs are located, which describe the lateral boundary of a sarcomere. The H-Zone originates in the center of the A-Band and consists of the so-called thick filaments. This H-zone is divided by the central M- Band (Figure 1.1).

In striated muscle the sarcomere is the fundamental molecular unit of contraction and is defined as a dynamic network of proteins, which is involved in force-generation and is able to generate signaling with other cellular compartments (Lewis *et al.*, 2018; Ono, 2010; Ghosh and Hope, 2010; Rudolph *et al.*, 2019).

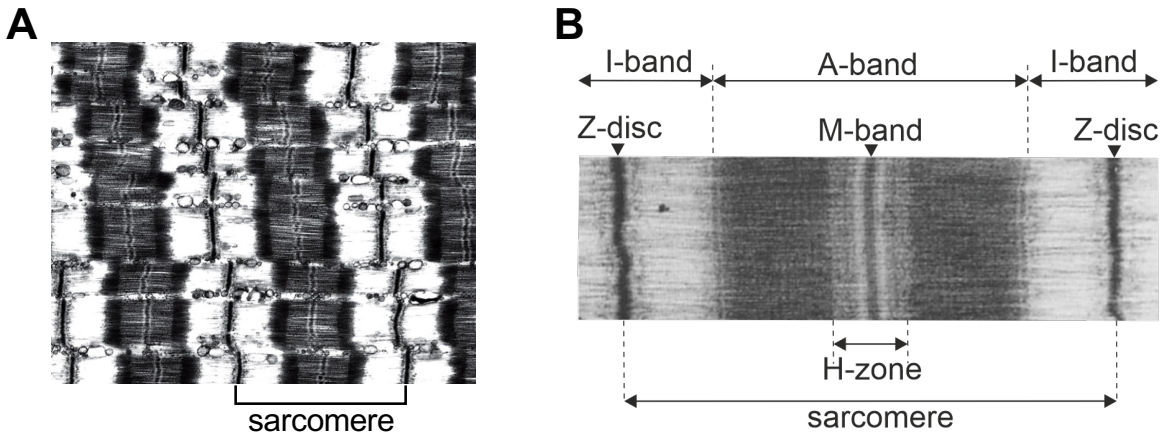

Figure 1.1: Electron-micrograph of the skeletal muscle. (A) Arrangement of the sarcomeres in skeletal muscle longitudinal section (modified from Alberts *et al.*, 2007). (B) Detailed view of a sarcomere with depiction of important structures (modified from Fürst *et al.*, 1988).

1.2.1 Skeletal muscle

Skeletal muscles are primarily responsible for the voluntary body movements and are composed of multiple parallelly arranged muscle fascicles which are surrounded by a connective tissue called perimysium (Figure 1.2). The muscle fascicles consist of large cells, the muscle fibers, which are surrounded by a further layer of connective tissue called endomysium (Schünke, 2000). The layers of the connective tissue which cross the entire muscle are essential for the stability and the force transmission (Berthier and Blaineau, 1997; Purslow, 2002). The muscle is connected to the tendons via myotendinous junctions and thus to the skeleton which allows its contraction to result in a movement of the bones.

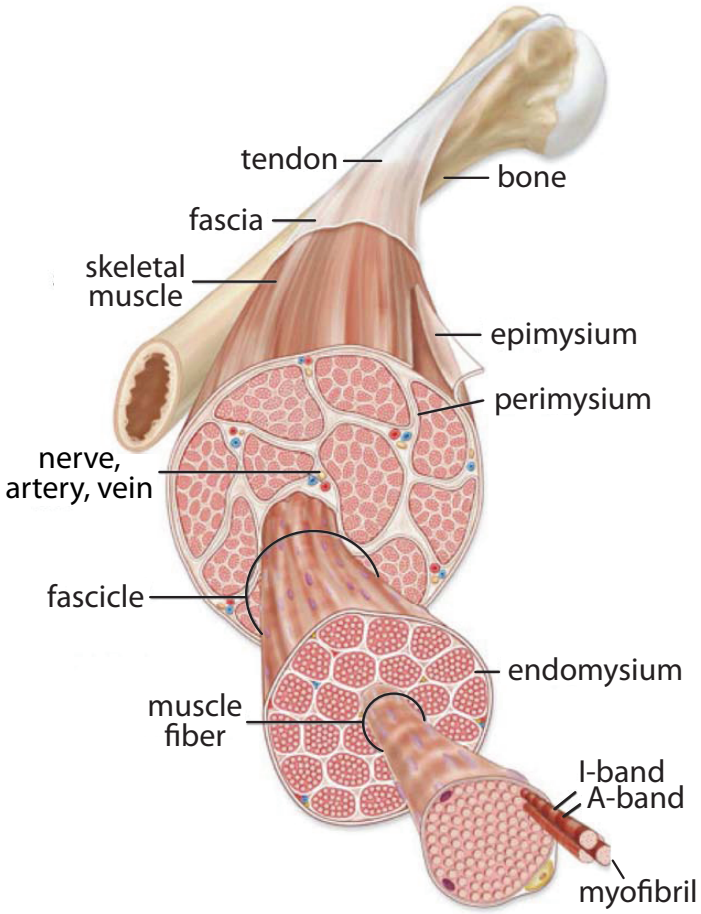

Figure 1.2: Schematic figure depicting the structure of a skeletal muscle. The skeletal muscle is connected with the bones through the tendon. It consists of bundles of muscles, which are surrounded by perimysium. These bundles of muscles are composed of muscle fibers and these fibers are surrounded by endomysium (modified from Michael McKinley, 2009).

Each muscle fiber represents a polynuclear syncytium which is emerged during the embryonic development as a result of the fusion of the muscle precursor cell, the myoblasts. During the differentiation of these syncytia numerous contractile myofibrils are developed which proceed parallel over the entire length of the muscle cell. The myofibrils are constructed by the smallest contractile unit of the cross-striated musculature, the sarcomeres and mainly consist of specialized actin- and myosin-filaments (Figure 1.3). The thin actin-filaments are anchored in the Z-discs (Clark *et al.*, 2002) and interact with a variety of muscle specific proteins including nebulin, troponin and tropomyosin (McLachlan und Stewart, 1975).

A special characteristic of the skeletal muscle lies in the ability to contract quickly in a targeted manner. This is caused by the interplay of the thin actin-filaments and the thick myosin-filaments. A low concentration of calcium leads to the inhibition of the myosin binding site. However, the release of calcium ions from the sarcoplasmic reticulum in response to an action potential lead to a troponin dependent conformation change of tropomyosin which then leads to an uncovering of the binding site. Subsequently, myosin heads bound to the filaments and the ATP bound to the globular myosin heads is hydrolyzed. The hydrolysis of ATP to ADP + P_i leads to a conformational change of the myosin molecule, which pushes the thin filaments to the M-band direction. Nevertheless, the length of the filaments remains constant during this process (Huxley und Hanson, 1954)

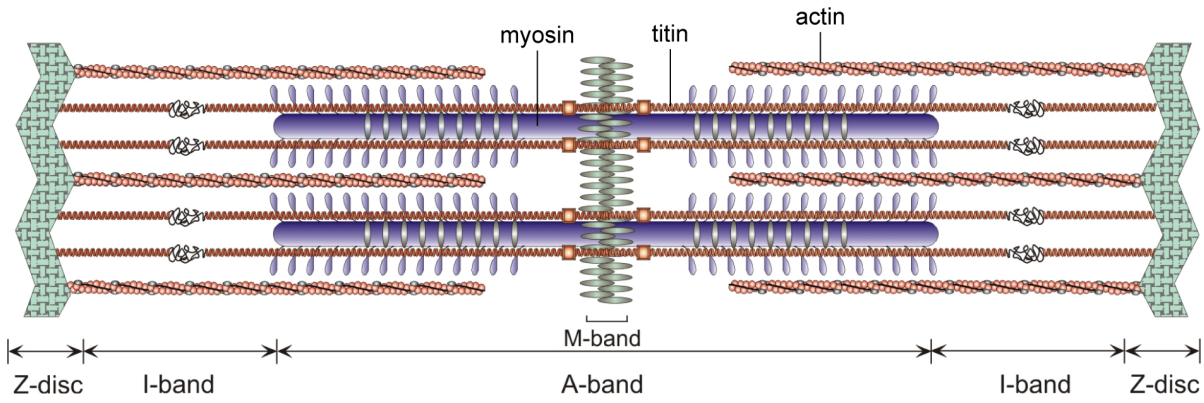

Figure 1.3: Schematic overview of the sarcomere. Thin actin filaments stretch out from the Z-disc towards the M-band which is the origin of the thick myosin filaments. Titin extends from the Z-disc to the M-band (modified from D. O. Fürst).

A third filament system composed of the gigantic protein titin is responsible for the stability and the elasticity of skeletal muscle cells. After actin and myosin, titin belongs to the main elements of the sarcomere (Clark *et al.*, 2002) and serves as scaffold protein for the myosin filaments (Tskhovrebova and Trinick, 2010). It is the largest protein expressed in the human body with a molecular weight of 3 to 3.7 MDa. The N-terminal domains of the titin molecules of opposite sarcomeres overlap (Pyle and Solaro, 2004) and it extends from the Z-disc to the M-band, thereby connecting both structures (Fürst *et al.*, 1988).

1.3 Myofibrillogenesis

Myofibrillogenesis describes the process of the development of sarcomeres in myofibrils as precursor structures. Since there is yet no complete clarification for the underlying process, there are different models describing it (summarized in Sanger *et al.*, 2005). The preferred model used by authors is the three-stage pre-myofibril model (Figure 1.4). According to this model the development of the nascent myofibril in the periphery starts with the development of pre-myofibrils from fused muscle cells. The nascent myofibrils consist of mini-sarcomeres containing actin, actin-binding proteins, and filamentous non-muscle myosin II. These mini sarcomeres are laterally confined by the Z-disc precursors called Z-bodies, which already express sarcomere-specific proteins like actin, α-actinin and filamin (Rhee *et al.*, 1994; Sanger *et al.*, 2000). In the later stage Z-bodies form the Z-discs through linearization. In the process of the myofibrillogenesis muscle-specific myosin II and titin are added, and the Z-bodies start to align and form Z-disc precursors of the nascent myofibrils. The characteristic cross striation is still lacking in the nascent myofibrils, since the thick filaments are still randomly arranged. Through the full exchange of non-muscle myosin IIb to muscle myosin II and the incorporation of M-band proteins the nascent myofibrils mature into differentiated myofibrils (Sanger *et al.*, 2000; Du *et al.*, 2003).

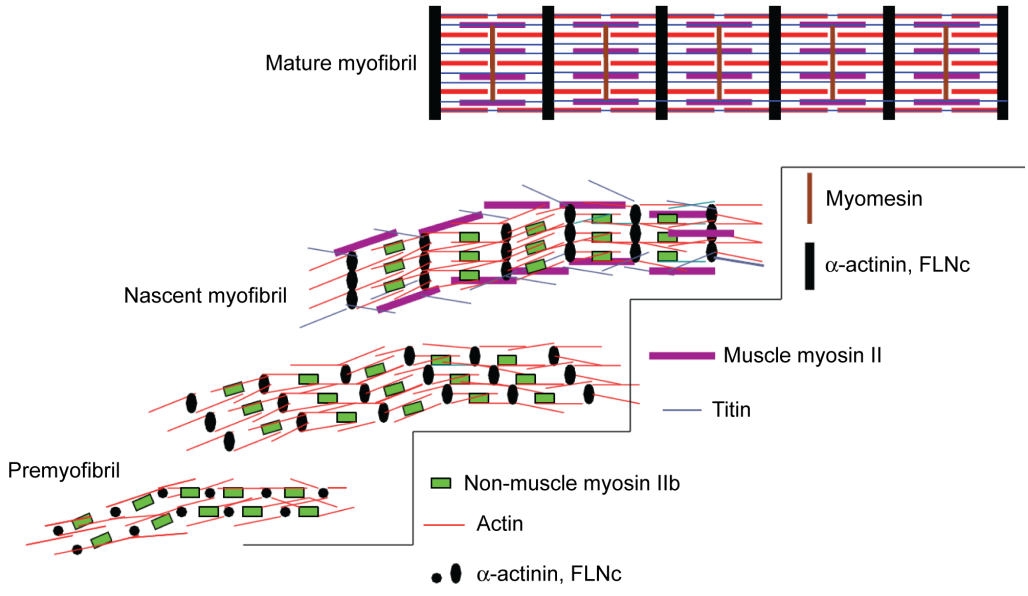

Figure 1.4: Pre-myofibrils model according to Sanger. Pre-myofibrils consists of mini sarcomeres containing Z-bodies, actin, actin-binding proteins, and non-muscle myosin II. The Z-bodies align to each other, linearize and the non-muscle myosin II is replaced by muscle myosin II and titin is incorporated. The terminal differentiated myofibril is characterized by the formation of Z-discs and the sarcomeric structure (modified from Sanger *et al.,* 2005).

1.4 Muscle regeneration and remodeling

The complex, essentially crystalline macromolecular arrangement of the contractile apparatus of striated muscles is optimized for directional movement. Numerous individual protein constituents have to associate consecutively during its development, eventually leading to the formation of the contractile myofibrils. Subsequently, it is equally important to maintain the structure and functionality of the myofibrils throughout the lifetime of an organism, although it is constantly challenged by mechanical forces.

Injury may occur at two levels: the more severe kind of damage ultimately means the total loss of a muscle cell, which subsequently has to be replaced by a new cell. These processes can be divided into the three phases of damage, repair, and remodeling. First, the damaged tissue undergoes necrosis and hematoma formation, and subsequently inflammatory cells migrating to the site of damage will phagocytose the necrotic tissue. To replace the lost myofibers, a special population of muscle stem cells, called satellite cells, are activated. Much like embryonic muscle progenitor cells they divide, proceed with development and ultimately fuse into mature, differentiated muscle fibers (Ten Broek *et al.*, 2010). These satellite cells are located between the plasma membrane and the surrounding basal lamina (Wagers and Conboy, 2005). They are characterized by the expression of the transcription factor Pax7 and transform into myoblasts after the expression of the myogenic factors MyoD and Myf5 (Wagers and Conboy, 2005). The specific microenvironment of the satellite cells, called the niche, controls their behavior. The niche contains various stimulatory and inhibitory growth factors that ensure that the cells are kept in a resting state until they become activated (Ten Broek *et al.*, 2010). Only in response to muscle injury, the satellite cells are activated and reenter the cell cycle. However, some of the activated satellite cells do not proliferate and differentiate, but instead undergo a self-renewing cycle and replenish the satellite stem cell pool (Ten Broek *et al.*, 2010). Depending on the severity of the injury, activated satellite cells either form new, multinucleated muscle fibers or repair existing muscle fibers by fusing with them (Ten Broek *et al.*, 2010).

These regenerative processes require extensive proliferation, and the pool of renewable cells may become exhausted at some point, which is an evident problem in several neuromuscular diseases (e.g., Duchenne Muscular Dystrophy; reviewed in Moser, 1984). It is therefore beneficial to develop alternative strategies for repair of muscular damage, limiting the need for complete cell replacement to the severest cases. In addition, this is even a must in cardiomyocytes, where there is no or only a very limited amount of stem cells that could replace severely damaged cells. Minor myofibrillar damages due to mechanical stress and other kinds

of cellular or physical stress occur constantly at the level of individual sarcomeres or myofibrils, and the repair of these damages requires efficient and rapid repair mechanisms (Yu and Thornell, 2002; Yu *et al.*, 2003). Muscle fibers exposed to eccentric contraction may adapt to this higher activity by adding new sarcomeres (Yu *et al.*, 2003). Zones of repair and/or regeneration are characterized by longitudinal strands bridging two or more sarcomeres and appearing as broad bands in immunofluorescence studies (Vijayan *et al.*, 1998; Vijayan *et al.*, 2001; Yu and Thornell, 2002; Yu *et al.*, 2003; Otten *et al.*, 2012; Eulitz *et al.*, 2013; Orfanos et al., 2016). In these areas α-actinin and titin are absent, whereas actin-filament and desmin intermediate filaments are enriched (Yu and Thornell, 2002; Yu *et al.*, 2004). Staining against the actin-crosslinking protein filamin C and its binding partners Xin and XIRP2 enable efficient detection of these myofibrillar lesions (van der Ven *et al.*, 2006; Otten *et al.*, 2012; Eulitz *et al.*, 2013; Kley *et al.*, 2013). However, the exact mechanisms of these remodeling processes are not yet known.

It is possible to study these processes with skeletal muscle cells in cell culture by applying electrical pulse stimulation (EPS). This method enables the investigation of remodeling processes independent of complex animal models or the taking of human biopsies. By using EPS, it is possible to induce contractile activity of for example cultured C2C12 myotubes (Thelen *et al.*, 1997) and to accelerate the *de novo* assembly of sarcomeres (Fujita *et al.*, 2007). The changes in gene expression and metabolic properties induced by EPS are comparable to those in skeletal muscle cells *in situ*, and the EPS-induced contractions have been shown to mimic the situation of a stimulated, contracting muscle in humans (Nedachi *et al.*, 2008; Burch *et al.*, 2010). Likewise, enhanced stimulation leads to the formation of myofibrillar lesions. EPS is therefore a suitable method for the analysis of mechanical stress-induced biological processes in skeletal muscle cells and represents a useful model to assess the effects of muscle contraction as well as different states of contraction (Manabe *et al.*, 2012). The actin crosslinking protein filamin C was particularly detectable in lesions. Therefore, the analysis of the role of filamin C associated proteins in these events is of interest. Due to their involvement in the chaperone assisted selective autophagy, the podin proteins are of particular interest.

1.5 The Z-disc

Z-discs define the lateral borders of the sarcomere and are located at the center of the I-band (Pyle and Solaro, 2004). The thin actin-filaments of adjacent sarcomeres are cross-linked in the Z-discs by their tight interaction with antiparallel α-actinin homodimers (Frank *et al.*, 2006;

Hoshijima, 2006). In addition, titin and nebulin/nebulette, which is among others responsible for the stabilization of actin-filaments, are also connected to the Z-disc via α-actinin. Z-discs of adjacent sarcomeres are arranged in parallel and laterally linked by desmin intermediate filaments (Frank *et al*., 2006) and desmin forms an important link between the costameres and the sarcomeric Z-discs (Patel and Lieber, 1997). Costameres establish a communication center between the extracellular matrix, the sarcolemma, and the myofibrils and are made up of a collection of proteins that include α-actinin, integrin-associated protein talin, β-integrin which is involved in the force transmission from Z-disc to extracellular matrix, dystrophin and vinculin among others (Pyle and Solaro, 2004). Vinculin indirectly binds to the integrins via the integrin-associated proteins talin and α-actinin and thus connecting the costameres to the actin-based cytoskeleton. Intermediate filaments also connect the Z-discs to focal adhesion contacts and the nucleus (Hoshijima, 2006). Thus, changes of the extracellular matrix composition can affect signaling pathways between the costameres, the peripheral and central Z-discs and the nucleus, and vice versa, these signaling pathways can also lead to changes in the extracellular matrix.

The main task of the Z-discs was restricted to the passive power transmission and mechanical stabilization in the past. But in addition to these structurally and mechanically stabilizing functions, the Z-disc is today also known to be involved in signal transduction processes. It serves as an accumulation point of various transcription factors, proteins of calcium ion-coupled signal transduction as well as phosphatases and kinases, which primarily influence phosphorylation state but also the function and gene expression and thus characterize the Z-disc as a biochemical sensor (Pyle and Solaro, 2004; Frank *et al*., 2006; Hoshijima, 2006; Faul *et al*., 2007; Gautel, 2008). Taken together, these properties demonstrate the inseparability of the mechanical, structural, and biochemical functions of the Z-disc complex. Moreover, it has been shown that a variety of nonstructural proteins are localized in the Z-disc. These proteins are involved in signal transduction from the contractile machinery to other compartments such as the cell nucleus. Thereby, they operate as mechanical stress-sensor complexes or as a part of the protein kinase signaling pathway (Gautel, 2008). Additionally, several signaling proteins and a diversity of anchoring proteins for signal components including the members of the calsarcin protein family are localized in the Z-discs (Pyle und Solaro, 2004).

The central role of Z-discs in the sarcomere maintenance is further supported by the fact that cardiomyopathies and muscular dystrophies have been linked to mutations in different genes encoding Z-disc proteins (Frank *et al*., 2006).

In addition, the Z-disc was also shown to be involved in protein turnover and autophagy (Willis *et al.*, 2009; Arndt *et al.*, 2010; Ulbricht *et al.*, 2013).
In the following, the proteins α-actinin and filamin C are described in more detail as crucial components of the Z-disc.

1.5.1 α-Actinin

The actin-bundling protein α-actinin has a molecular mass of approximately 94 kDa and belongs to the spectrin superfamily, which in addition to spectrin includes dystrophin and utrophin as well (Sjöblom *et al.*, 2008). In mammals, four α-actinin isoforms are encoded by four genes (ACTN1, ACTN2, ACTN3, and ACTN4) and expressed in a tissue-specific manner. The α-actinin isoforms 2 and 3 are expressed in skeletal muscle, whereas α-actinin 1 and 4 are restricted to non-muscle cells (Blanchard *et al.*, 1989). The molecular structure of all four isoforms is identical and is characterized by an N-terminal, globular actin-binding domain (ABD), which is followed by a central rod with four so-called spectrin repeats and a calmodulin-like domain at the C-terminus (CAM domain) (Davison and Critchley, 1988; Castresana and Saraste, 1995; Travé *et al.*, 1995)

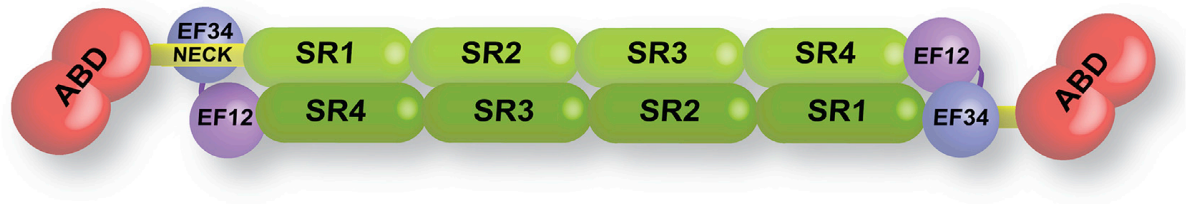

Figure 1.5: Schematic representation of the domain structure of an α-actinin dimer. The N-terminal ABD is followed by four spectrin-like repeats (SR) and the CAM domain at the C-terminal, containing the EF hand motif (from Ribeiro Ede *et al.*, 2014).

The central rod allows α-actinin to form antiparallel dimers with an actin-binding site at each end which enables the molecule to crosslink actin-filaments into tight bundles. During the dimerization of α-actinin, the central spectrin domains of two α-actinin molecules interact in pairs via polar interactions (Figure 1.5). The crystal structure has shown that dimerization occurs in detail via the positively charged spectrin repeats R1 and R2 with the negatively charged repeats R3 and R4 of a second α-actinin molecule (Djinović-Carugo *et al.*, 1999). The actin-binding site has two calponin homology domains (CH domains) and is similar in structure

to the actin binding sites of other actin-binding proteins, such as filamins or dystrophins (Djinović-Carugo *et al.*, 1999; Van Troys *et al.*, 1999).

Binding of non-muscle α-actinins 1 and 4 to actin is calcium-dependent. However, due to a mutation of the EF hands of the calmodulin-like domain, the muscle-specific α-actinin isoforms 2 and 3 have lost this ability and are no longer able to bind actin in a calcium-dependent manner (Blanchard *et al*., 1989). In these two isoforms, the affinity of α-actinin for actin filaments is ensured by the binding of phosphatidylinositol-4, 5-bisphosphate (PIP_2) (Fraley *et al.*, 2003). In its inactive form, the α-actinin homodimer is mainly held together by contacts between the spectrin repeats and by PIP_2-sensitive contacts between the CAM and ABD. When PIP_2 binds to the ABD the contact with the CAM domain is broken. This exposes a binding site for the titin domain Z-repeat 7 (ZR7) and activates the actin binding site in the ABD (Young and Gautel, 2000).

In skeletal and cardiac muscle, α-actinin is localized in the Z-discs, where its main function is to cross-link antiparallel actin filaments of adjacent sarcomeres. As described above, many Z-disc-associated proteins bind to α-actinin, resulting in stabilization of the sarcomere during contraction. This interaction between the CAM domain of α-actinin to the ZR-domain of titin leads to Z-disc localization of α-actinin and further plays a possible role in the assembly and regulation of Z-disc thickness (Ohtsuka *et al.*, 1997; Young and Gautel, 2000). In addition, α-actinin interacts with a variety of proteins in the contraction machinery of adult striated muscle, including nebulin (Nave *et al.*, 1990), CapZ (Papa *et al.*, 1999), calsarcin (Faulkner *et al.*, 2000; Takada *et al.*, 2001; Frey and Olson, 2002), the scaffolding protein myotilin (Salmikangas *et al.*, 1999) and the multi-adapter protein synaptopodin-2 (Linnemann *et al.*, 2010).

1.5.2 Filamin

The protein Filamin was described for the first time in chicken gizzard by Hartwig *et al.* in 1975. A key feature of filamin is its capacity to bundle F-actin. With this feature filamin regulates the actin filament system in a variety of dynamic cellular processes (Wang and Singer, 1977). There are three different isoforms of filamin coded in mammalians, named filamin A, filamin B and filamin C, which all have a molecular weight of approximately 280 kDa. Filamins consist of a N-terminal ABD and the two CH domains as well as the 24 immunoglobulin-like (Ig-like) domains. The Ig-like domains consist of two antiparallel ß-pleated sheets. One of the antiparallel ß-pleated sheets is four stranded and the other one is three stranded (Fucini *et al.*, 1997; Pudas *et al.*, 2005). Filamins form V-shaped homodimers and the dimerization takes place in the C-terminal Ig-like domain 24 (Himmel *et al.*, 2003; Pudas *et al.*, 2005; Seo *et al.*,

2009). The order of the Ig-like domain is disrupted by one or two hinge regions and is isoform dependent. These hinge regions lead to additional flexibility (Gorlin *et al.*, 1990) and they lie between the domain 15 and 16 as well as domain 23 and 24. The Ig-like domain 16 and 17, 18 and 19 as well as 20 and 21 are arranged pairwise in filamin A and play a role in the regulation of different protein interactions by functioning as auto-inhibitory and stress-activated mechanosensors. This structure is also suggested to be the same for filamin C (Heikkinen *et al.*, 2009; Ehrlicher *et al.*, 2011; Rognoni *et al.*, 2012). All three isoforms share 60 to 80 % homology and present an almost identical domain structure with only the hinge regions being an exception with a homology of only 45 % (Gorlin *et al.*, 1990).

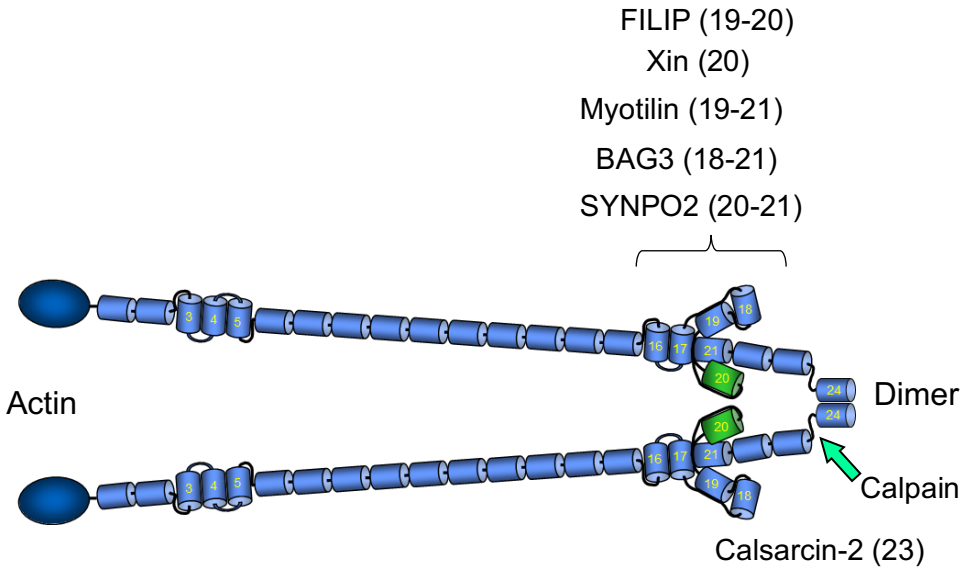

Figure 1.6: Schematic representation of filamin C molecule. The N-terminal ABD is followed by 24 Ig-like domains. The last Ig-like domain (24) is responsible for dimerization. Domain 20 marked in green has an insertion consisting of 82 amino acids. Some of the known binding partners of the molecule are noted in the figure. (Modified from van der Ven *et al.*, 2006).

Besides to the bundling of actin-filaments, filamin is also involved in their anchoring of the transmembrane proteins such as the integrins, with the actin filament network (Kim and McCulloch, 2011). Furthermore, filamins play an important role in signal transduction processes since the C-terminus interacts with the various GTPases of the Rho-family (Rac, Rho, Cdc42) which act as switches in modulating the organization of the actin cytoskeleton (Ohta *et al.*, 1999).

There are 90 different binding partners of filamins known including receptors, intracellular signaling molecules and transcription factors (Nakamura *et al.*, 2011). The filamin A and filamin B isoforms are expressed ubiquitous and are localized in the cortical actin network and in actin stress fibers (Xie *et al.*, 1998; Chiang und Greaser, 2000; Thompson *et al.*, 2000). Filamin C has an insertion of 82 amino acids in the Ig-like domain 20, which is lacking in the other filamins. This insertion serves as the interaction site for many binding partners and is probably involved in the Z-disc localization of the protein (van der Ven *et al.*, 2000b; Fürst *et al.*, 2013). The filamin C isoform is predominantly expressed in cross-striated muscles (Xie *et al.*, 1998). This isoform is associated with the Z-disc, the sarcolemma, the myotendinous junctions and the intercalated discs (van der Ven *et al.*, 2000a). Interaction partners of filamin C are for example myotilin (van der Ven *et al.*, 2000b), calsarcin (Frey und Olson, 2002), FILIP1 and FILIPL (Reimann *et al.*, 2020), synaptopodin-2 (Linnemann *et al.*, 2010), actin-binding xin-repeat proteins (XIRPs) (van der Ven *et al.*, 2006; Kley *et al.*, 2013) and aciculin (Molt *et al.*, 2014) (Figure 1.6).
Mutations of the genes coding filamin lead to myofibrillar or distal myopathies (Vorgerd *et al.*, 2005; Duff *et al.*, 2011; Fürst *et al.*, 2013) and thus, filamin is of clinical significance.

1.6 The Podin protein family

The podin protein family consists of three members named synaptopodin, synaptopodin-2 and synaptopodin-2-like which are encoded by the genes SYNPO, SYNPO2 and SYNPO2L, respectively. All podins contain two regions of high homology, each comprising about 90 amino acids, are highly proline-rich, and are mostly unfolded under physiological conditions. In addition, each podin has multiple isoforms resulting from alternative splicing (see Figure 1.7). In striated muscle cells podins are localized at the Z-discs, where they interact with multiple binding partners. (Mundel *et al.*, 1997; Khaymina *et al.*, 2007)

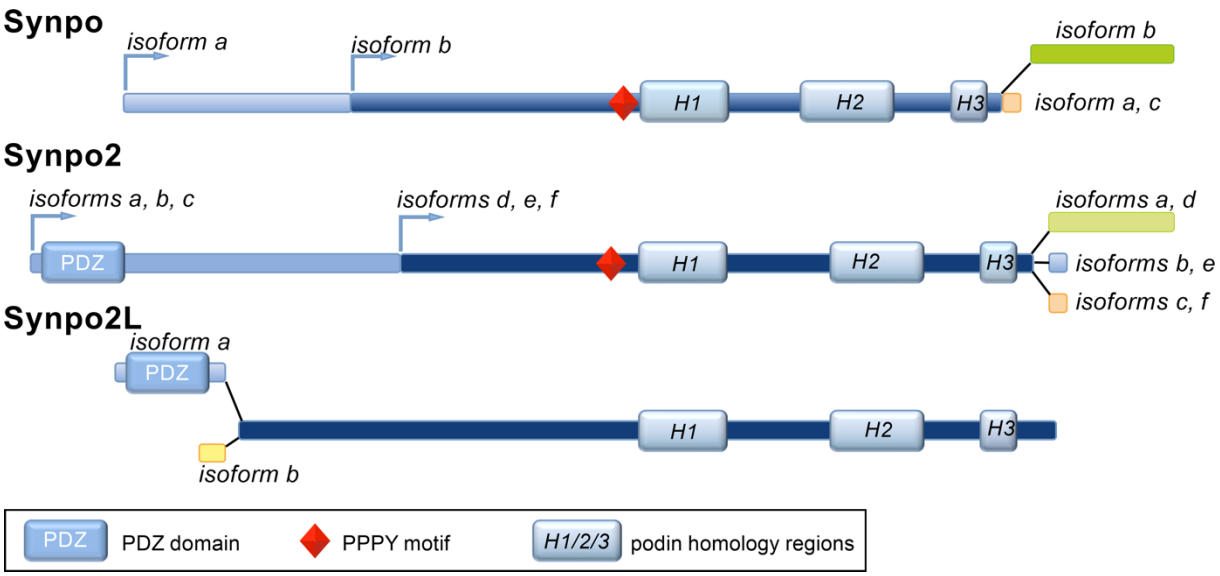

Figure 1.7: Schematic overview of the podin protein family. Synaptopodin, synaptopodin-2 and synaptopodin-2-like occur in several isoforms due to alternative splicing processes. The colored boxes represent protein regions originating from different exons. The N-terminal PDZ-domain, PPPY motif and the proline-rich podin homology regions are marked.

1.6.1 Synaptopodin-2

Synaptopodin-2 (Synpo2), also known as myopodin was first identified by Weins *et al.* in 2001, but a corresponding orthologue in birds called fesselin had already been described two years earlier (Leinweber *et al.*, 1999). Synpo2 was found in smooth muscle, where it is predominantly localized in dense bodies, and in cardiac and skeletal muscles, where it is predominantly located in Z-discs (Leinweber *et al.*, 1999; Renegar *et al.*, 2009; Weins *et al.*, 2001; Schroeter *et al.*, 2008; Linnemann *et al.*, 2010).

Two alternative transcriptional promotors and alternatively spliced exons of the human SYNPO2 gene result in 6 isoforms with a distinction at both the N- and C-terminus. A major, distinguishing difference is the N-terminal PDZ-domain, which is only found in the long isoforms a-c but not in the short isoforms d-f (de Ganck *et al.*, 2008; Linnemann *et al.*, 2010; Kai *et al.*, 2012). An overview of these isoforms is shown in Figure 1.8. It is described that isoform e, composed of 698 amino acids, is predominatly expressed in skeletal muscle while isoform b, composed of 1109 amino acids, is predominant in heart muscle (Linnemann, 2010).

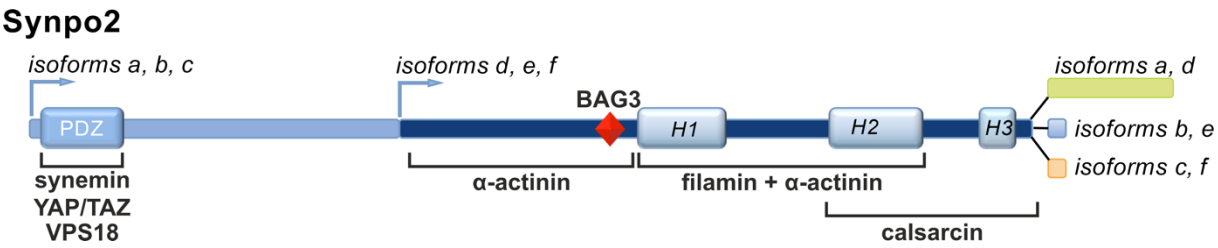

Figure 1.8: Schematic overview of Synpo2. Due to alternative transcriptional start points and differently spliced 3´exons 6 isoforms of Synpo2 can be described. The binding sites of several cytoskeletal proteins with Synpo2 is depicted.

Immunofluorescence studies of skeletal muscle cells revealed that in differentiated muscle Synpo2 is colocalized with α-actinin in sarcomeric Z-discs (Weins *et al.*, 2001). Synpo2 has been described as an interaction partner of α-actinin (Takada *et al.*, 2001; Pham and Chalovich, 2006; Faul *et al.*, 2007), with this interaction promoting the 14-3-3 dependent targeting of Synpo2 in the cell nucleus (Faul *et al.*, 2007). Previously observed co-sedimentation or co-localization with actin (Leinweber *et al.*, 1999; Weins *et al.*, 2001) was confirmed and characterized in more detail by Linnemann *et al.*, (2010, 2013). They identified two independent actin-binding regions and showed that Synpo2 can cross-link actin filaments into bundles. Binding of Synpo2 to several cytoskeletal proteins was found and some of these are depicted in Figure 1.8.

A direct interaction with filamin A and filamin C could also be shown (Linnemann *et al.*, 2010). The interaction between Synpo2 and filamin C was narrowed down to the Ig-like domains 20-21 by Linnemann *et al.*, (2010) using biochemical binding studies, while the Ig-like domain 20 and the Ig-like domain 21 alone did not show any interaction. Therefore, both Ig-like domains appear to be essential for binding.

In addition, Synpo2 binds to VPS18, a vacuolar Protein Sorting Homolog 18, which is involved in vesicle transport, via its PDZ-domain and to the co-chaperone BAG3 via a PPPY motif (Ulbricht *et al.*, 2013). As a result of these interactions, Synpo2 represents a link between the machinery of chaperone-assisted selective autophagy (see 1.7.1) and membrane fusion processes that generate autophagosomal membranes (Ulbricht *et al.*, 2013; Ulbricht and Höhfeld, 2013).

The Zinc-binding protein zyxin, which is enriched at focal contacts (Yu and Luo, 2006) and calmodulin, the binding of which is regulated in a calcium-dependent manner, have been described as further binding partners of Synpo2 (Kolakowski *et al.*, 2004). Furthermore, Synpo2 also inhibits actin-activated myosin ATPase activity, which is why Synpo2 is assigned a role similar to the protein caldesmon, which is known to inhibit myosin binding to actin in smooth muscle cells. In addition, binding of Synpo2 to smooth muscle myosin II has also been demonstrated (Schroeter and Chalovich, 2005).

Finally, integrin-linked kinase (ILK), an *in vitro* bona-fide protein kinase with additional framework functions (Hanningan *et al.*, 2011), binds to Synpo2. This is thought to induce phosphorylation at the N-terminus of Synpo2, which is necessary for Synpo2-mediated suppression of PC3 cell growth and migration (Yu and Luo, 2011).

1.7 Autophagy in the skeletal muscle

Autophagy occupies a fundamental position in numerous pathological and physiological processes from cell proliferation, protein and lipid homeostasis to neurodegeneration, muscle dystrophy and cancer (Levine and Kroemer, 2008). It represents a conserved system in which components of the cytoplasm and organelles are enclosed in vesicles, the autophagosomes, to be subsequently degraded (Mizushima *et al.*, 2011). Newly formed autophagosomes are first transported to lysosomes before they fuse with these. This leads to degradation of their cargo, with amino acids and most likely also lipids and sugars are made available again to the cell for the *de novo* synthesis of various molecules and organelles (Zoncu *et al.*, 2011; Liu and Czaja, 2013; Nascimbeni *et al.*, 2012a; Nascimbeni *et al.*, 2012b).

In most tissues, autophagy occurs constantly at a low level. However, under stress conditions such as protein aggregation, limited nutrient supply or during the requirement of structural remodeling, autophagic flux is enhanced as a compensatory mechanism to maintain energy demands and to stabilize cellular functions (Levine and Kroemer, 2008).

Constant movement and vigorous physical activity expose striated muscle to a large amount of reactive oxygen species, which can lead to damages of cellular components (Jackson, 2005). Moreover, under conditions of metabolic stress and starvation, skeletal muscle is an important source of amino acids.

Autophagy ensures that damaged or aged organelles and accumulated protein aggregates are recycled (Mizushima *et al.*, 2008). It could be shown that inhibition or impairment of autophagy leads to muscle degeneration and muscle weakness and that the adaptation of autophagic

activity to respective situation is essential for maintaining integrity of muscle fibers (Nascimbeni *et al.*, 2012b).

1.7.1 Chaperone-assisted selective autophagy

The sarcomeric Z-disc is under intense mechanical stress during muscle cell contraction, and thus effective mechanisms of protein homeostasis to maintain protein levels must be in place. Here, chaperone-assisted selective autophagy (CASA) represents a selective, autophagic degradation pathway of the flexible mechanosensor and actin-crosslinker filamin (Arndt *et al.*, 2010). When there is intracellular tension or an external force is applied, filamin's Ig-like domain interactions are disrupted, resulting in single domain unfolding (Yamazaki *et al.*, 2002, Rognoni *et al.*, 2012). This alters the binding of this protein to cytoskeletal and signaling proteins. In addition, unfolding of individual Ig-like domains and associated lengthening of the protein enables filamin to function as a flexible linker between actin filaments (Nakamura *et al.*, 2011; Ehrlicher *et al.*, 2011; Lad *et al.*, 2007; Chen *et al.*, 2011; Zhou *et al.*, 2010). Moreover, there is a high risk of irreversible damage and aggregation in the case of unfolded proteins or protein domains. Here, the CASA complex takes over an essential function in controlling protein quality (Ulbricht *et al.*, 2013).

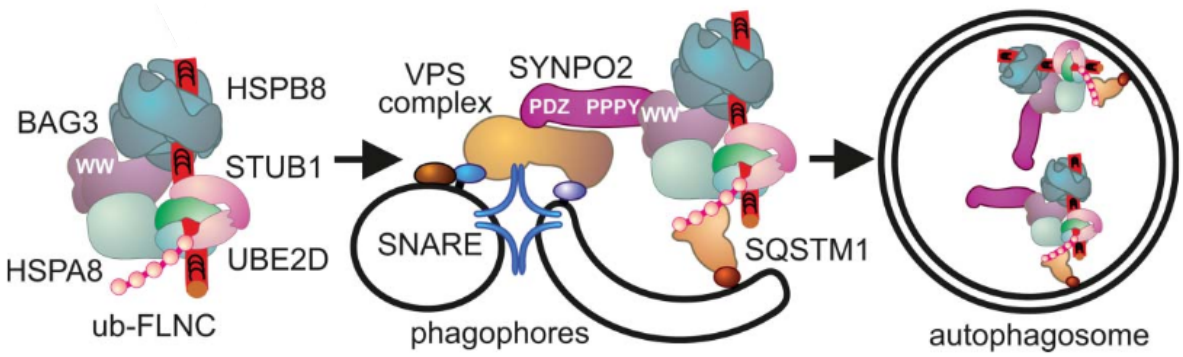

Figure 1.9: Schematic depiction of the CASA chaperone complex. During ubiquitination of the bound client protein, STUB1 plays a role as a chaperone-associated ubiquitin ligase and cooperates with the ubiquitin-conjugating enzyme UBE2D. Synpo2 binds to the membrane fusion complex containing VPS18 protein and Synpo2 interacts with BAG3, which is essential for the formation of autophagosomes. This complex is responsible for the assembly of ATG16L1- and LC3-positive phagophores. After this, the syntaxin-7-mediated membrane fusion takes place (modified from Ulbricht *et al.*, 2013).

The CASA complex consists of the molecular chaperones HspA8/Hsc70, and HspB8/Hsp22 together with the co-chaperones BAG3 and STUB1/CHIP (Figure 1.9). HspA8 is both a cytoplasmic and nuclear localized member of the Hsp70 chaperone family that is constitutively expressed. HspB8 belongs to a group of small heat shock proteins, which form large oligomers that stabilize non-native proteins. Further processing of these stabilized proteins is supported by Hsp70 chaperones (Haslbeck *et al.*, 2005). The co-chaperone BAG3 in turn has binding sites for both HspA8 and HspB8 and thus enables their functional interaction (Arndt *et al.*, 2010). In muscle cells, J-domain co-chaperone DNAJB6 can also be found in the CASA complex (Sarparanta *et al.*, 2012). These co-chaperones are often the first components of the chaperone machinery that recognize client proteins and enable high-affinity client binding through regulation of ATP-gated chaperone cycle of Hsp70 (Hartl *et al.*, 2011). Subsequently, the bound client filamin is ubiquitinated by chaperone-associated ubiquitin ligase STUB1 in conjunction with ubiquitin-conjugating enzymes of the UBE2D family (Arndt *et al.*, 2010). By binding BAG3 to the microtubule-associated motor protein cytoplasmic dynein, it directs client proteins into aggregate-like structures, which are then subjected to efficient autophagic digestion (Gamerdinger *et al.*, 2011). Furthermore, BAG3 favors recognition of ubiquitinated clients by the autophagic ubiquitin adapter SQSTM1/p62 (Arndt *et al.*, 2010; Gamerdinger *et al.*, 2009; Shaid *et al.*, 2013). In addition to the ubiquitin binding region, UBA-domain (ubiquitin-associated domain), this SQSTM1/p62 adapter has a LC3 interaction region, which mediates the interaction of LC3 to phagophores. Simultaneous binding of the adapter to ubiquitinated filamin and to phagophores induces the formation of the autophagosome (Shaid *et al.*, 2013), a process in which Synpo2 is also involved (Ulbricht *et al.*, 2013). In this process Synpo2 acts as an adapter protein by interacting to the membrane fusion complex containing VPS18 with its PDZ-domain and with the PPPY motif to the co-chaperone BAG3, which is crucial for the formation of autophagosomes (Ulbricht *et al.*, 2013). VPS18 is an essential component of diverse protein complexes that bring intracellular membrane systems together in preparation of fusion events (Wickner, 2010; Epp *et al.*, 2011; Bröcker *et al.*, 2012). Synpo2-associated VPS protein complex appears to be specific for attachment of the phagophore membranes, as corresponding marker proteins such as ATG16L1 and LC3 could be detected in these complexes (Ulbricht et al., 2013). In addition, these structures contain the SNARE protein syntaxin-7, which facilitates phagophore fusion (Moreau and Rubinsztein, 2012). In summary, Synpo2 likely acts as a link between the CASA chaperone complex, which processes the client protein filamin, and a membrane attachment and membrane fusion machinery (Ulbricht *et al.*, 2013).

1.7.2 BAG3

The co-chaperone BAG3 belongs to the Bcl2-associated anthanogene (BAG) protein family. It contains a proline-rich PXXP-motif, a WW-domain and two IPV-regions, which all mediate binding to other proteins (Takayama *et al.*, 1999; Doong *et al.*, 2003; Berre, 2005; Ulbricht *et al.*, 2013) (Figure 1.10). The C-terminal domain of BAG3 interacts with the ATPase domain of Hsp70 (Takayama *et al.*, 1999).

Figure 1.10: Schematic representation of a BAG3 molecule. The N-terminal WW domain is followed by the two IPV-regions. Proline-rich PxxP-motif is depicted next to the C-terminal BAG domain (modified from D.O. Fürst).

BAG3 is highly abundant in skeletal and cardiac muscle, where it is localized diffusely distributed throughout the cytoplasm and Z-discs (Homma *et al.*, 2006). Via its interaction with HspA8, HspB8 and Synpo2, it plays an important role in the degradation of unfolded filamin by the CASA machinery (Arndt *et al.*, 2010; Ulbricht *et al.*, 2013).
A huge number of dominant BAG3 mutations have been identified some of which resulting in cardiomyopathy or in BAG3-related severe myofibrillar myopathies (Selcen *et al.*, 2009; Arimura *et al.*, 2011; Norton *et al.*, 2011; Lee *et al.*, 2012; Feldman *et al.*, 2014; Franaszczyk *et al.*, 2014).
BAG3 was also shown to regulate contractility and calcium homeostasis in ventricular myocytes (Feldmann et al., 2016).

1.8 Protein Phosphorylation

As Synpo2 was described as a multi-adapter protein of the Z-disc with diverse functions, it was a central goal of this work to unravel how the multiplicity of resulting interactions and functions could be regulated, and which cellular mechanisms would allow the reversible and dynamic regulation of Synpo2 activities. A very widespread mechanism of regulating protein-protein interactions is their modulation by introduction of post-translational modifications. Until now,

more than 400 of these post-translational modifications are known, allowing the cells to dynamically adapt to changing conditions (Wilkins *et al.*, 1996). One of the best-studied and most crucial post-translational modifications is the phosphorylation of certain amino acids with probably about 30 % of the whole proteome affected (reviewed by Cohen, 2002b).

A plethora of biological processes, including the activity, synthesis, degradation/turnover, binding capacity, conformational changes, and localization of proteins are regulated and modulated by phosphorylation. Protein phosphorylation is a reversible process, where protein kinases, an enzymatic sub-class that is encoded by different genes in the human genome, mediate the addition of the gamma phosphate group from an ATP molecule to an acceptor amino acid residue (Manning *et al.*, 2002). The enzymatic removal of this phosphate residue is catalyzed by protein phosphatases (Figure 1.11).

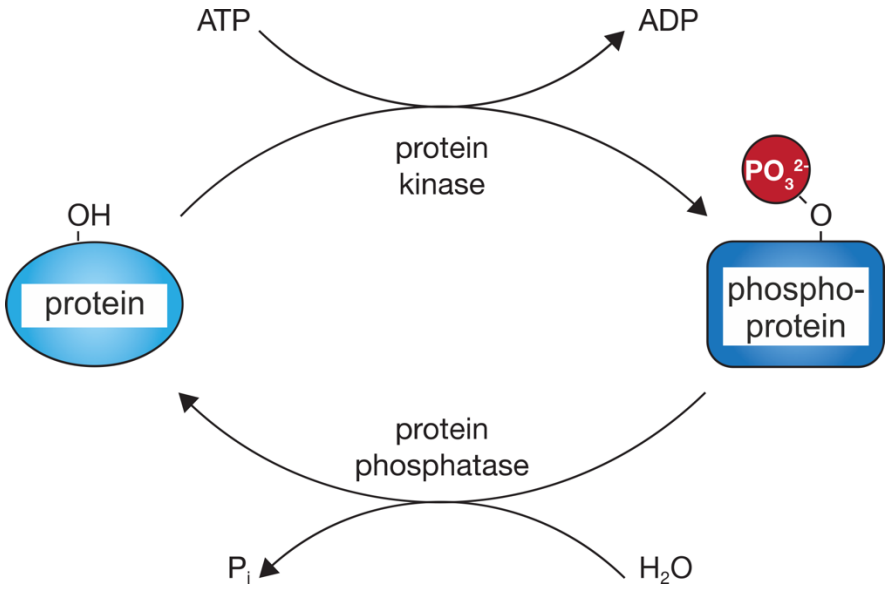

Figure 1.11: Schematic overview of kinase-mediated O-phosphorylation and phosphatase-dependent dephosphorylation. A phosphate group is added to the hydroxyl-groups of the amino acids serine, threonine, or tyrosine by transfer of a phosphate group from ATP, catalyzed by protein kinases. Thereby the respective amino acid of the respective protein is modified, and ADP is released. The reverse reaction i.e., the removal of the phosphate group is mediated by protein phosphatases and leads to the release of the dephosphorylated protein and an inorganic phosphate group (P_i) (modified from Lena Reimann, 2016).

Of the 20 known essential amino acids, nine can be modified with a phosphate group (PO_4^{3-}) via the four following mechanisms. The N-phosphorylation, acylphosphorylation, S-phosphorylation, and O-phosphorylation. The latter represents the most crucial phosphorylation mechanism in eukaryotes (Lottspeich and Engels, 2005).

In a previous publication, murine Synpo2 was shown to be phosphorylated by protein kinase A (PKA) and calmodulin-dependent kinase II (CaMKII). These phosphorylations were purported to regulate the interaction of Synpo2 with 14-3-3 proteins, which has the capability to bind to a huge number of kinases, phosphatases, and transmembrane proteins (Faul *et al.*, 2007), however the phosphorylation sites are not conserved between mouse and man. Therefore, further attempts were made in this work to characterize specific phosphorylations of Synpo2. Database searches using *Phosphonet* (**http://www.phosphonet.ca/default.aspx**) predicted 138 potential phosphorylation sites for the Synpo2b isoform in human. Moreover, the research group of Bettina Warscheid (University of Freiburg/ University of Würzburg) experimentally identified several phosphorylation sites in numerous Z-disc-associated proteins, including filamin C, the co-chaperone BAG3 and the podin protein family members by performing phosphoproteomic studies (Reimann *et al.*, 2017 and unpublished data, Figure 1.12).

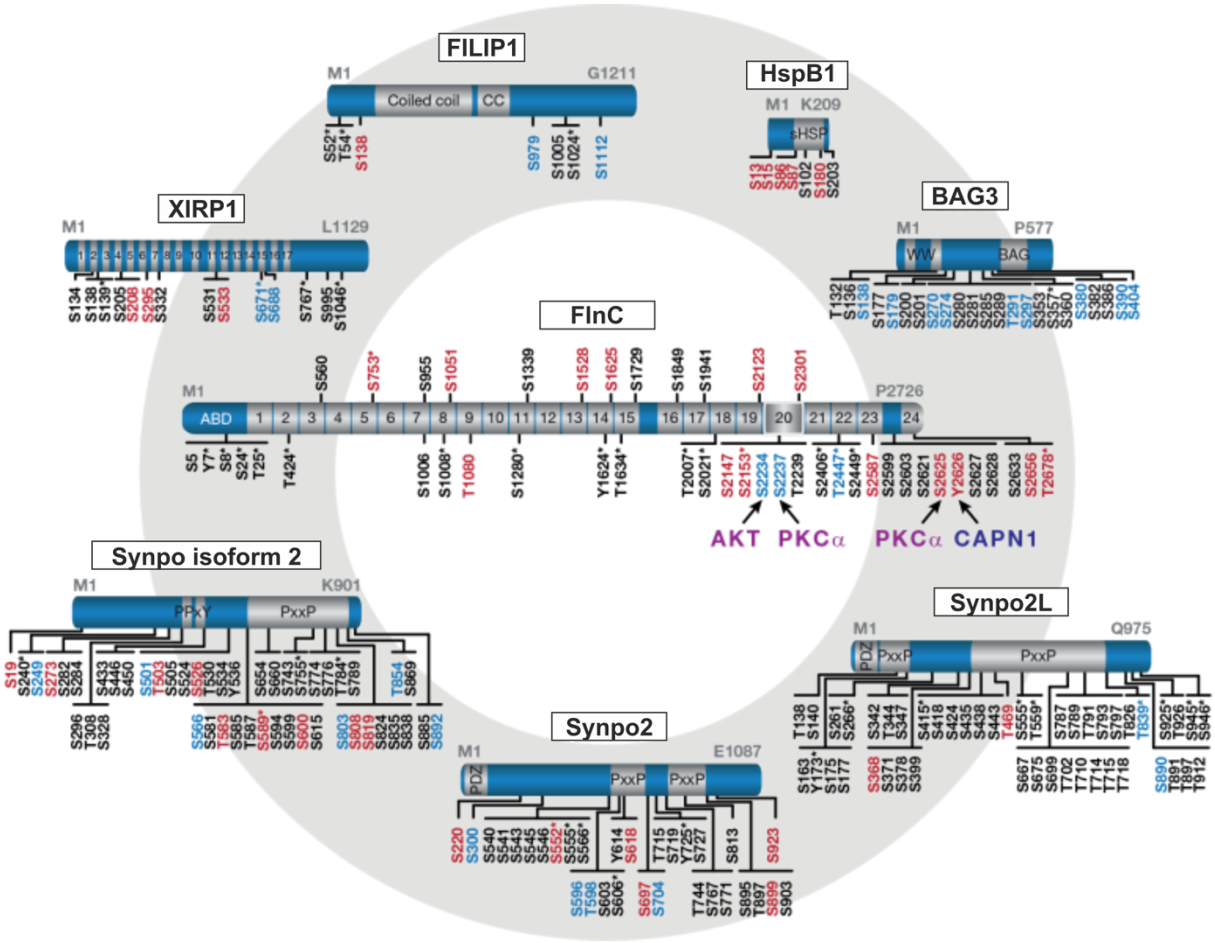

Figure 1.12: Schematic overview of highly phosphorylated Z-disc-associated proteins. Shown are the molecular layouts of the proteins indicated. Filamin C Ig-like domains and Xin actin-binding domains in XIRP1 are numbered, and important binding motifs highlighted. The phosphosites in the murine proteins, known from the PhosphoSitePlus database, are indicated in black, the phosphosites known by the similarity to orthologues sites in human are shown in blue, and the recently identified sites in red. (Modified from Reimann *et al.*, 2017)

The Warscheid lab has so far performed three phosphoproteome studies in cultured C2C12 cells: (1) differential global phosphoproteomics of differentiated versus immature myotubes (Reimann *et al.*, 2017), (2) PI3K/Akt signaling in contracting skeletal muscle cells (Reimann *et al.*, 2020), and (3) phosphoproteome changes induced by enhanced mechanical stress in myotubes (unpublished work). In all three investigations Synpo2 showed a large number of phosphosites, which were either up- or downregulated, with the most interesting ones being regulated by mechanical activity (see Table 1.1). These findings demanded analyzing potential effects of these phosphorylations on the properties and function of Synpo2 (see Aims and Results of this work).

Table 1.1: Overview of selected Synpo2 phosphosites. The positions of the respective amino acid residues in the mouse and human Synpo2b and Synpo2e isoforms are given. Arrows indicate up- or downregulation upon EPS experiment.

Synpo2b			Synpo2e		
mouse	**human**	**upon EPS**	**mouse**	**human**	**upon EPS**
Ser220	Ser226	↓			
Ser300	Ser310	↑			
Ser596 Thr598	Ser604 Thr606	↑	Ser211 Thr213	Ser209 Thr211	↑
Ser697	Ser705	↓	Ser312	Ser310	↓
Ser704	Ser712	↑	S319	Ser317	↑
Tyr725 Ser727	Tyr735 Ser737	LIR ↑	Tyr340 Ser342	Tyr340 Ser342	LIR ↑
Ser895 Ser899 Ser903	Ser902 Ser906 Ser910	↓	Ser510 Ser514 Ser518	Ser507 Ser511 Ser515	↓
Ser923	Ser930	↓	Ser538	Ser535	↓

1.9 Calcineurin regulation

A phosphatase that was shown to be involved in the dephosphorylation of Synpo2 is the serine/threonine phosphatase calcineurin (Faul *et al.*, 2007). Calcineurin forms a heterodimer composed of a catalytic subunit (CnA) and a regulatory subunit (CnB). The activity of the latter is regulated by calcium-dependent binding to calmodulin (reviewed in Parra and Rothermel, 2017). Three different genes encode CnA in mammals (α, β, and γ) (Klee *et al.*, 1998; Rusnak and Mertz, 2000; Hogan *et al.*, 2005), which consists of an N-terminal catalytic-, a CnB-binding, a calmodulin-binding, and a C-terminal autoinhibitory domain (AID) (Taigen *et al*., 2000; Haq *et al.*, 2001; Oka *et al.*, 2005). In addition to these 3 variants a truncation of CnA to remove AID results in a constitutively active phosphatase (CnA*) which is no longer calcium/calmodulin-dependent (reviewed in Parra and Rothermel, 2017). The CnB regulatory

subunit is encoded by two genes and contains four EF-hand calcium-binding sites with different calcium binding affinities (Kakalis *et al.*, 1995; Dolmetsch *et al.*, 1997; Molkentin *et al.*, 1998).

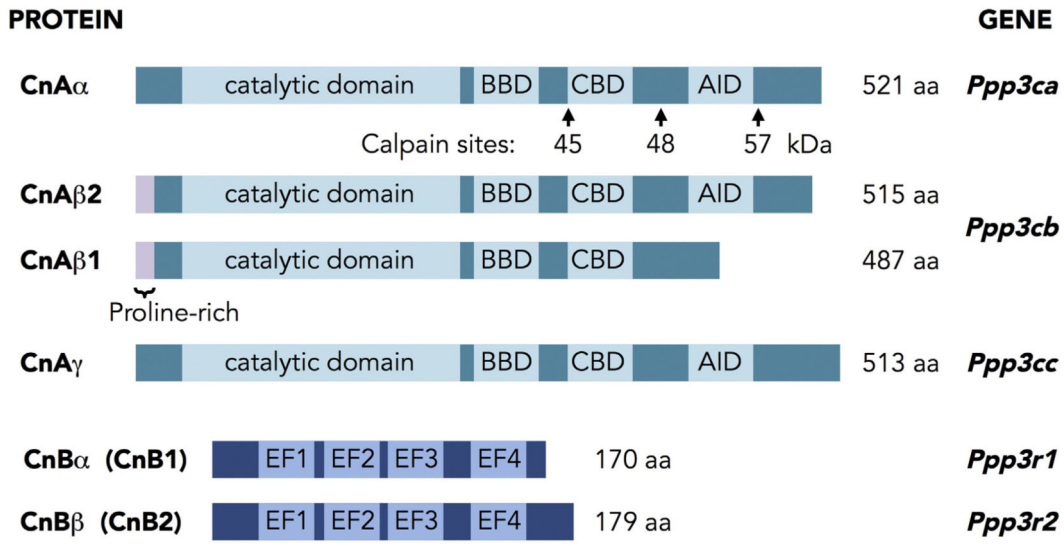

Figure 1.13: Schematic overview of calcineurin proteins and genes. CnA is encoded by three genes (Ppp3ca, Ppp3cb, Ppp3cc) in mammals (α, β, and γ) is composed of a catalytic-, a regulatory- and an autoinhibitory domain. The CnAβ has a proline-rich region at the N-terminus. A truncated CnAβ variant lacking the AID domain results in a calcium/calmodulin independent constitutively active phosphatase. CnB contains 4 EF-hands and is encoded by two genes (Ppp3r1, Ppp3r2) (Parra and Rothermel, 2017).

Due to an increase in calcium concentration calcineurin and calmodulin, a calcium-sensing protein, bind to calcium. After binding calcium, calmodulin binds to calcineurin via the calmodulin-binding site in CnA and this complex displays an active state of the phosphatase (Aramburu *et al.*, 2000). Calcineurin was shown to be a key factor regulating the activity of several transcription factors, such as NFAT (Hogan *et al.*, 2005; Liu *et al.*, 2009; Li *et al.*, 2011), FOXO (Tremblay and Giguère, 2008; Lapierre *et al.*, 2015), and MEF2 (Sakuma *et al.*, 2010; Dewenter *et al.*, 2017; Parra and Rothermel, 2017). These transcription factors, in turn, activate transcriptional programs involved in (among others) T-cell activation (Hogan *et al.*, 2005), cardiac function, or autophagy (Sakuma *et al.*, 2010; Dewenter *et al.*, 2017; Parra and Rothermel, 2017).

An interesting interaction partner of calcineurin in muscle cells is the protein calsarcin (also known as FATZ or myozenin), which is localized to the Z-discs of skeletal muscle. Calsarcin,

in turn, interacts with α-actinin and thus tethers calcineurin to the sarcomere of cardiac and skeletal muscle (Frey *et al.*, 2000; Faulkner *et al.*, 2002; Takada *et al.*, 2002). The calsarcin protein family consists of 3 members: calsarcin-1 is mainly expressed in slow-twitch fibers of skeletal muscle and in adult heart muscle, whereas calsarcin-2 and calsarcin-3 are found in fast-twitch fibers of skeletal muscle (Frey *et al.*, 2000; Frey *et al.*, 2002). Calsarcin-2 was shown to have an inhibitory role on calcineurin and by inhibiting the phosphatase, calsarcin-2 negatively regulates NFAT activity. As a result, phosphorylated NFAT remains in the cytoplasm and is no longer dephosphorylated and translocated to the nucleus (Frey *et al.*, 2008). The combination of these findings raises the interesting question, whether Synpo2 is only passively regulated by calcineurin, or whether it might be involved in the regulation of calcineurin activity via calsarcin instead.

Figure 1.14: Domain structure of Calsarcin-2. Calsarcin-2 is composed of the calsarcin homology region (CHD) at the N-terminus, which is highly conserved in all isoforms of the calsarcin family and the ABD at the C-terminus (modified from Frey *et al.*, 2008).

1.10 Aims of this study

The sarcomeric Z-disc is assumed to have an essential function as a platform for intracellular signaling processes occurring in response to mechanical stress, which requires special mechanism of protein homeostasis (reviewed by Pyle and Solaro, 2004). In this process Synpo2 has obviously an important role as an adapter protein being engaged in the homeostasis of the actin cross-linking protein filamin C.

This work was focused on the isoforms Synpo2b containing a PDZ-domain and Synpo2e lacking this PDZ-domain, as these variants show the highest expression in skeletal muscle cells (Linnemann, 2010). A first aim was to analyze the specific localization of both isoforms in muscle cells under mechanical stress applied by EPS using C2C12 cells as model system. Transient transfections with fluorescent constructs of Synpo2b and Synpo2e should microscopically reveal their precise subcellular localization. Additionally, using this model system for fluorescence recovery after photobleaching (FRAP) experiments should allow to determine the dynamics and mobility of these isoforms as further features of their specific cellular functions.

In a second approach, the before biochemically shown interaction of the co-chaperone BAG3 with Synpo2 during autophagic processes in the muscle (Ulbricht *et al.*, 2013) should be validated and characterized microscopically on the cellular level under EPS-induced mechanical stress conditions employing bimolecular complementation assays (BiFCs).

A further central goal of this work was to verify recent phosphoproteomic data (B. Warscheid, University of Freiburg/ University of Würzburg, unpublished work) pointing to a possible role of amino acid phosphorylations/dephosphorylations in regulating Synpo2 isoforms in muscle cells under mechanical stress. Therefore, phosphomimetic constructs of relevant phosphosites should be generated by mutagenesis to determine the influence of force-dependent (de)phosphorylation on protein-protein interactions biochemically by co-immunoprecipitation (co-IP) assays. Moreover, fluorescent constructs of the mutated Synpo2 isoforms should be expressed in cultivated muscle cells to allow microscopical analysis of the impact of reversible phosphorylation on their cellular localization, as well as on their dynamics and mobility performing FRAP experiments.

2.0 Materials and Methods

2.1 Materials

2.1.1 Chemicals

The origin of utilized chemicals, consumables, kits, and enzymes is indicated in the corresponding sections. Restriction enzymes were sourced from Thermo Scientific (Karlsruhe, Germany) and New England Biolabs Inc. (Massachusetts, USA), the fine chemicals for electrophoresis from Biorad (Munich, Germany), oligonucleotides from TIB-Molbiol (Berlin, Germany) or Invitrogen, cell culture media, and additions, if not described differently from Gibco/Invitrogen (Karlsruhe, Germany) and further consumable supplies were from Sigma-Aldrich (Taufenkirchen, Germany).

2.1.2 Culture Medium

Table 2.1: Composition of culture media. The utilized masses refer to a final volume of 1l.

Name	Composition
LB-medium	10 g tryptone, 5 g yeast extract, 10 g NaCl, pH 7.5
SOB-medium	20 g tryptone, 5 g yeast extract, 0.59 g NaCl, 0.19 g KCl, pH 7.0
SOC-medium	5 mM $MgCl_2$, 5 mM $MgSO_4$, 20 mM Glucose in SOB-medium

For preparation of all media ddH_2O was used. Media were sterilized in an autoclave (Systec, Wettenberg, Germany) at 125 °C and 1.4 bar for 20 min. To obtain solid media, 1.5 % agar was added.

2.1.3 Antibiotics

Antibiotics were added to the autoclaved culture medium immediately before the use.

Table 2.2: Final concentration of antibiotics used in culture medium.

Antibiotic	Final concentration
carbenicillin	100 µg/ml
chloramphenicol	34 µg/ml
kanamycin	50 µg/ml

2.1.4 Bacteria Strain

2.1.4.1 Cloning

The following bacterial strain was used for routine cloning of defined cDNAs:
E. coli JM109 (Stratagene Co, Heidelberg, Germany)
Genotype: e14- (McrA-) recA1 endA1 gyrA96 thi-1hsdR17 (r-k m+k) supE44 relA1 Δ (lacproAB) [F' traD36 proAB lacIqZΔM15]

2.1.4.2 Protein Expression

For routine recombinant protein expression of defined cDNA, the following bacterial strain was used:
E. coli BL21(DE3)CodonPlus(DE3)-RP (Stratagene Co, Heidelberg, Germany)
Genotype: B F^- ompT hsdS(r^-_B m^-_B) dcm^+ Tet^r gal λ(DE3) endA Hte [argU proL Cam^r]

2.1.5 Plasmids

All utilized plasmids were derivatives of commercially available vectors with modified multiple cloning sites, promotors, or fusion proteins. The sources of the plasmids and the modification made are depicted below. The corresponding vector maps of the relevant plasmids are included in the appendix. The pET23aEEF and pET23aT7 plasmids had a carbenicillin resistance cassette, and all the remaining vectors contained a kanamycin resistance cassette. By replacing the existing cloning cassette of the original vectors, suitable restriction sites (MluI or BamHI, EcoRI and SalI or XhoI) became available.

Table 2.3: Application and features of used plasmids.

Plasmid	Application and features	origin
pET23aEEF	procaryotic expression, His and EEF-*Tag*	modified pET23a, Novagen
pET23aT7	procaryotic expression, His and T7-*Tag*	modified pET23a, Novagen
pEGFPC2 Pd	eukaryotic expression, EGFP-*Tag*	modified pEGFP-C2, Clontech
Venus2-C	eukaryotic expression, EYFP-*Tag* (AS 155-238)	modified pECFP-C1, Clontech
Venus CT	eukaryotic expression, EYFP-*Tag*	modified pECFP-C1, Clontech
Venus1-N3	eukaryotic expression, EYFP-*Tag* (AS 1-154)	modified pECFP-N1, Clontech
Venus NT	eukaryotic expression, EYFP-*Tag*	modified pECFP-N1, Clontech

2.1.6 Antibodies

Table 2.4 lists the primary antibodies used in this work. The utilized secondary antibodies, horseradish peroxidase conjugates (HRPO) for Western blots (WB), fluorescent dye conjugated for Western blots (WB), and immunofluorescence staining (IF) are listed in table 2.5.

Table 2.4: Primary antibodies

Name	Epitope	Type	WB	IF	origin
BAG3	BAG3	rabbit	1:2500	-	Proteintech
GAPDH	GAPDH	mouse IgG1	1:10000	-	Calbiochem
GST	GST-tag	rabbit	1:10000	-	Proteintech
HH9	Synpo2	mouse IgG1	1:1	-	Linnemann *et al.,* 2010
HspB7	heat-shock protein beta-7	rabbit	1:700	-	Proteintech
HspB8	heat-shock protein beta-8	rabbit	1:1000	-	Proteintech
LC3BII	LC3BII	rabbit	1:800	-	Novus
p62	p62/SQSTM1	guinea pig	1:1000	-	Progen
T7	T7-tag	mouse IgG2b	1:10000	-	Novagen
T12	titin	mouse IgG1	-	1:20	Fürst *et al.* 1988
YL1/2	EEF-tag, tubulin	rat IgG2a	1:700	-	Invitrogen

Table 2.5: Secondary antibodies

Name	donor	epitope	conjugate	dilution	origin
GAM IgG1 Alexa594	goat	mouse IgG1	Alexa 594	1:300	Jackson
GAM IgA488	goat	Mouse IgA	Alexa 488	1:200	SBA 1040-31
GAM-PO	goat	mouse IgG	HRPO	1:10000	Jackson
GARat-PO	goat	rat	HRPO	1:10000	Jackson
GAR-PO	goat	rabbit	HRPO	1:10000	Jackson
GAM IRdye800CW	goat	mouse IgG	IRDye800	1:10000	LI-COR
GARat IRdye800 CW	goat	rat	IRDye800	1:10000	LI-COR
GAR IRdye800 CW	goat	rabbit	IRDye800	1:10000	LI-COR

2.2 Molecular Biological Methods

2.2.1 Polymerase chain reaction

To amplify DNA fragments out of an existing plasmid DNA or cDNA polymerase chain reaction (PCR) (Mullis *et al.*, 1992) was used. The fragments for cloning were produced using the Pfu-polymerase to minimize errors during amplification. In addition, the ready to use Taq-DNA-polymerase system *Firepol* (Solis Biodyne, Tartu, Estonia) was utilized, and the reaction was optimized according to the length and the GC-content of the template DNA and manufacturer instructions (Table 2.6).

Table 2.6: Composition of a PCR reaction

Component	**Concentration**
Template DNA	10 - 100ng
dNTPs	200 µM each (Fermentas)
sense Primer	0.4 µM (TIB Molbiol, Invitrogen)
antisense Primer	0.4 µM (TIB Molbiol, Invitrogen)
$MgCl_2$	1.5 - 6 mM (Fermentas)
Buffer	1x (provided with polymerase)
DNA polymerase	0.05 U/µl
ddH_2O	added to 20 - 50 µl

The cycles were performed in a thermocycler (Biometra, Göttingen, Germany). The temperature settings of a PCR are shown in Table 2.7. The PCR product was analyzed by agarose gel electrophoresis (see 2.2.2) and purified using the PCR clean up and gel extraction Kit (Machery-Nagel, Düren, Germany).

Table 2.7: Temperature profile of PCR

Cycle Step	Temperature	Time	No. of Cycles
Initial Denaturation	95 °C	5 min	1
Denaturation	95 °C	30 s	
Annealing	58 - 65 °C	30 s	30
Elongation	72 °C	30 s/kb	
Final Elongation	72 °C	5 min	1

2.2.2 Agarose Gel Electrophoresis

Agarose gel electrophoresis served as a method for separation of DNA fragments according to their size. For this purpose, agarose was solved in TAE buffer (40 mM Tris-Acetate, 1 mM EDTA, pH 8.3) by heating. In order to get a proper segregation of DNA fragments, the concentration of the agarose (0.6 % to 2 % (w/v) agarose) had to be adjusted depending on the size of the expected fragment. 1 µg/ml ethidiumbromide was added to the agarose gel, which intercalated with the double-stranded DNA. Via fluorescence stimulation using UV light, the DNA fragments separated by size can be detected. Before loading, 1 x loading buffer (6 x MassRuler DNA Loading Dye, Thermo Scientific, Karlsruhe, Germany) was added to all samples. Based on the marker (100 bp or 1 kb DNA ladder ready to load, Solis BioDyne, Tartu, Estland), which contained DNA fragments of defined length, the size of the analyzed DNA fragments could be approximately determined. The loaded samples were separated by using 80 to 100 V in TAE buffer. Thereafter the DNA fragments were detected through the exposure of the gel to UV light with the gel documentation system (GelDoc 2000, BioRad). The images were exported using Quantity One Software (Version 4.6).

2.2.3 DNA Extraction and Purification from Agarose Gel

For preparative methods DNA fragments separated by size were visualized by UV light exposure. The corresponding band was then cut out of the gel using a scalpel. Subsequently, the DNA was purified using the NucleoSpin® Gel and PCR Clean-up Kit (Machery-Nagel, Düren, Germany) according to the manufacturer's information.

2.2.4 Restriction Digest of DNA

Restriction endonuclease are enzymes which bind to specific sequences of the DNA. The DNA fragments were cut by double digest and cloned into vectors which were cut with the same restriction enzymes before. For the double digest the buffers recommended by the provider (Thermo Scientific, Karlsruhe, Germany) were used.

2.2.4.1 Analytical Restriction Digest

In order to check whether a cloning process was successful and to check for the quality of DNA an analytical restriction digest was performed. For this purpose, a 10 µl mixture containing 0.2 µg DNA, 1 U of each restriction enzyme, respective amount of buffer and ddH_2O to reach the end volume, was produced. The mixture was incubated in an incubator at 37 °C for 1 to 2 h or overnight. Further on for analysis the digested mixture was loaded on an agarose gel and the fragments were separated by size.

2.2.4.2 Preparative Restriction Digest

The preparative restriction digest is performed to produce cut DNA which is further used for cloning. For this 1 to 5 µg DNA was used with 2 U of each restriction enzyme per 1 µg of DNA with an appropriate amount of buffer (Thermo Scientific, Karlsruhe, Germany) and ddH_2O with an end volume of 20 µl. The mixture was incubated at 37 °C overnight. Thereafter, loading buffer (6 x MassRuler DNA Loading Dye, Thermo Scientific, Karlsruhe, Germany) was added to the digested mixture and entire sample was loaded on an agarose gel (see 2.2.2).

2.2.5 Ligation

During the ligation the DNA fragments were linked with cut vectors via their particular cohesive ends. This reaction was catalyzed by a T4-DNA-Ligase (Thermo Scientific, Karlsruhe, Germany) in an ATP dependent reaction. One ligation mixture contained approximately 50 ng

vector-DNA with a threefold molar excess of the insert-DNA and 1 U T4-DNA ligase in ligation buffer (Thermo Scientific, Karlsruhe, Germany). In order to reach an end volume of 10 µl ddH_2O was added. The total ligation mixture was incubated at 16 °C overnight and afterwards used for the transformation of chemically competent bacteria.

2.2.5.1 Dephosphorylation

Sticky 5' overhang end or blunt-end vector DNA was efficiently dephosphorylated with the *Rapid DNA Dephos & Ligation Kit* (Thermo Scientific, Karlsruhe, Germany). Therefore, 1 U rAPid Alkaline Phosphatase, rAPid Alkaline Phosphatase buffer, vector DNA and ddH_2O to reach an end volume of 20 µl were incubated for 30 min at 37 °C. Then the rAPid Alkaline Phosphatase was inactivated at 75 °C for 2 min. The dephosphorylated reaction mixture was further used for ligation (see 2.2.5).

2.2.6 Production of chemical competent *E. coli*

The competent bacterial cells for transformation of plasmid DNA were produced as described in Inoue *et al.* (Inoue *et al*., 1990). The bacterial strains were taken from glycerol stocks stored in -80 °C.

The transfection efficiency was obtained by transformation of the competent bacterial cells with either 100 pg, 10 pg or 1 pg of plasmid DNA. After an overnight incubation, the colonies were counted. 100 colonies per 10 pg plasmid DNA correlated with 10^7 colonies/µg plasmid DNA.

2.2.7 Transformation of competent *E. coli*

Using heat shock transformation, the plasmid DNA can be introduced to competent bacteria cells. Therefore, the competent *E. coli* strain stored at -80 °C, was thawed on ice for 20 min. For transformation of 100 µl competent bacteria cells, 30 to 500 ng plasmid DNA or 10 µl of ligation mixture was added to the cells, carefully mixed, and then incubated on ice for 30 min. Further on the cells were exposed to a heat shock at 42 °C for 60 s and then again incubated on ice for 2 min. After adding 200 µl of LB medium/SOC medium the cells were incubated on a shaker at 37 °C for 1 h. Then the entire bacteria suspension was plated on a LB agar plate which contained the relevant antibiotics for a successful selection of transformed bacteria cells. On the following day the colonies were picked, and overnight cultures (5 ml LB medium +

antibiotics) were inoculated to check the clones. The positive clones were stored as glycerol stocks at -80 °C (see 2.2.8).

2.2.8 Preparation of Glycerol stocks

In order to store the successfully cloned constructs in transformed bacteria, glycerol stocks were produced. Therefore 820 µl of the overnight culture and 180 µl of pure glycerin were properly mixed in a cryovessel (TPP, Trasadingen, Schweiz) and then stored at -80 °C.

2.2.9 DNA Plasmid Preparation

To perform a mini plasmid preparation 4 ml LB medium with the appropriate antibiotics was inoculated with one single colony of the selection plate and cultivated overnight at 37 °C. In order to purify the DNA with a high purity the NucleoSpin® Plasmid Mini Kit (Machery-Nagel, Düren, Germany) was used according to the manufacturer's information. The purification of high amounts of DNA with a very high purity was performed by using the NucleoBond® Xtra Midi Kit (Machery-Nagel, Düren, Germany) pursuant to the manufacturer's information. The purified DNA was solved in Tris/HCL buffer (10 mM, pH 8). Thereafter the purity as well as the concentration of the DNA were defined using spectrophotometry.

2.2.10 Spectral Concentration Measurement of DNA

The level of purity and the concentration of the DNA was observed using a Cary 50 Scan UV-Vis spectral photometer (Varian, Darmstadt, Germany). For measurements the samples were diluted 1:1000 in Tris/HCL buffer (10 mM, pH 8) and added into a quartz cuvette (1 cm thickness, Hellma, Mühlheim, Germany). An undiluted Tris/HCL buffer (10 mM, pH 8) was used as a reference and the extinction was measured by the spectral photometer. The extinction from 1 to 260 nm corresponds to a double-stranded DNA concentration of 50 µg/ml. Since proteins have an absorption maximum of 280 nm the ratio of the OD260/OD280 gives information about the rate of purity, which should be around 1.8 for double-stranded DNA. A value under 1.8 indicates an impurity of the DNA through UV absorbing substances like proteins and phenols. The value of the OD260/OD230 ratio describes the impurity by RNA. The absorbance value of 320 nm should be 0 since it describes whether the DNA solution contains particular ingredients.

2.3 Protein Biochemical and Biophysical Methods

2.3.1 Expression of recombinant protein in *E. coli*

Recombinant proteins were expressed in *E. coli* using either the pET expression system (Novagen, EMD Millipore, Darmstadt, Germany) or the GST gene fusion system (GE Healthcare, Solingen, Germany). Expression was performed under the control of the T7 promoter and induced by the addition of Isopropyl-β-D-1-thiogalactopyranoside (IPTG).

2.3.1.1 Small scale protein expression

To perform the mini expression analysis, precultures were inoculated with pET or pDEST plasmid transformed bacteria of the *E. coli* BL21 codon plus strain (single colonies). 4 ml of fresh LB medium, mixed with the antibiotics carbenicillin and chloramphenicol, were mixed with 1 ml of the overnight preculture and incubated for 1 h at 37 °C in a shaker. A pre-induction sample (1 ml) was taken from the culture and protein expression was induced by adding of IPTG followed by an incubation for 3 h at 37 °C in a shaker. Afterwards, a post-induction positive sample (1 ml) was taken and centrifuged alongside with the pre-induction negative sample in a microcentrifuge for 5 min at 5000 rpm. Cell pellets were dissolved in 100 µl of 2 x concentrated SDS sample buffer (2 mM EDTA, 12 % glycerol, 24 mM Tris/HCl, 6 % SDS, 3 % β-mercaptoethanol, 0.04 % bromophenol blue, pH 6.8). The samples were heated at 95 °C for 5 min, sonicated (Ultrasonic Processor UP100H, Hielscher, Teltow, Germany) and tested for successful expression of the protein using SDS-polyacrylamide gel electrophoresis (see 2.3.5). Clones showing a successful expression were stored as glycerol stocks at -80 °C (see 2.2.8).

2.3.1.2 Large scale protein expression

For preparative protein expression, 200 ml of fresh LB medium, mixed with the antibiotics carbenicillin and chloramphenicol, were inoculated with 3 ml of preculture. The culture was incubated in a shaker at 37 °C until an absorbance of 0.6 to 0.8 optical density (OD) at 600 nm could be measured (BioPhotometer plus, Eppendorf, Hamburg, Germany). The expression was induced by adding 0.5 mM IPTG to the culture. The protein was expressed for 3 h at 18 °C with constant shaking. Subsequently, the culture was pelleted in a refrigerated centrifuge (Allegra

X-15R, Beckmann Coulter, Krefeld, Germany) at 4 °C by a 15 min centrifugation step at 4500 rpm. The supernatant was discarded, while the pellet was stored at -20 °C.

2.3.2 Purification of recombinant protein

The expressed proteins contained an additional hexahistidine (His_6)-tag, which enabled their purification using immobilized metal affinity chromatography. The usage of the nitrilotriacetate acid (NTA) chelator, which partially complexes divalent ions, a chelator/ His_6-tag complex can be formed. The NTA complexes four nickel ion binding sites and leaves two unoccupied for histidine binding. The fusion protein can be reversibly bound to the Ni-NTA agarose by this complex.

The bacterial pellet stored at -20 °C (see 2.3.1.2) was thawed on ice for 15 min to purify the protein. Afterwards, the pellet was resuspended in 4 ml lysis buffer (50 mM NaH_2PO_4, 300 mM NaCl, 10 mM imidazole, 1 mg/ml lysozyme, pH 8.0, 4 °C) and lysed on ice for 30 min. The lysate was sonicated (Ultrasonic Processor UP100H, Hielscher, Teltow, Germany) 10 times for 10 s and centrifuged at 4500 rpm at 4 °C for 30 min (Labofuge 400R, Heraus, Thermo Fisher Scientific, Karlsruhe, Germany) to separate the cell debris and soluble proteins. The supernatant was transferred to 500 µl of previously in lysis buffer washed Ni-NTA-agarose and incubated for 1 to 2h at 4 °C on a rotating wheel. In the following the Ni-NTA-agarose-protein mixture was centrifuged for 1 min at 1500 rpm and 4 °C and subsequently the supernatant with the unbound proteins was discarded. The Ni-NTA agarose with the bound proteins was washed three times with 5 ml wash buffer (50 mM NaH_2PO_4, 300 mM NaCl, 20 mM imidazole, pH 8.0, 4°C). Subsequently, the supernatant was removed down to 1 ml, the Ni-NTA agarose with the bound protein was resuspended in this volume and transferred to an empty column (mini columns, Sigma-Aldrich) equilibrated previously with lysis buffer. Finally, the protein was eluted from the column by adding 500 µl of elution buffer (50 mM NaH_2PO_4, 300 mM NaCl, 250 mM imidazole, pH8.0) three times in a row. To test the protein content in a rapid test, 1 µl of each eluate was applied to a nitrocellulose membrane (Whatman, GE Healthcare, Solingen, Germany) and stained with Ponceau red (0.1 % (w/v), 3 % (w/v) Trichloroacetic acid). The purity of the protein purification was determined using an SDS-polyacrylamide gel, followed by Coomassie staining (0.1 % (w/v) Coomassie Brilliant Blue G-250 (Thermo Fisher Scientific, Karlsruhe, Germany), 50 % (v/v) methanol, 20 % (v/v) acetic acid) analysis.

2.3.3 Protein quantification via Bradford Assay

To determine the concentration of the purified proteins, Bradford assay (Bradford, 1976) was performed using the Protein Assay Kit (Biorad, Munich, Germany) according to the instructions of the manufacturer. Therefore, the proteins were diluted in PBS (137 mM NaCl, 3 mM KCl, 8 mM NaH_2PO_4, 1.5 mM KH_2PO_4, pH 7.3) and the calorimetric reaction was started by adding the Bradford reagent (Biorad, Munich, Germany). The reagent forms a colored complex with the protein which can be absorbed at 595 nm. The complex formation proceeds linearly with increasing protein concentration. After 5 min of incubation at RT, the extinction at 595 nm was measured in an ELISA reader (Elx800, BioTek, Bad Friedrichshall, Germany). A dilution series of bovine γ-globulin in PBS (0 - 200 µg/ml) served as the calibration standard. The linear regression was calculated using the extinction values of the calibration standard in an Excel spreadsheet (Microsoft). The concentration was calculated by substituting the variable for the absorbance with the measured value of the protein dilution in the resulting linear equation. A triplicate determination was performed to minimize pipetting errors.

2.3.4 Production of cell extracts

Cultured cells were washed twice with cold PBS containing Mg^{2+} and Ca^{2+} (DPBS, Gibco, Carlsbad, USA). After adding 100 µl of prewarmed 5 x SDS sample buffer the cells were detached from the culture dish (ø 10 cm, TPP, Trasadingen, Switzerland /ø 10 cm, Sarstedt, Nümbrecht, Germany) using a cell scraper (Sarstedt, Nümbrecht, Germany). The cell lysates were incubated for 5 min at 95 °C and sonicated (UP100, Hielscher). Insoluble components were pelleted by centrifugation at 13000 rpm for 15 min (Biofuge pico, Heraeus) and the supernatant was transferred to a new micro reaction vessel. The lysates were stored at -20 °C until further use.

2.3.5 SDS polyacrylamide gel electrophoresis (SDS-PAGE)

Proteins were separated according to their molecular weight in a *SE250 Mighty Small II MINI Vertical Electrophoresis Unit* (Höfer, Holliston, USA) as described by Laemmli (1970). The discontinuous gel contained a separation gel and a stacking gel.

First, the separation gels of different pore sizes due to varying acrylamide concentrations were poured (6 -12 % (v/v) acrylamide/bisacrylamide (37.5:1), 1,5 M Tris-HCl, pH 8.8, 0.8 % (w/v)

sodium dodecyl sulfate (SDS), 0.083 % (v/v) ammonium persulfate (APS), 0,1 % (v/v) tetramethylethylenediamine (TEMED)). This was followed by the stacking gel (4 % (v/v) acrylamide/bisacrylamide (19:1), 0.5 M Tris-HCl, pH 6.8, 0.8 % (w/v) SDS, 0.45 % (v/v) APS, 0.3 % TEMED). The respective samples were mixed with SDS sample buffer (5 mM EDTA, 30 % glycerol, 60 mM Tris-HCl, 15 % SDS, 7.5 % β-ME, 0.1 % bromophenol blue, pH 6.8) and heated for 5 min on a thermomixer at 95 °C. The samples were loaded on the gel and a constant voltage was used for electrophoresis (80 V stacking gel, 120 V separation gel) in electrophoresis buffer (25 mM Tris, 250 mM glycine, 0.1 % (w/v) SDS, pH 8.8). After that, gels were either stained with Coomassie Blue solution (0.1 % (w/v) Coomassie Brilliant Blue G-250 (Thermo Fisher Scientific, Karlsruhe, Germany), 50 % (v/v) methanol, 20 % (v/v) acetic acid) or further processed for immunoblots (see 2.3.6).

2.3.6 Protein transfer

For the application of antibody-based detection methods the proteins separated using SDS-PAGE (see 2.3.5), were transferred from the gel to a nitrocellulose membrane (Whatman, GE Healthcare, Solingen, Germany).

2.3.6.1 Semidry Western blot

For the protein transfer using the semidry method (Towbin *et al*., 1979), filter papers soaked in transfer buffer (20 % methanol in electrophoresis buffer) were placed on the electrodes. The gel was placed on this, coated with the membrane, and again covered with filter paper. The proteins were transferred for 70 to 90 min at 1 mA per cm^2 gel. The efficiency of the transfer was checked by staining with Ponceau red (0.1 % (w/v) Ponceau red, 3 % (w/v) Trichloroacetic acid).

2.3.6.2 Tankblot transfer

The tankblot transfer method was used for more efficient transfer of proteins with a high molecular mass. For this purpose, the polyacrylamide gel was equilibrated in transfer buffer (25 mM Tris-Base, 192 mM glycine, 20 % (v/v) methanol, 0.01 % SDS), placed on a nitrocellulose membrane and, as previously described for the semidry transfer process (see 2.3.5.1) arranged between filter papers soaked in transfer buffer. The entire setup was held together by a blotting cassette and transferred to a blotting chamber (Höfer, Holliston, USA) filled with transfer

buffer. The transfer was performed overnight at a constant current of 250 mA at 4 °C and was then verified by Ponceau red staining of the membrane.

2.3.7 Immunodetection

First, the nitrocellulose membrane was incubated in blocking buffer (4 % (w/v) skimmed milk powder dissolved in TBST (50 mM, Tris-HCl (pH 7.9), 150 mM NaCl, 0.05 % (w/v) Tween-20) to prevent non-specific antibody binding. Thereafter the membrane was incubated with the primary antibody (see table 2.4) for 1 h at RT, followed by three washes for 5 to 10 min each with TBST. The membrane was then incubated with horseradish peroxidase (HPR)-coupled secondary antibody diluted in TBST for 1 h at RT. After three washes in TBST, the HRP-conjugated secondary antibodies were analyzed by chemiluminescence (enhanced chemiluminescence, ECL). For this purpose, the membrane was incubated with the SuperSignal West Pico chemiluminescence substrate (Thermo Fisher Scientific, Karlsruhe, Germany) for 5 min and enclosed with a film after the incubation time had expired. The membrane was placed in a light-tight film cassette (Sigma-Aldrich) overlayed with an X-ray film (Fujifilm, Minato, Japan). The exposure time was adjusted to the intensity of the signal. The exposed film was then developed using a developer machine (Curix 60, AGFA, Mortsel, Belgium). Alternatively, after the enclosure with the film the membrane was analyzed using the ChemiDoc (Biorad, Munich, Germany).

To quantify protein amounts, the blot was incubated with secondary antibodies coupled with infrared fluorophore (IRDy® Infrared Dyes), washed as described above with an extra last washing step with ddH_2O and then detected on the Odyssey® Infrared Imaging System (LI-COR) or the Chemidoc System (Biorad, Munich, Germany). The images for the Odyssey® were evaluated using the Odyssey software version 3.0.16 and the Chemidoc images were analyzed with the BioRad software Image Lab version 6.0.1.

2.3.8 Protein Interaction Studies

2.3.8.1 Co-Immunoprecipitation

For co-immunoprecipitation (co-IP) experiments, 1 µM protein with a T7-tag and 15 µM protein with an EEF-tag were isolated in IP buffer (1 % BSA (bovine serum albumin), 0.5 %

Triton X-100, protease inhibitors (Roche mini complete, Roche, Basel, Switzerland) in PBS) and incubated for 1 h at RT with shaking. After the addition of 0.7 µl of a monoclonal antibody which specifically detects the T7-tag, the mixture was incubated for a further 30 min at RT with shaking. Then 20 µl of pre-washed protein G-coupled magnetic beads (Dynabeads Protein G Invitrogen, Life technologies, Carlsbad, USA) were added and the mixture was incubated for 1 h at 4 °C on a rotating wheel. In the following the samples were washed three times with washing buffer (0.05 % Triton X-100 in PBS) in a magnetic stand and the bound proteins were eluted with 20 µl of 2 x SDS sample buffer by incubating the mixture for 5 min at 95 °C. The proteins were separated using SDS-PAGE and transferred to a nitrocellulose membrane. Antibodies specifically directed against the tags were used for the immunodetection. Controls without T7 antibodies and without the T7-tagged protein were carried out in all co-IPs. With these controls the specific precipitation of the protein of interest via the T7-tag were demonstrated and non-specific binding of the interaction partner to the dynabeads were ruled out.

2.3.8.2 Peptide Array

Peptide arrays represent a highly efficient and very accurate method for the identification of a certain binding motif within a full-length protein. Therefore, specific short synthetic peptides consisting of a binding motif of interest were synthesized on a cellulose membrane (Peptides&Elefants, Hennigsdorf, Germany). Further on to investigate the importance of each amino acid of the binding motif of interest each amino acids of the motif were mutated. After blocking the cellulose membranes with blocking buffer (4 % (w/v) skimmed milk powder dissolved in TBST (50 mM, Tris-HCl (pH 7.9), 150 mM NaCl, 0.05 % (w/v) Tween-20) to prevent non-specific binding, peptide interactions with GST or GST fusion proteins of a protein of interest were tested by overlaying the membrane with 1 µg/µl of recombinant protein for 2 h at RT. In this way the binding motif can be verified and furthermore the impact of certain amino acid mutation (e.g., phosphomimic mutation) on the binding of two proteins of interests can be investigated. Afterwards, filters were washed three times in TBST and incubated with HRP-conjugated anti-GST antibodies before analysis by chemiluminescence using the ChemiDoc (Bio-Rad, Munich, Germany).

2.4 Cell biological Methods

2.4.1 Cell Culture

All utilized cells were cultivated in an incubator (Heracell 240i CO_2-Incubator) at 37 °C, 5 % CO_2 and with 100 % relative humidity. The composition of all used culture media is listed in Table 2.8 and Table 2.9. The respective media and solutions were warmed up to 37 °C in a water bath. All steps were performed under a sterile workbench.

2.4.2 Cultivation of C2C12 Cells

The used C2C12 cells originated from a cell line of myoblasts of the skeletal muscles. Originally, they were isolated from the leg musculature of a mouse stem called C3H (Yaffe and Saxel, 1977). In order to cultivate the cells, a 1 ml aliquot of cell which was stored in liquid nitrogen, was thawed at 37 °C in the water bath and then added to 9 ml of preheated medium. After 3 min of centrifugation at 800 rpm (Labofuge 400R, Heraeus) the supernatant was discarded, and the pellet was solved in 1 ml of preheated proliferation medium. This suspension was then added to 9 ml preheated proliferation medium in a 10 cm culture dish (Sarstedt, Nümbrecht, Deutschland). The C2C12 cells were propagated in the nutritious proliferation medium. After reaching a confluency of 80 % the cells were passaged in a 1:10 ratio. For the passaging the cells were washed with 0.5 mM ethylenediaminetetraacetate (EDTA) in 1x CMF PBS (Ca^{2+} and Mg^{2+} free). To detach the cells from the culture dish, 1 ml of 0.25 % trypsin was added. Following the resuspension in fresh preheated culture medium the appropriate number of cell suspension was added to cell culture dishes. After reaching a confluency between 90 to 100 % the nutrient deficient differentiation medium was added to the cells to induce the differentiation.

Table 2.8: Composition of the C2C12 cell culture media

Type of Medium	Composition
Proliferation Medium	DMEM Glutamax (Gibco)
	15 % FCS (Sigma)
	1 % Pen/Strep
	1 % NEAA
Differentiation Medium	DMEM Glutamax (Gibco)
	2 % Horse serum
	1 % Pen/Strep
	1 % NEAA

2.4.3 Cultivation of IMM cells

Immortalized mouse myoblasts (IMM) were isolated and cultured as described previously (Winter *et al.*, 2014). The IMM were propagated in nutrient-rich proliferation medium on collagen-coated (Bornstein and Traub Type I, 0.1 mg/ml, Sigma-Aldrich) cell culture dishes and passaged at a ratio of 1:3 every two days after reaching 90 % confluency. Cells were detached as already described for the C2C12 cells, but with 3 ml of 0.05 % trypsin (Gibco in PBS). After adding 7 ml of fresh culture medium, the cells were transferred to a 15 ml centrifuge tube with a conical bottom and pelleted by centrifugation for 3 min at 800 rpm. The pellet was resuspended in fresh proliferation medium. Further on the cell suspension was then transferred to an uncoated culture dish and incubated for 60 to 120 min under the previously described conditions to remove contaminating fibroblasts (pre-plating). Subsequently, the IMM cells were transferred to a collagen-coated culture dish and cultivated. Depending on the aim of the experiments the cells were stimulated to differentiate by changing to nutrient-poor differentiation medium at a confluency of 90 to 100 %. The differentiation medium was changed every second day. For the examination under the microscope, the cells were placed on laminin-coated coverslips (2.5 µg/cm^2, Sigma-Aldrich).

Table 2.9: Composition of the IMM cell culture media

Type of Medium	Composition
Proliferation Medium	HAM´s F-10 Nutrient Mix (Gibco)
	20 % FCS (Sigma)
	1 % Pen/Strep
	2,5 ng/ml rhFGF-b
Differentiation Medium	DMEM Glutamax (Gibco)
	5 % Horse serum (Gibco)
	1 % Pen/Strep (Gibco)

2.4.4 Transient Transfection of C2C12

C2C12 cells were transfected using the Amaxa Cell Line Nucleofector Kit V (Lonza, Basel, Switzerland). For this purpose, C2C12 cells with a 70 to 80 % confluency on a 10 cm cell culture dish were used. These cells were detached from the cell dish using 0.25 % trypsin and transfected by applying the nucleofection technology according to the manufacturer information and based on the program B-032. After the transfection the cells were seeded on 3 cm cell culture dishes containing 2 ml of preheated proliferation medium. 24 h post-transfection the cells reached a 100 % confluency, and the proliferation medium was exchanged with differentiation medium. The cells were differentiated up to seven days and the medium was changed every second day.

2.4.5 Transient Transfection of IMM

Cells were cultured on coverslips in microtiter plates (6-well plates, TPP, Trasadingen, Switzerland) to a confluency of 50 to 60 %. The transfection was performed according to the instructions of the manufacturer with 3 µg DNA, 3 µl of JetPrime *in vitro* transfection reagent (jetPRIME®, Polyplus, Illkirch, France) and 200 µl of transfection buffer in proliferation medium. The medium was changed 4 h after transfection to proliferation medium. Once the cells reached a confluency of 90 % the medium was changed to nutrient-poor differentiation medium. After four days of differentiation the transfection was repeated as described before. Finally, the cells were differentiated up to six days and the medium was changed every second day. For further analysis the cells were fixed as described in section 2.5.1, stained, and microscopically analyzed.

2.4.6 Bimolecular Fluorescence Complementation

In order to depict protein interactions in living cells BiFC analysis (Hu *et al*., 2002) were performed. For this experiment, one of two non-fluorescent fragments of a fluorescent protein (Venus) is carried by each protein of interest. Only if the two potential interaction partners are in close proximity to each other, the non-fluorescent fragments complement and an intact, fluorescent complex is generated (Kerppola, 2006). While performing the experiment, it was important to note that different BiFC combinations were available for the transient double transfection of the cells using the Amaxa Cell Line Nucleofector Kit V (Lonza, Basel, Switzerland). The Venus1 construct (AA 1-154) as well as the Venus2 construct (AA 155-238) can be expressed at both the N- and C-terminus of each protein of interest. This resulted in eight different possible combinations. The transfected cells were differentiated for six days by changing the differentiation medium each day before they were fixed (see 2.5.1) and immunofluorescence stained (see 2.5.2) for confocal laser scanning microscopy.

2.4.7 Electrical Pulse Stimulation (EPS)

To investigate the contraction-dependent dynamics of Synpo2 in FRAP (Fluorescence Recovery after Photobleaching) studies myoblasts from transfected C2C12 cells were seeded on 35 mm imaging µ-dish with a polymer coverslip bottom (Ibidi, Gräfelfing, Germany) and electrically stimulated. For this purpose, a 6-well C-Dish (Ion Optix, Westwood, MA, USA) was used. A pulse of 10 V for 4 ms duration at a frequency of 0.5 Hz was applied as standard setting to achieve mechano-adaptation of the cells, using a C-Pace EP Culture Pacer (Ion Optix, Westwood, MA, USA). Cells were analyzed as described in 2.6.2.

To study the behavior and localization of certain proteins under mechanical stress by transfecting them and to analyze protein-protein interactions in mechanically stressed C2C12 cells using BiFC analysis the cells were transfected with the respective proteins and differentiated for six days. The cells were then stimulated with EPS for 2 h of 10 V for 10 ms duration at a frequency of 1 Hz using a 6-well C-Dish (Ion Optix) and the C-Pace EP Culture Pacer. Thereafter, the cells were fixed and stained as depicted in section 2.5.

2.5 Immunostaining of cells

To investigate protein localization *in vivo*, cells and tissue sections were incubated with specific primary antibodies and fluorochrome-coupled secondary antibodies (see Table 2.4 and Table 2.5). Fixed cells or tissue sections were incubated in two consecutive steps with the primary and secondary antibodies and finally embedded with a mounting solution (Fluoromount-G, Southern Biotech).

2.5.1 Paraformaldehyde Fixation of Cells

Primarily, the cells cultivated on 35 mm plastic dishes (Greiner Bio-One, Kremsmünster, Austria) were washed twice with pre-heated PBS containing Ca^{2+} and Mg^{2+} (DPBS, Gibco, Life technologies, Carlsbad, USA). After that they were fixed with 4 % paraformaldehyde (Carl Roth, Karlsruhe, Germany) in PBS for 10 min at RT. Then the dishes were again washed twice with Ca^{2+} and Mg^{2+} containing PBS followed by the permeabilization of the cells with 0.5 % Triton X-100 (Carl Roth, Karlsruhe, Germany) in PBS for 10 min at RT.

2.5.2 Indirect Immunostaining of cells

The used primary and fluorochrome-coupled secondary antibodies are listed in Table 2.4 and Table 2.5 respectively. Fixed cells were treated with blocking solution (10 % NGS, 1 % BSA in PBS) for 45 min at RT. Primary antibodies were diluted in PBS and added to the dishes followed by an incubation for 1 h in a wet chamber. Afterwards the cells were washed twice with PBST (0.5 % Tween-20 in PBS) and once with PBS. Then the secondary antibody, diluted in PBS was added to the dishes and incubated for 1 h. In the following the dishes were washed three times with PBST and once with ddH_2O. Eventually, the cells were embedded on object slides (Menzel-Glasses, Thermo Fisher Scientific, Waltham, USA) using a mounting solution (Fluoromount-G, Southern Biotech).

2.6 Microscopic Analysis

2.6.1 Confocal Laser Scanning Microscopy

For visualization of fluorescence-labelled cells confocal laser scanning microscopes were employed (LSM 710 and LSM 900 Airy Scan, both Carl Zeiss, Oberkochen, Germany) using either an EC Plan-Apochromat DICII 40x/1.3 oil or an EC Plan-Apochromat DIC 63x/1.4 oil objective (both Carl Zeiss, Oberkochen, Germany). The diameter of the pinhole was set to one airy unit (AU) for all wavelengths. To prevent signal crosstalk when imaging multi-channel lebelling, line-by-line scanning was performed recording each channel separately and sequentially. The mean value of four recordings was formed for each pixel, with the pixel dwell time set as high as possible. Digital image acquisition took place using ZEN black software at LSM 710 (Version 2012 SP5) and ZEN blue software at LSM 900 (Version 3.5) (Carl Zeiss, Oberkochen, Germany).

Evaluation of fluorescence-stained myoblasts was performed using a spinning disk microscope (Cell Observer SD, Carl Zeiss, Oberkochen, Germany). The rotating Nipkow disc of the confocal scanning unit CSU-X1 contained thousands of spirally arranged pinholes allowing hundreds of pixels to be scanned simultaneously, which made it possible to rapidly produce overview images of several myoblasts at high resolution. An EC Plan-Neofluar DIC 40x/1.3 oil objective (Carl Zeiss, Oberkochen, Germany) was used employing Zen blue software (Version 2.5) for digital image acquisition.

2.6.2 Fluorescence Recovery after Photobleaching (FRAP)

FRAP experiments were performed on a confocal laser scanning microscope (LSM900) equipped with a CO_2 chamber. The transfected C2C12 cells were analyzed at 37 °C and 5 % CO_2. The image processing took place with the help of the ZEN software (Carl Zeiss, Jena) using a 40x objective (EC Plan-Apochromat DICII 40x/1.3 oil). The regions of interest (ROIs) were defined and bleached with a 405 nm laser beam at 100 % intensity. The experiment was only included in the evaluation if the fluorescence intensity was reduced by at least 80 %. Pictures were taken before and immediately after the bleaching process. For FRAP analysis, 20 to 30 cells were analyzed in three to four individual experiments. For each cell, one to two ROIs limited to either the Z-discs or the myofibrillar lesions were selected and bleached. After

bleaching, fluorescence signal regeneration was detected for 400 to 900 seconds, depending on the intensity of the bleaching process. Normalized FRAP curves were generated based on the raw data as described in the following (Al Tanoury *et al*., 2010): First, the background fluorescence intensity ($I_{base}(t)$) was subtracted from the intensity in the region of interest ($I_{frap}(t)$) and subtracted from the fluorescence intensity of the whole cells ($I_{whole}(t)$) at all measured timepoints. The corrected intensities were adjusted to the intensity measured into corresponding regions before bleaching (pre-bleaching) ($I_{frap\text{-}pre}$ and $I_{whole\text{-}pre}$). This resulted in the following equation for the normalized FRAP curve:

$$I_{frap-norm}(t) = \frac{I_{whole-pre}}{I_{whole}(t) - I_{base}(t)} * \frac{I_{frap}(t) - I_{base}(t)}{I_{frap-pre}}$$

The normalized fluorescence intensity was plotted against time using Prism 6.0 (GraphPad Software). If it is a dual exponential regeneration phase, it fits into the following function.

$$y\,(t) = y_{max_1} * \,[1 - e^{-K_1 * x}] + y_{max^2} * [1 - e^{-K_2 * x}\,]$$

The half-lives $t_{1/2\ slow}$ and $t_{1/2\ fast}$ of the fluorescence recovery were calculated as follows:

$$t_{\frac{1}{2}slow} = \frac{\ln(2)}{K_1}\ and\ t_{\frac{1}{2}fast} = \frac{\ln(2)}{K_2}$$

The mobile fraction (M_f) results from the following equation:

$$M_f = \frac{F_{end} - F_{post}}{F_{pre} - F_{post}}$$

F_{end} refers to the values at which the fluorescence intensity has reached a plateau. F_{post} is the value of the fluorescence intensity after bleaching and F_{pre} indicated the initial fluorescence intensity. The FRAP data are presented as the mean of at least three individual experiments each.

2.7 Statistical Analysis

Statistical evaluation and graphic representation of collected data was carried out employing GraphPad Prism 6.0 (GraphPad Software Inc. USA). Since data could not be assumed to have a Gaussian normal distribution, first a statistical analysis was carried out with calculation of the minimum and maximum values, the median, the standard deviation, the standard error, and a test for normal distribution. Then an unpaired Student's t-test was performed to check for a difference between normally distributed samples. Statistical significance was assumed for a probability of error of less than 5 % ($p < 0.05$). Differences between samples which did not show a Gaussian normal distribution were evaluated using Mann-Whitney U test, with considering $p < 0.05$ as statistically significant.

For lesion area quantification ImageJ software (Schneider *et al.*, 2012) was used before further statistical analysis using GraphPad Prism was performed.

3.0 Results

3.1 Isoform-specific Synpo2 localization

In order to analyze the specific localization of different Synpo2 isoforms in muscle cells, C2C12 cells were used as a model system for muscle cell differentiation. Since the available anti-Synpo2 antibodies are not isoform-specific, EGFP-fusion proteins of different isoforms were transiently transfected into C2C12 cells. In this work I focused on isoforms Synpo2b (containing the PDZ-domain) and Synpo2e (without the PDZ-domain), since these variants show the highest expression in skeletal muscle cells (Linnemann, 2010). Subsequent to transfection, cells were differentiated into myotubes for six days. To monitor potential changes in the localization of isoforms upon mechanical stress, cells were analyzed before and after EPS. Muscle cells were fixed and counterstained with an antibody against the Z-disc epitope of the cytoskeletal protein titin and analyzed using confocal light microscopy. Both tested isoforms showed prominent localization at Z-discs (Figure 3.1 B, E). In addition, Synpo2b was also revealed in vesicular structures (Figure 3.1 C, arrows), whereas Synpo2e was partially found in myofibrillar lesions (Figure 3.1 F, arrow heads). Upon EPS, Synpo2b mainly remained associated with Z-discs (Figure 3.1 D), while Synpo2e was additionally found in sarcomeric lesions. In some myotubes even a complete recruitment of Synpo2e to these lesions was observed (Figure 3.1, G).

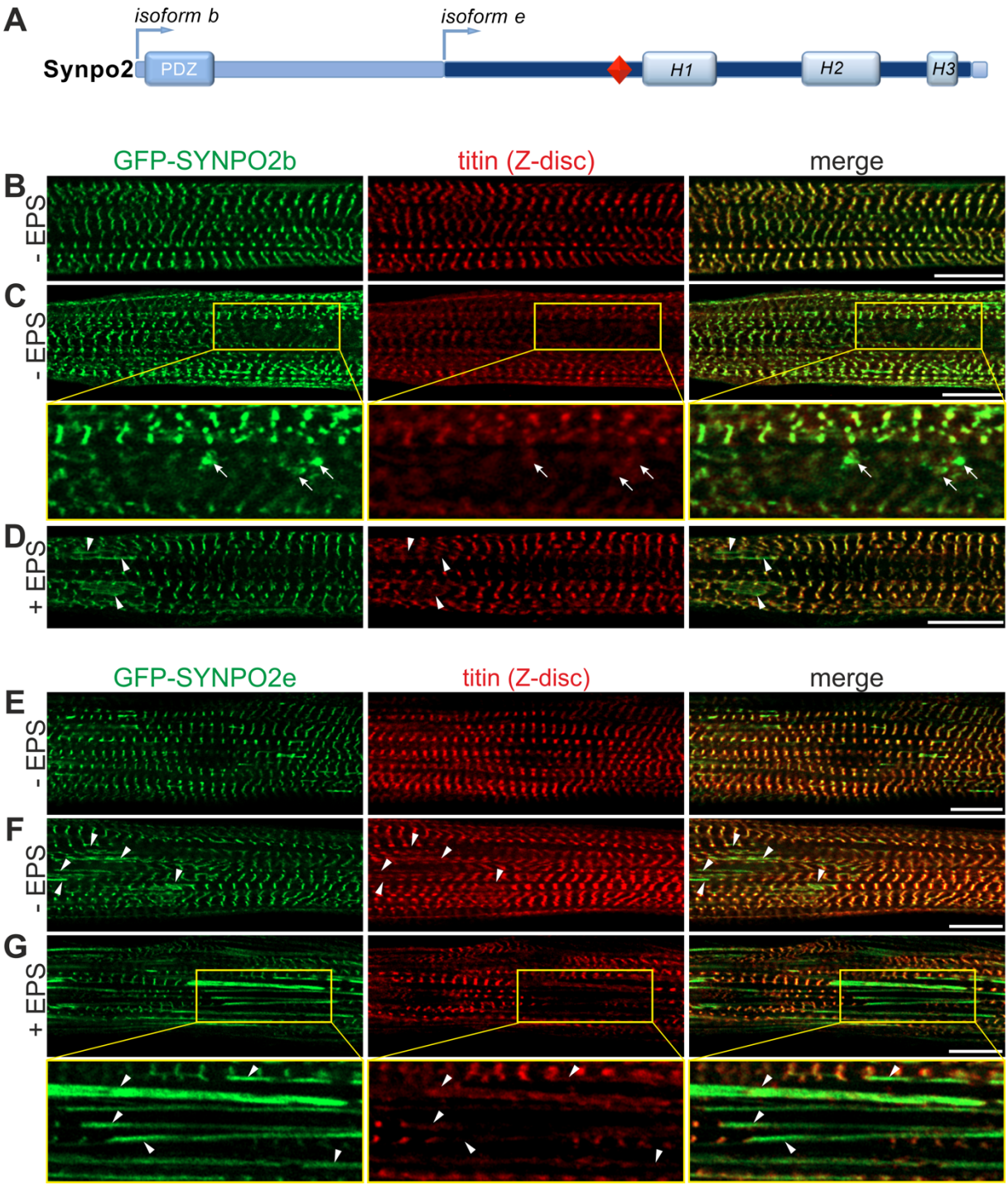

Figure 3.1: Localization of Synpo2 isoforms before and after EPS. (A) Molecular layout of Synpo2b and Synpo2e isoforms, the two variants used in this work: arrows illustrate the two alternative transcriptional start points. Only Synpo2b harbors an N-terminal PDZ-domain. (B - G) Isoform-specific localization of Synpo2b and Synpo2e. After transient transfection into C2C12 cells, EGFP-fusion proteins of both Synpo2b and Synpo2e localize to Z-discs (B, E). In addition, Synpo2b localizes to vesicular structures (C, arrows) and Synpo2e partially to myofibrillar lesions (F, arrow heads). EPS results in efficient recruitment of Synpo2e to lesions (G, arrow heads), whereas Synpo2b mainly remained located to Z-discs (D). Scale bars: 10 µm.

Furthermore, the striking and selective redistribution of Synpo2e to myofibrillar lesions under mechanical stress conditions (in comparison to Synpo2b) was analyzed by quantifying the lesions per area and the number of lesions per area. For this purpose, multiple images of at least 20 myotubes, transiently transfected with EGFP-Synpo2b or EGFP-Synpo2e, treated with EPS and counterstained for the Z-disc epitope of titin from separate experiments were utilized. Both, the total lesion area, and the number of lesions per area were determined and statistically evaluated. Forced contractions induced by EPS revealed a mean total lesion area of around 4 % for Synpo2b and 10 % for Synpo2e. Statistical evaluations showed a significant difference in both, the total lesion area, and the number of lesions per area (Figure 3.2). These quantification results confirm the prominent redistribution of Synpo2e to lesions upon mechanical stress stimulation.

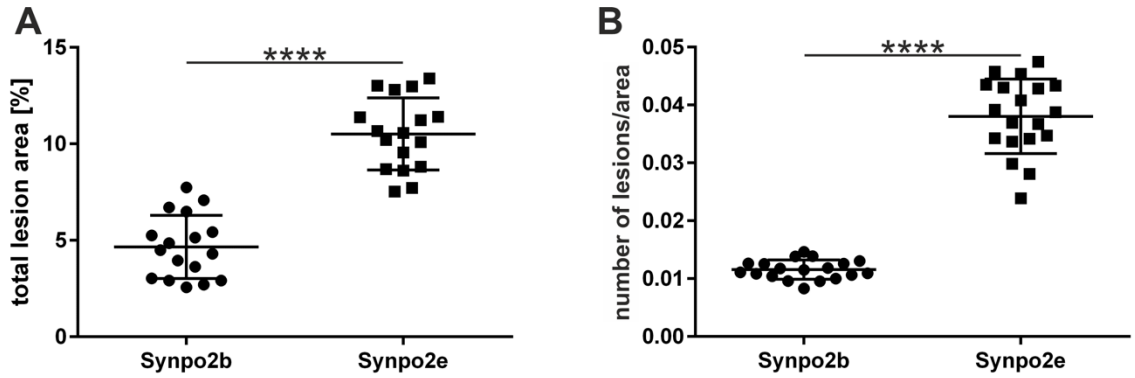

Figure 3.2: Synpo2e is redistributed to myofibrillar lesions after EPS. Representative images of myotubes transfected with EGFP-fusion proteins of Synpo2b and Synpo2e counterstained for the Z-disc epitope of titin were used to analyze the total area of myofibrillar lesions and their number per area using ImageJ software (Schneider *et al.*, 2012) and Prism 6.0 (GraphPad software). Both, the total lesion area (A), and the number of lesions per area (B, area: pixel/µm) were significantly higher in the Synpo2e isoform lacking the PDZ-domain, compared to the Synpo2b isoform containing this domain. Error bars represent the standard deviation of at least 20 analyzed images from four different experiments. The p-values were calculated using Student's t-test. ****: $p < 0.00001$.

3.2 The importance of the BAG3 WW domain for its targeting to the Z-disc

BAG3 was identified as an interaction partner of Synpo2 by Ulbricht *et al.* (2013). More precisely, the WW domain of BAG3 was shown to bind to the PPPY motif of Synpo2, which is contained in all Synpo2 isoforms. In order to analyze the importance of the WW domain for

the localization of BAG3 in skeletal muscle cells, a BAG3 WAWA mutant was employed, where the tryptophane residues of the WW domain were mutated to alanine. C2C12 cells were transiently transfected with constructs expressing EGFP-BAG3 and EGFP-BAG3 WAWA, respectively, and allowed to differentiate for six days. Both constructs, BAG3 and BAG3 WAWA, were found in a diffuse distribution throughout the cytoplasm (Figure 3.3 -EPS). However, clear differences in their localization were obtained after treating the transfected cells with EPS. Here, EGFP-BAG3 WAWA remained diffusely distributed (Figure 3.3 C, +EPS), whereas EGFP-BAG3 showed an association to Z-discs and also slightly to lesions (Figure 3.3 B, +EPS). This indicates that the interaction of BAG3 with Synpo2 is probably essential for BAG3 recruitment to Z-discs.

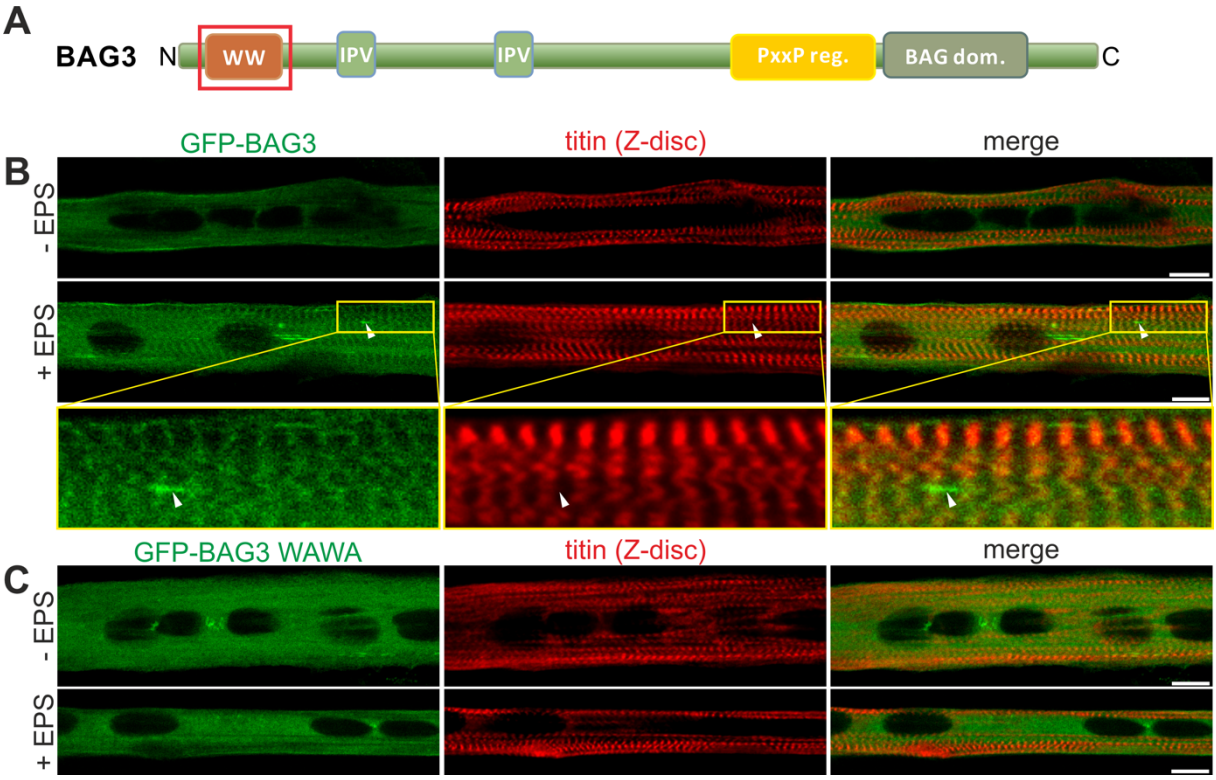

Figure 3.3: Localization of BAG3 variants in EPS and untreated myotubes. (A) Schematic overview of the structure of BAG3 with the WW domain outlined in a red box. (B) Transiently transfected EGFP-BAG3 is found in a diffuse distribution throughout the cytoplasm (-EPS). Consecutive EPS leads to a redistribution from this diffuse cytoplasmic localization to a clear Z-disc association (+EPS). In addition, a localization to myofibrillar lesions can be detected (B, +EPS, arrow heads). (C) EGFP-BAG3 WAWA mutant with the Synpo2 binding WW domain of BAG3 modified by exchanging both tryptophanes (W) to alanine (A), shows a diffuse distribution (-EPS). Even after EPS the BAG3 WAWA EGFP-fusion protein remains diffusely distributed throughout the cells (+EPS). Scale bars: 10 µm.

To further elucidate this finding, the EGFP-fusion protein of BAG3 was transiently transfected into IMM control cells, transduced with a scrambled shRNA-expressing lentivirus, and Synpo2 knockdown (kd) IMM cells, differentiated for six days and afterwards treated with EPS. In control cells the co-chaperone showed a partial association to Z-discs, whereas in Synpo2kd cells EGFP-BAG3 was diffusely distributed even after mechanical stress (Figure 3.4). This confirms the necessity of the interaction between BAG3 and Synpo2 for the association of BAG3 to Z-discs.

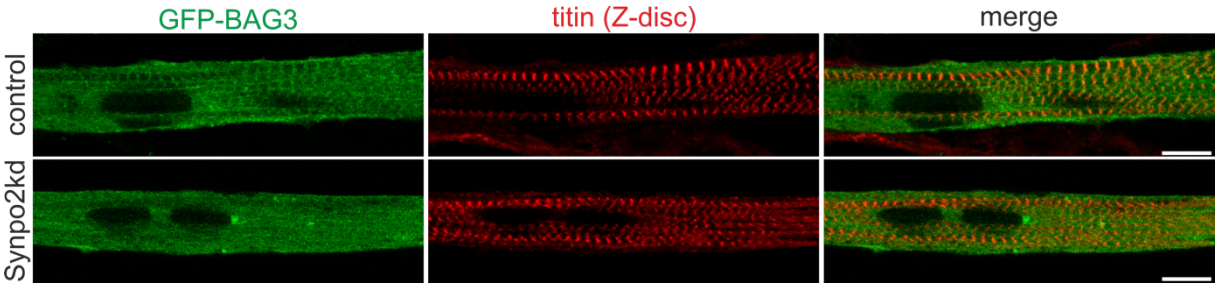

Figure 3.4: Synpo2-dependant localization of BAG3 to Z-discs. Upon EPS EGFP-BAG3 partially localizes to Z-discs in control cells, whereas Synpo2 deficient IMM Synpo2kd myotubes show a diffuse cytoplasmic distribution. Scale bars: 10 µm.

3.3 BAG3 forms two distinct molecular complexes with Synpo2 isoforms

The dynamic force-regulated interaction between BAG3 and Synpo2 in contracting myotubes was investigated by performing BiFC assays. For this experiment, one of two non-fluorescent fragments of a fluorescent protein (Venus) was connected to each protein of interest. If the two potential interaction partners are in close proximity to each other, the non-fluorescent fragments complement each other and an intact, fluorescent complex of Venus is generated (Kerppola, 2006). It is important to note that different BiFC combinations are in principle available for the transient double transfection of the cells. The Venus 1 construct (AA 1-154) as well as the Venus 2 construct (AA 155-238) can be expressed at both the N- and C-terminus of BAG3 and Synpo2, which would result in eight different possible combinations. However, since it is already known from previous experiments (Ulbricht *et al.*, 2013) that Synpo2 interacts with the N-terminal portion of BAG3, only double transfections were performed with BAG3 constructs expressing the Venus 1 or 2 construct at their N-terminus. Thus, only four possible transfection combinations had to be tested for successful complementation of the fluorescence signal.

C2C12 myotubes were transiently transfected with the different combinations, followed by a differentiation for six days. After EPS, successful complementation was detected by co-expressing Venus1C-BAG3 with Venus2C-Synpo2b or Venus2C-Synpo2e. The binding of BAG3 with both analyzed isoforms was confirmed (Figure 3.5 C, D). The BAG3-Synpo2b complex showed a BiFC signal in Z-discs and in vesicular structures (Figure 3.5 C). The BAG3-Synpo2e complex also interacted in Z-discs, but in addition also in sarcomeric lesions (Figure 3.5 D). Interestingly, the myotubes co-expressing BAG3 and Synpo2b did not exhibit any lesions (Figure 3.5 C).

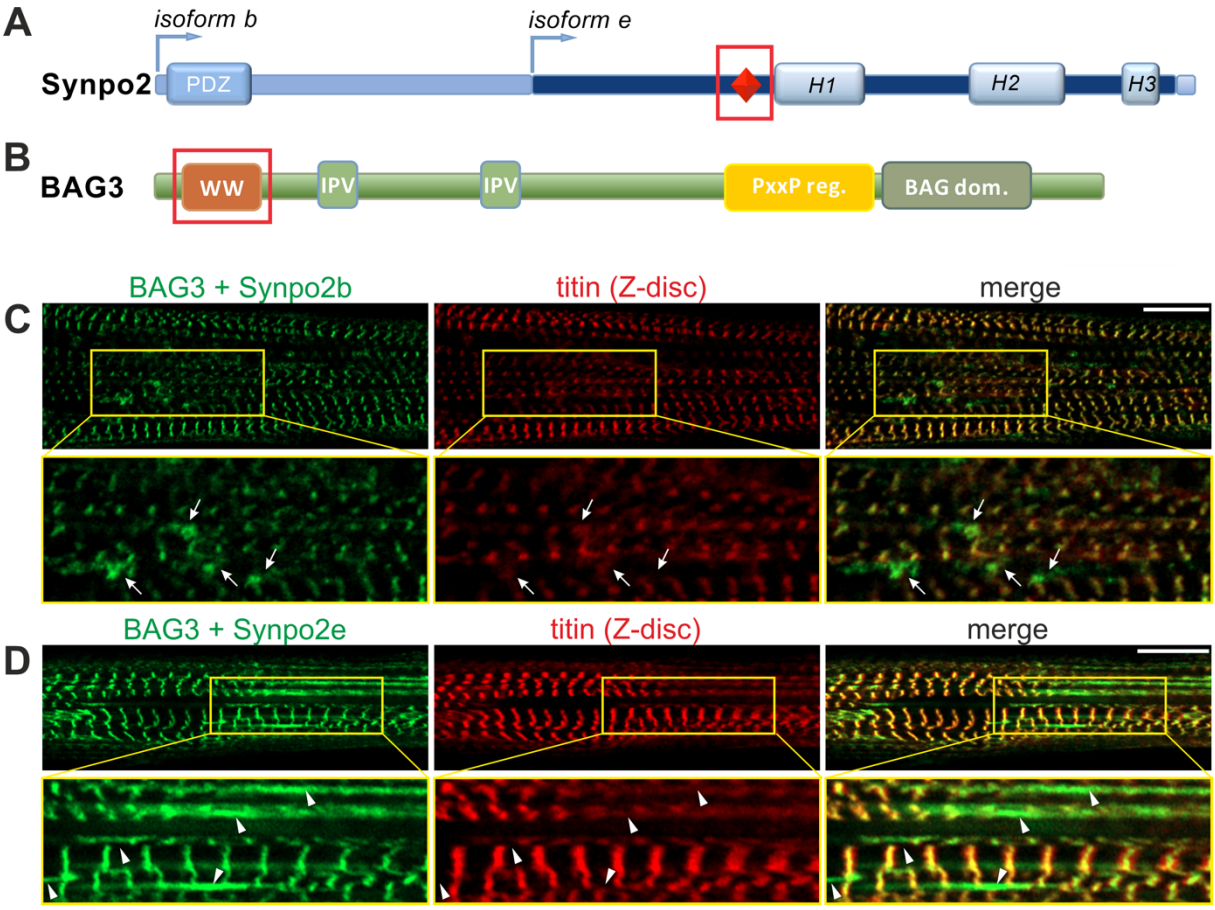

Figure 3.5: BiFC assay confirming the interaction of Synpo2 isoforms b and e with BAG3. (A, B) Schematic overview of Synpo2b/e and BAG3 with the PPPY motif of Synpo2 and the WW domain of BAG3 emphasized by a red box. (C, D) C2C12 myotubes were co-transfected with Venus1C-BAG3 and Venus2C-Synpo2b or Venus2C-Synpo2e before EPS. (C) EPS-induced mechanical stress induced a localization of the BAG3-Synpo2b complex to the Z-disc. Moreover, a BAG3-Synpo2b complex BiFC signal was detected in vesicular structures (C, arrows), whereas the BAG3-Synpo2e complex localized both in Z-disc and in lesions (D, arrow heads). Scale bars: 10 µm.

3.4 Isoform-specific Synpo2 dynamics

To analyze the impact of mechanical stress on isoform-specific dynamics and mobility of Synpo2, FRAP experiments were performed. C2C12 myotubes were transiently transfected with EGFP-Synpo2b and EGFP-Synpo2e and differentiated for six days. Before performing FRAP experiments, cells were "mildly" treated with EPS overnight in order to achieve their mechanical adaptation (EPS setting: 10 V, 4 ms, 0.5 Hz). Both fusion proteins were targeted to Z-discs, with EGFP-Synpo2e additionally located to myofibrillar lesions as well. Mobility and dynamics of both Synpo2 isoforms were determined by photobleaching individual Z-discs and analyzing the regeneration of the fluorescence signal over a certain period of time until recovery was reached. Recovery of Synpo2b half-life was about 130.5 s, whereas Synpo2e recovered with a half-life of around 50.2 s (Figure 3.6 B-D). This indicates, that the Synpo2b isoform containing a PDZ-domain at the N-terminus is more stably associated with Z-discs than the Synpo2e isoform that lacks the PDZ-domain. The mobile fraction of Synpo2b and Synpo2e exhibited a mobility of 87 and 92.3 %, respectively (Figure 3.6 E).

Since Synpo2e was strongly redistributed from Z-discs to myofibrillar lesions, FRAP analyses were also performed by photobleaching individual lesions and studying the recovery time of this isoform. Synpo2e-containing lesions recovered with a half-life of 80.5 s and had a mobile fraction of 88 % indicating that Synpo2e is bound more firmly to lesions compared to Z-discs, implying a stabilizing function of Synpo2e (Figure 3.7 D, E). To sum up, these data reveal different subcellular molecular dynamics and functions of both analyzed Synpo2 isoforms upon induction of mechanical stress by EPS.

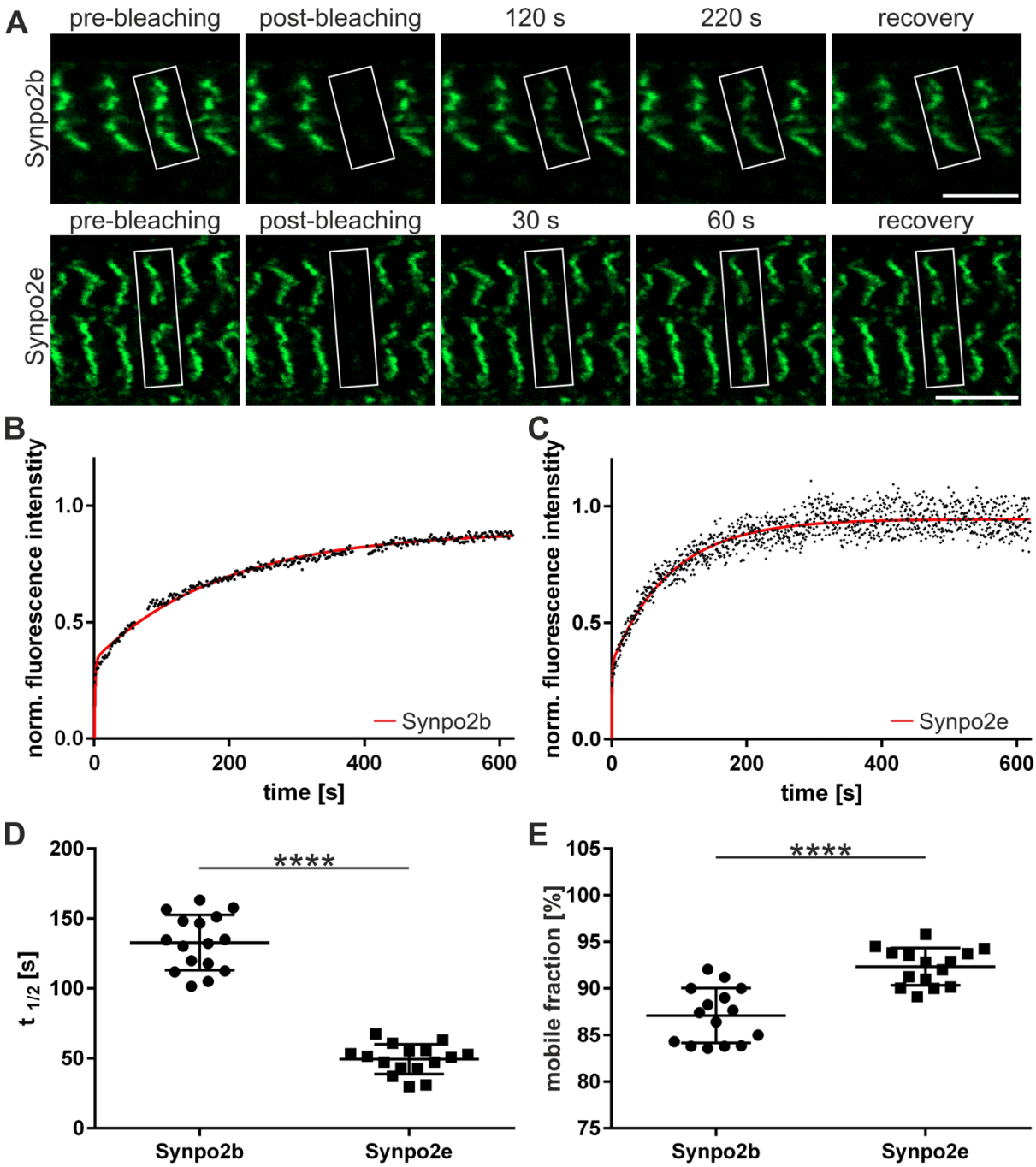

Figure 3.6: Isoform-specific mobility and dynamics of Synpo2. FRAP experiments performed on C2C12 myotubes expressing EGFP-Synpo2b or Synpo2e. Cells were "mildly" treated with EPS (10 V, 4 ms, 0.5 Hz) overnight in order to achieve their mechanical adaptation. (A) The intensities of Synpo2b and Synpo2e fusion proteins are shown before bleaching (pre-bleaching), directly after bleaching (post-bleaching) and 120 / 220 s after bleaching for Synpo2b and 30 / 60 s after bleaching for Synpo2e, and after maximum recovery. White rectangles indicate the regions bleached. Statistical analysis of the results shown in panels B - E. (B - D) The half-life of Synpo2b is significantly higher compared to that of Synpo2e. (E) Significant differences were observed between the mobilities of Synpo2b and Synpo2e. Error bars show the standard deviation of at least 15 FRAP assays from three individual experiments. The p-values were calculated using Student's t-test. ****: $p < 0.00001$. Scale bars: 5 µm.

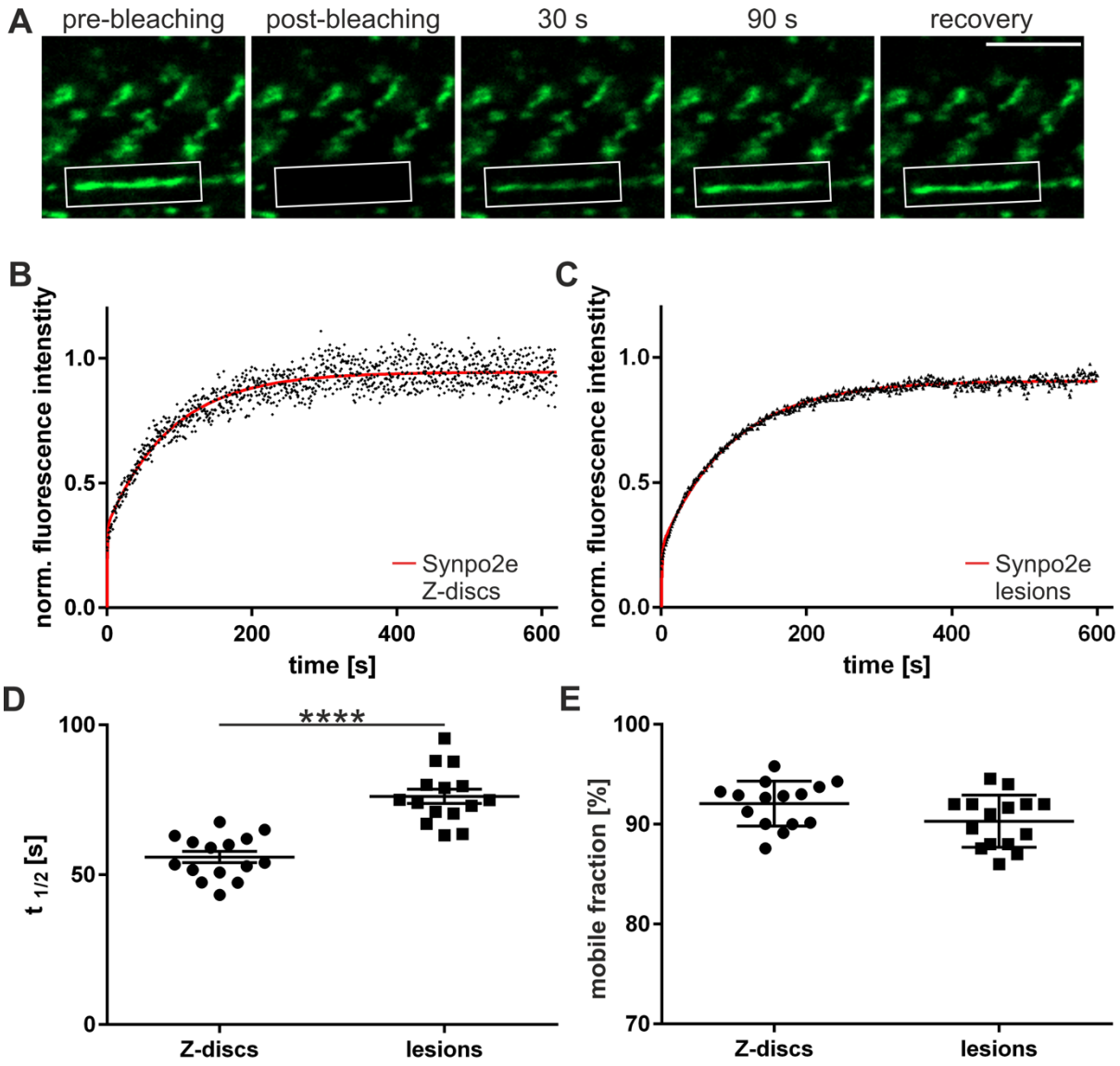

Figure 3.7: Synpo2e associated with myofibrillar lesions is less dynamic than that located at Z-discs. (A) FRAP assay in EGFP-Synpo2e-expressing C2C12 myotubes after six days of differentiation, Respective frames show pre-bleaching, post-bleaching and multiple timepoints during recovery. The bleached area is marked by white rectangles. (B - D) The biphasic course of the curves (red line) indicates a slower regeneration of Synpo2e in the bleached regions of myofibrillar lesions compared to Z-discs. The half-life of Synpo2e in lesions was significantly higher than that of the recovery of Z-discs. (E) No significant differences were obtained for the mobile fractions. The error indicator shows the standard deviation for at least 15 FRAP assays from three individual experiments. The p-values were calculated using Student's t-test. ****: $p < 0.00001$. Scale bar: 5 µm.

3.5 Synpo2 knockdown has an impact on autophagic flux

We recently showed that a knockdown of Synpo2 results in highly enhanced sarcomeric lesion formation upon mechanical stress simulation using EPS (Lohanadan *et al.*, 2021) and formation of lesions led to a redistribution of filamin C from Z-discs to lesion. These results suggested an increased instability of myofibrils under mechanical stress upon loss of Synpo2 (Lohanadan *et al.*, 2021).

This demanded to analyze the relative levels of LC3BII (the lipidated form of LC3B, which is involved in the formation of autophagosomal membrane) compared to non-membrane bound LC3BI. The ratio of these two forms, which is an indicator of autophagic flux, was studied in cell lysates of control as well as Synpo2kd cells differentiated for six days. Furthermore, the effect of EPS on these levels was analyzed by comparing cell lysates of six days differentiated and EPS treated cells. In control myotubes, extended mechanical stress induced by EPS caused an increase in the conversion of LC3BI to LC3BII (Figure 3.8). In contrast, in Synpo2kd cells the LC3BII/LC3BI ratio was lower in the untreated cells and did not increase by application of EPS (Figure 3.8) (see also Lohanadan *et al.*, 2021).

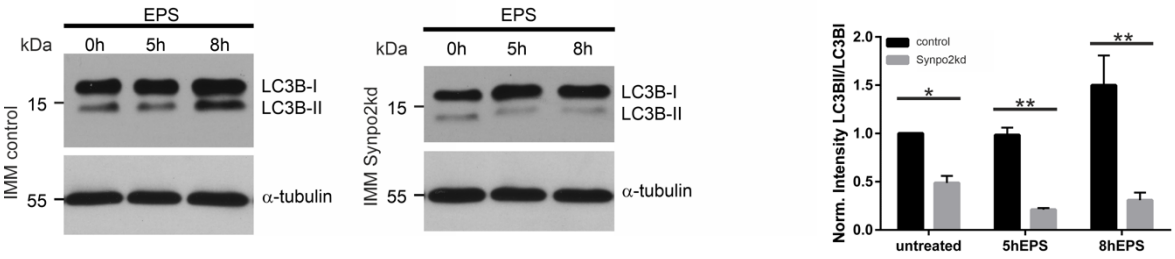

Figure 3.8: Knockdown of Synpo2 reduces autophagic flux. The relative amount of lipidated LC3BII and non-lipidated LC3BI quantified in cell lysates of six days differentiated IMM control and Synpo2kd cells, which were either untreated or treated with EPS for 5 h or 8 h. The ratio of LC3BII/LC3BI was significantly lower in Synpo2kd cells. Upon EPS, the ratio of LC3BII/LC3BI increased in the control cells, whereas it was even slightly reduced in the Synpo2kd cells (Blots by Julia Braune, unpublished results). The p-values were calculated using Student's t-test. *: $p < 0.05$, **: $p < 0.001$.

Since these results indicated that the deficiency of Synpo2 reduces autophagic flux (Lohanadan *et al.*, 2021) and because Synpo2 was described to play a role as an adapter protein in CASA-mediated degradation (Ulbricht *et al.*, 2013, Ulbricht and Höhfeld, 2013), the expression levels of several autophagy-associated proteins, the heat shock proteins, namely HspB7 and HspB8, the co-chaperone BAG3, and the autophagic ubiquitin adapter p62, were investigated. For this purpose, Synpo2kd IMM cells and control IMM cells transduced with a scrambled shRNA-expressing lentivirus were cultivated, and cell lysates generated before differentiation (d0) as well as after three (d3) or six (d6) days of differentiation. Protein levels of Synpo2kd cell lysates were normalized to GAPDH and compared with their levels in GAPDH normalized control cells. In Synpo2kd cells the expression of Synpo2 was reduced by approximately 70 % (Figure 3.9 E) and HspB8 expression was elevated at all developmental stages (Figure 3.9 B), whereas HspB7 showed a significantly lower expression after differentiation for six days (Figure 3.9 A). In contrast, no significant change in expression of the co-chaperone BAG3 was observed between control and Synpo2kd cells (Figure 3.9 C). Interestingly, expression of p62 was decreased after three days of differentiation in Synpo2kd cells compared to control cells, whereas after six days of differentiation no difference in the p62 level was observed between both types of myotubes (Figure 3.9 D).

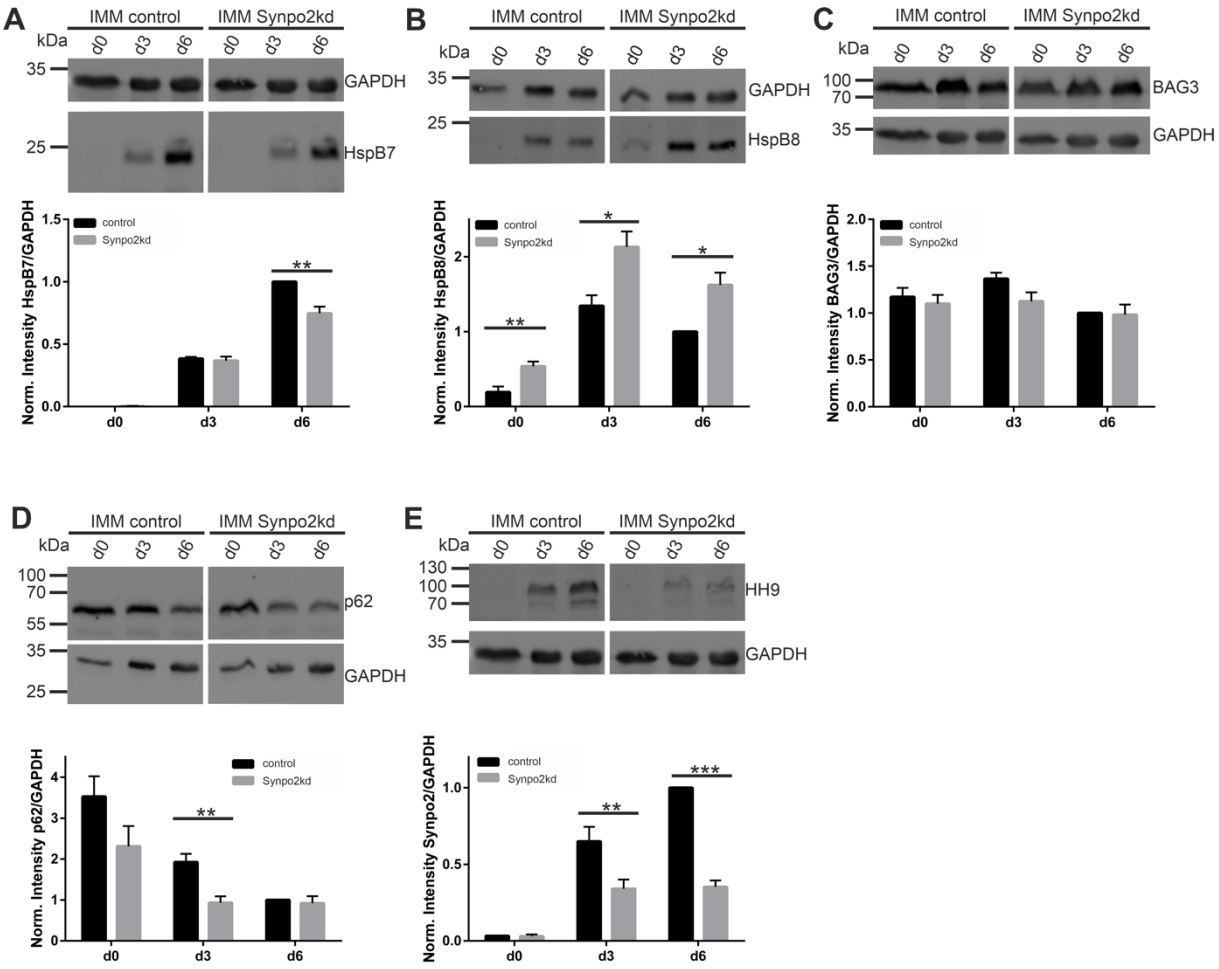

Figure 3.9: Knockdown of Synpo2 has an impact on autophagic flux. The expression levels of HspB7 (A), HspB8 (B), BAG3 (C) and p62 (D) were analyzed using cell lysates of undifferentiated (d0), three days differentiated (d3) and six days differentiated (d6) IMM control and Synpo2kd cells. HspB7 showed significantly lower expression in d6 Synpo2kd cells (A), whereas HspB8 had an overall increased expression at all timepoints tested (B). No changes in the expression level of BAG3 were obtained (C). In Synpo2kd cell p62 was expressed significantly lower after three days of differentiation but no differences were detectable between the cells after six days of differentiation (D). The overall knockdown-efficiency of the Synpo2kd cells amounted to approximately 70 % (E). Error indicators show the standard deviation from at least five individual experiments. The p-values were calculated using Student's t-test. *: $p < 0.05$, **: $p < 0.001$, ***: $p < 0.0001$.

3.6 Triple phosphorylation in homology region 2 (H2)

A further central goal of this work was to unravel the specific roles of different Synpo2 variants for maintenance of the cytoskeleton, autophagy, and signaling under conditions of mechanical stress in muscle cells. An important type of the regulation of protein-protein- interactions represents the post-translational modification by phosphorylation. It has previously been shown that Synpo2 may be phosphorylated by PKA and calmodulin-dependent kinase II (CaMKII) (Faul *et al.*, 2007). These phosphorylations regulate the interaction of murine Synpo2 with 14-3-3 proteins (Faul *et al.*, 2007), but at least one of the sites described is not conserved between mice and humans. Therefore, further attempts were made in this work to identify and characterize specific phosphorylations of Synpo2. The research group of Bettina Warscheid (University of Freiburg/ University of Würzburg) experimentally identified numerous phosphorylation sites in several Z-disc associated proteins including Synpo2 through phosphoproteomic studies (see table. 1.1). Several of these identified phosphosites were either up- or downregulated upon mechanical stress induced by EPS (Reimann *et al.*, 2017 and unpublished work).

Table 3.1: Overview of generated phosphosite mutants. The sequence and the position of the respective amino acid residues in human of the generated phosphosite mutants are depicted. Serine to alanine and serine to aspartic acid mutants were generated to mimic the dephosphorylated and phosphorylated state of the selected phosphosite.

Nomenclature	Sequence	residue in Synpo2b	residue in Synpo2e
3x mutant	HAARAQSPTPSLPASWKYSSNVRAPPPV	Ser902 Ser906 Ser910	Ser507 Ser511 Ser515
LIR mutant	GDSGPEEDYLSLGAEACN	Ser737	Ser342

A particularly interesting phosphosite region was found in the H2-region, in which three serine residues were identified in close proximity. Mechanical activity upon EPS showed a downregulation upon stimulation of these phosphorylation sites (see Table. 1.1). This area was found to be highly conserved in all podins and therefore this region and in particular the phosphorylation sites can be assumed to be of general relevance for the podin protein family (Figure 3.10). To characterize these phosphorylation sites in more detail, mutants with exchange of serine to alanine (3 x SA) and serine to aspartic acid (3 x SD) were generated to

mimic a dephosphorylated and phosphorylated state, respectively. The sequence and amino acid position of these phosphosites in Synpo2b as well as in Synpo2e are depicted in Table 3.1 (3 x mutant). As all the experiments in this study were performed using human cDNA, I will refer to the human amino acid sequence in the following.

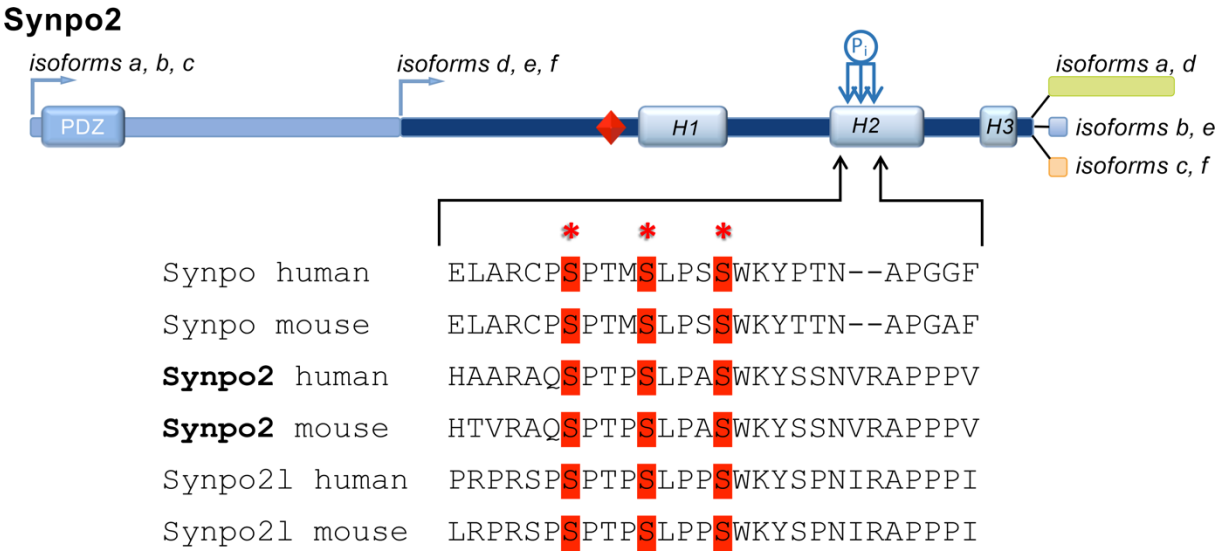

Figure 3.10: Schematic illustration of triple phosphorylation in the H2 region of Synpo2. The red stars mark the serine residues identified as phosphorylation sites located in the H2-region and found in all Synpo2 isoforms as well as in synaptopodin (Synpo) and synaptopodin-2-like (Synpo2l).

3.6.1 Phosphorylation in H2 weakens binding of Synpo2 to filamin C and α-actinin-2

The binding of Synpo2 to filamin C, more specifically to its d18-21 region, and to the muscle-specific α-actinin-2 is mediated by the two homology regions 1 and 2, referred to as H1+H2 in the following. Therefore, it was interesting to investigate the impact of the phosphorylation state of the triple serine residues (Synpo2b: S902 S906 S910, Synpo2e S507 S511 S515) on the interaction between Synpo2 and filamin C, as well as Synpo2 and α-actinin-2.

For this purpose, 3 x SA and 3 x SD mutants were generated in the Synpo2 fragment H1+H2, which simulated constitutively dephosphorylated and phosphorylated conditions, respectively. Using these phosphomimetic Synpo2 fragments and a Synpo2 WT fragment, co-IPs were carried out with the binding region of filamin C (filamin C d18-21) and α-actinin-2. The proteins were first expressed in *E. coli* and then purified using the His_6-tag. Filamin C as well as α-actinin-2 fragments were in the pET23aEEF vector. All Synpo2 H1+H2 fragments were cloned

into the pET23aT7 vector for binding studies. This facilitated the detection of each protein via the T7 or EEF-tag, respectively. The utilized secondary antibody was coupled to a fluorochrome, which made it possible to quantify the protein levels using a fluorescence imager (Odyssey, LI-COR).

Interestingly, the interaction of the Synpo2 fragment H1+H2 3xSD with filamin C d18-21 showed a significantly weaker binding compared to the interaction of filamin C d18-21 with Synpo2 WT and 3xSA fragments (Figure 3.11 B-D). Quantitative analysis of the filamin C d18-21 protein level after normalizing with the protein levels of the Synpo2 fragments, demonstrated that the protein level of filamin C d18-21 after a Co-IP with the Synpo2 H1+H2 3xSD construct was reduced by 47 % compared to the Synpo2 H1+H2 WT construct (Figure 3.11 E). This indicates that the phosphorylation state of Synpo2 plays a crucial role in the regulation of its interaction with filamin C.

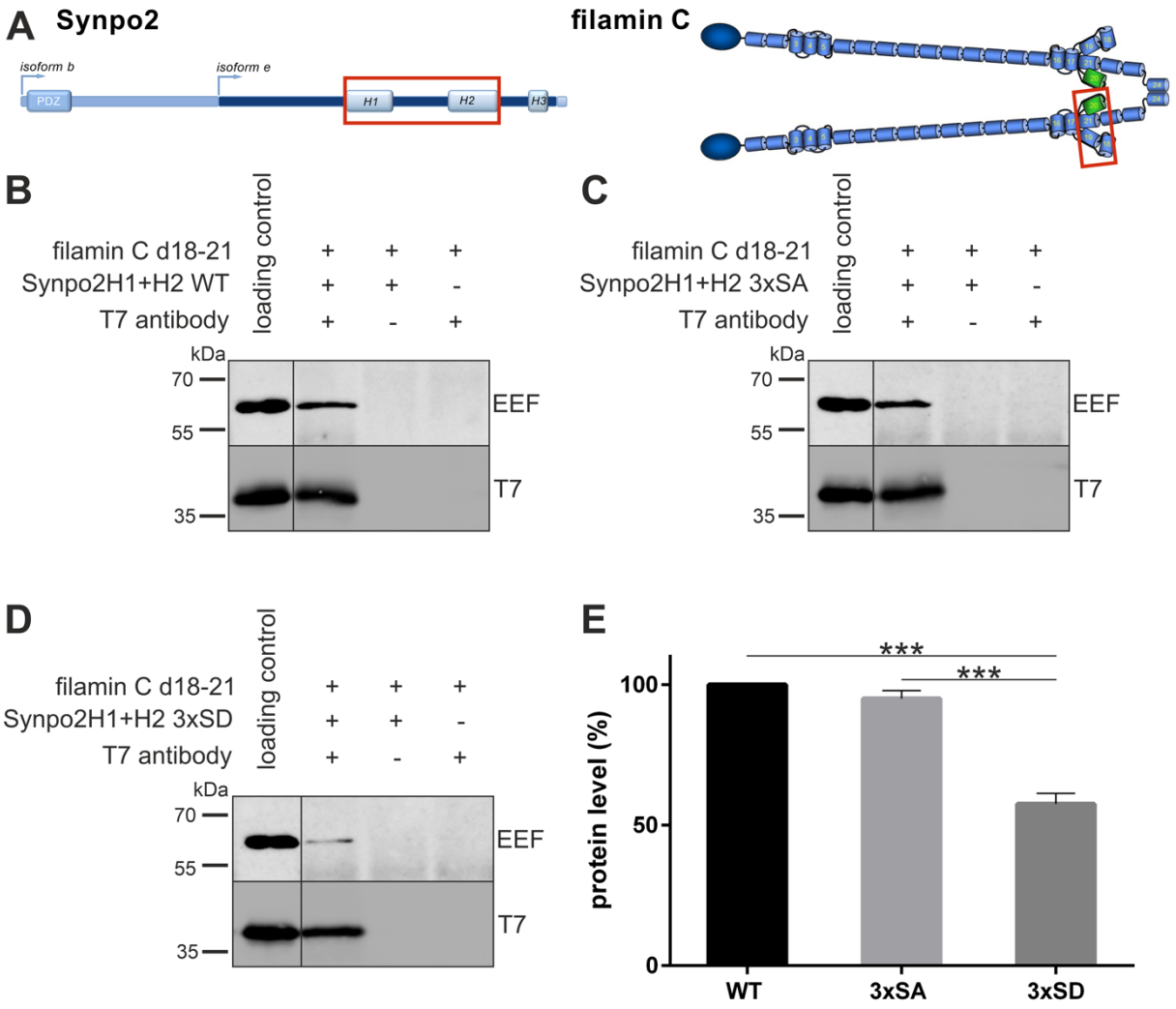

Figure 3.11: Phosphorylation in the H2-region of Synpo2 weakens its filamin C binding. (A) Schematic overview of the structure of filamin C (modified from van der Ven *et al.*, 2006) and Synpo2. The fragments used are outlined by a red box. (B-D) The co-IP of the bacterially expressed fragments Synpo2 H1+H2 WT/3xSA/3xSD and filamin C d18-21 showed a weaker interaction of the Synpo2 H1+H2 3xSD mutant with filamin C d18-21 compared to the WT and 3xSA mutant fragments. (E) Quantitative analysis of the normalized filamin C d18-21 protein level using a fluorescence imager revealed a filamin C d18-21 protein level in the co-IP with the 3xSD mutant fragment, which was reduced by 47 %. The protein level was normalized to the T7-tagged Synpo2 fragment and the filamin C level of the co-IP with the Synpo2 WT fragment set to 100 %. Error bars show the standard deviation of three measurements. The p-values were calculated using the Wilcoxon-Mann-Whitney test. ***: $p < 0.0001$.

Furthermore, a co-IP-assay of Synpo2 H1+H2 fragments (WT, 3xSA, 3xSD in pET23aT7 vector) and α-actinin-2 (in pET23aEEF vector) was performed. For this purpose, the Synpo2 fragments were precipitated using a T7-tag-specific antibody and the co-precipitated α-actinin-2 fragments were detected using an antibody directed against the EEF-tag. All used fragments of Synpo2 showed binding to α-actinin-2 (Figure 3.12 B-D). Interestingly, the results demonstrated a significantly weakened interaction of the Synpo2 H1+H2 3xSD mutant, mimicking the phosphorylated state, with α-actinin-2 (Figure 3.12 D). The α-actinin-2 protein level was quantified by normalizing it with the protein levels of the Synpo2 fragments and showed that the protein level of α-actinin-2 was reduced by 30 % after co-IP with the Synpo2 H1+H2 3xSD construct, comparted to the Synpo2 H1+H2 WT as well as the Synpo2 H1+H2 3xSA constructs (Figure 3.12 E). These results therefore suggest a strong influence of the Synpo2 phosphorylation state in the H2 region on the binding to α-actinin-2 (Figure 3.12 B-E). Taken together the results from the co-IP assays suggest an important role of the triple phosphosite in the H2 region for the regulation of the binding of Synpo2 to the two cytoskeletal proteins α-actinin and filamin C.

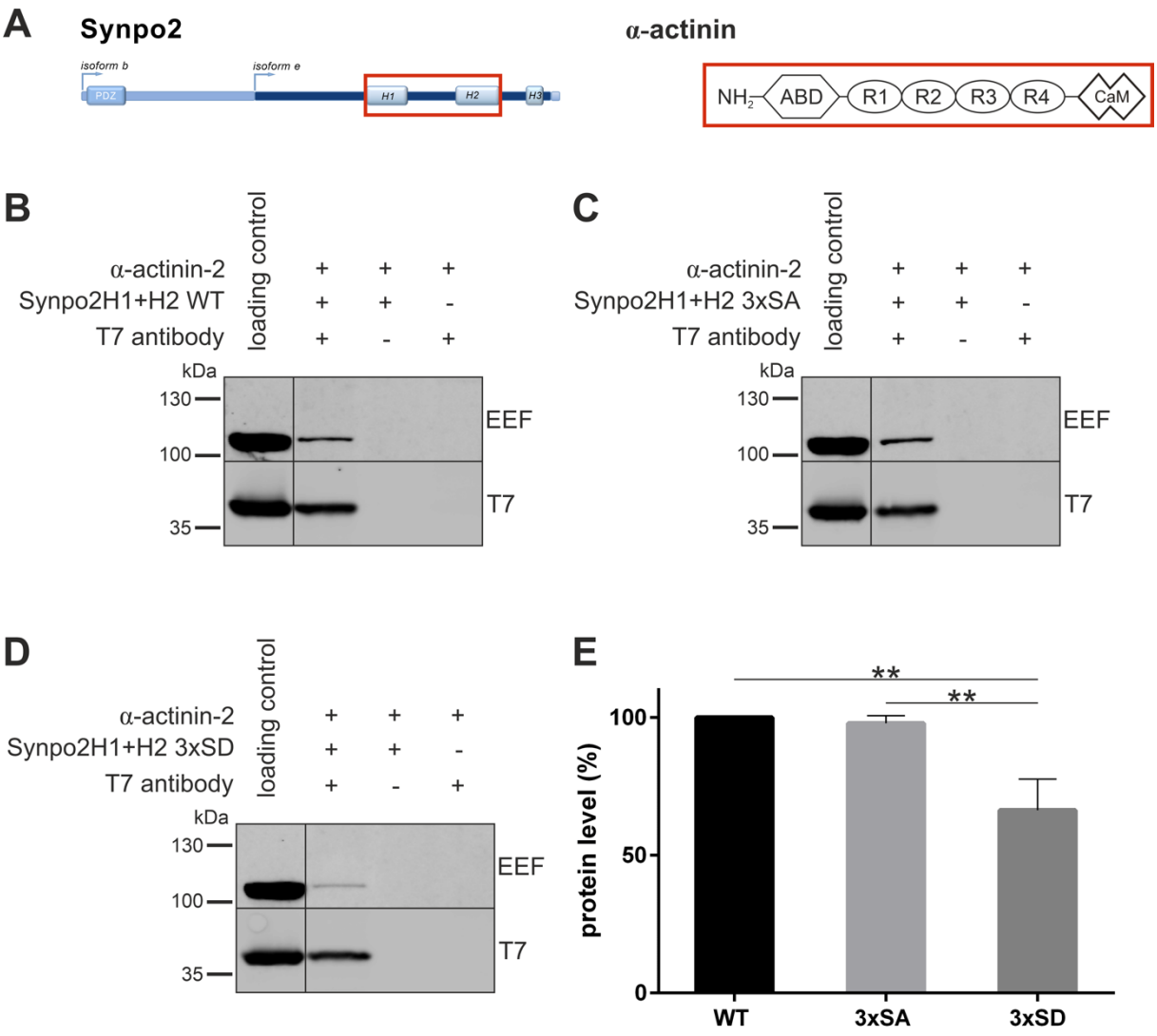

Figure 3.12: Phosphorylation-regulated affinity of the interaction of Synpo2 and α-actinin-2. (A) Schematic overview of α-actinin-2 and Synpo2. Utilized fragments of the proteins are outlined in red boxes. (B-D) Co-IPs were performed with T7-tagged Synpo2 H1+H2 WT/3xSA/3xSD and EEF-tagged α-actinin-2. Synpo2 fragments were precipitated using a T7-tag specific antibody and α-actinin-2 was co-precipitated. The detection of the co-IP using an EEF-tag specific antibody demonstrated a weaker interaction of α-actinin-2 with the constitutively pseudo-phosphorylated mutant Synpo2 H1+H2 3xSD compared to the WT and the consistently pseudo-dephosphorylated mutant Synpo2 H1+H2 3xSA. (E) Quantitative analysis of the α-actinin-2 protein level after normalizing it with the Synpo2 controls illustrates a level reduced by 30 % compared to the WT. The α-actinin-2 level obtained after normalization to the T7-tagged Synpo2 fragment was set to 100 %. Error bars show the standard deviation of three measurements. The p-values were calculated using the Wilcoxon-Mann-Whitney test. **: $p < 0.005$.

3.6.2 Mechanical-stress-induced lesion formation varies upon phosphorylation in H2

After elucidating the important regulatory role of the triple phosphosite for the *in vitro* binding to both filamin C and α-actinin-2, it was interesting to see whether the phosphorylation state exert an impact on the cellular localization of Synpo2 upon mechanical stress induced by EPS. Therefore, the isoform Synpo2b (EGFP-Synpo2bWT/3xSA/3xSD) was transiently transfected into C2C12 cells, differentiated for six days, and analyzed before and after EPS. The PDZ-domain-containing Synpo2b isoform showed an association with Z-discs and a partial association with vesicular structures of all the constructs tested (EGFP-Synpo2bWT/3xSA/3xSD) in the unpaced state (Figure 3.13 B-D, -EPS). Differences became evident upon EPS: EGFP-Synpo2bWT and EGFP-Synpo2b3xSA mainly remained localized at Z-discs, whereas EGFP-Synpo2b3xSD now showed a clear association with myofibrillar lesions (Figure 3.13 B-D, +EPS). In order to analyze this distribution in more detail, myofibrillar lesions were quantified. For this purpose, at least 25 images of transiently transfected EGFP-Synpo2bWT and both triple mutants were investigated. The EGFP-fusion proteins of Synpo2bWT as well as Synpo2b3xSA contained a comparable mean total lesion area of 4.7 % and 4.6 %, respectively. In contrast, EGFP-Synpo2b3xSD - mimicking the phosphorylated state - depicts a significantly higher mean total lesion area of around 10 % (Figure 3.14 A). In addition, the number of lesions per area is also significantly increased in the EGFP-Synpo2b3xSD construct compared to EGFP-Synpo2bWT and EGFP-Synpo2b3xSA constructs (Figure 3.14 B).

This leads to the assumption, that the triple phosphosite in the H2 region, which showed a downregulation upon EPS (unpublished work Bettina Warscheid, University of Freiburg/ University of Würzburg), depicts a different affinity to certain actin cytoskeleton-associated proteins in the phosphorylated state. The EGFP-Synpo2b3xSD construct, mimicking the phosphorylated state is strongly recruited to myofibrillar lesions, suggesting a reduced binding affinity to certain actin-associated proteins. The lower affinity to the cytoskeleton appears to result in more damage, apparent as myofibrillar lesions.

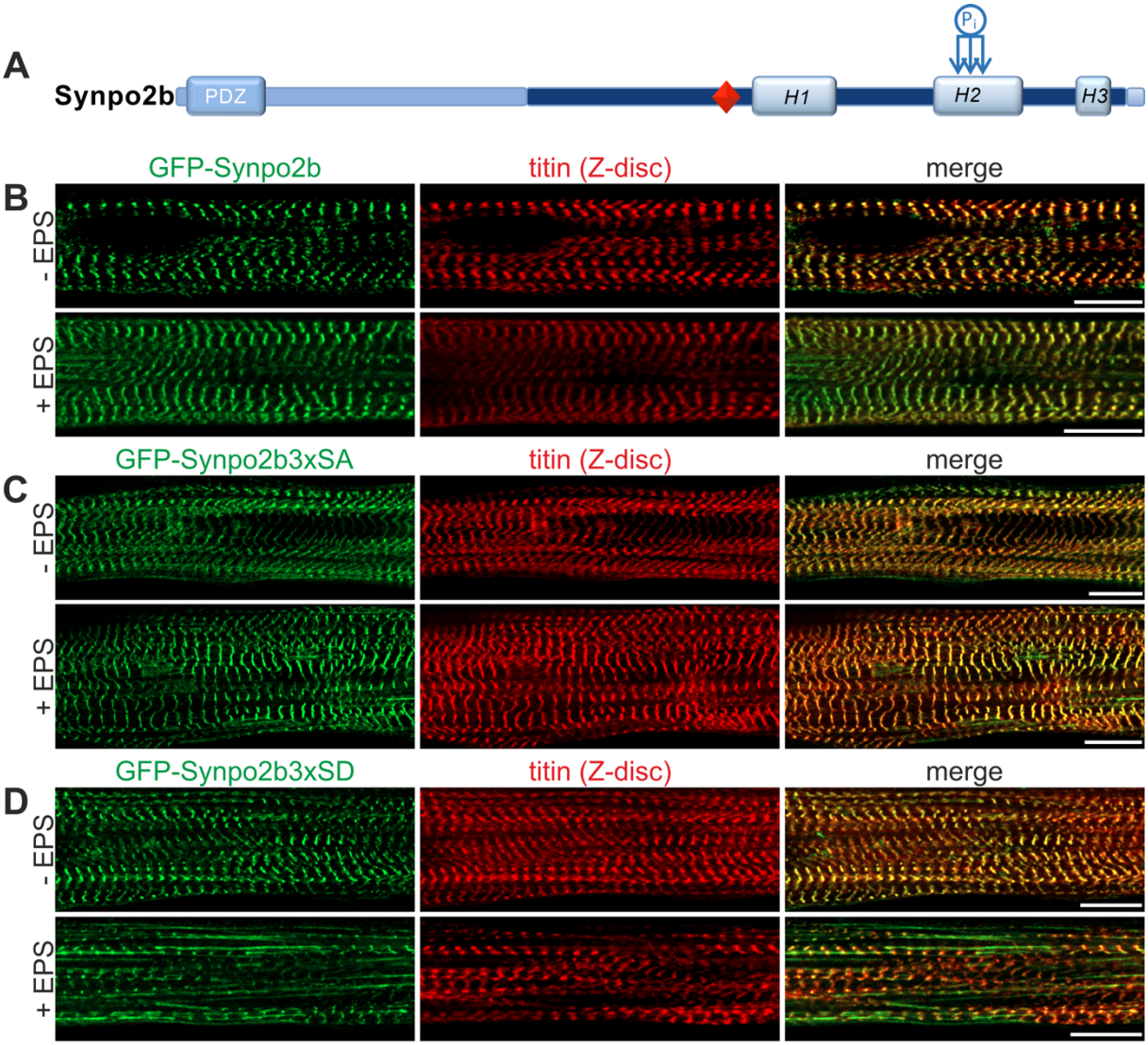

Figure 3.13: Phosphorylation-state-dependent formation of mechanical stress-induced lesions in Synpo2b. (A) Schematic overview of Synpo2b with the triple phosphosite highlighted in the H2-region. (B-D) C2C12 cells were transfected with EGFP-Synpo2bWT, EGFP-Synpo2b3xSA and EGFP-Synpo2b3xSD fusion protein constructs and differentiated for six days. Cells were analyzed either without pacing (-EPS) or after 2 h of EPS (+EPS). All three constructs show a localization at Z-discs without EPS (B-D, -EPS). Differences were however obtained upon EPS, where Synpo2bWT and Synpob3xSA mainly remained localized to Z-discs, while only showing a slight association with lesions. In contrast, Synpo2b3xSD exhibited a strong tendency for redistribution to lesions (B-D, +EPS). Scale Bars: 10 µm.

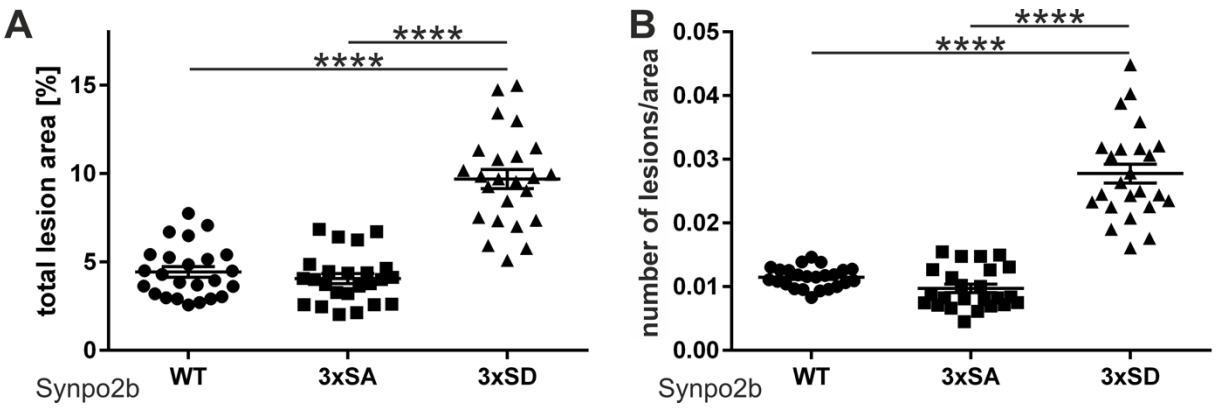

Figure 3.14: Quantitative analysis of phosphorylation state-dependent formation of mechanical stress-induced lesions in Synpo2b. After transfecting C2C12 cells with EGFP-Synpo2bWT, EGFP-Synpo2b3xSA and EGFP-Synpo2b3xSD fusion protein constructs, myotubes were differentiated for six days and microscopically analyzed after 2 h of EPS. Quantitative analysis of the total lesions area (A) and the number of lesions per area (B, area: pixel/µm) of each constructs demonstrate the significantly increased number of lesions in the cells transfected only with EGFP-Synpo2b3xSD mutant after EPS. Error bars represent the standard deviation of at least 25 analyzed images of at least three different experiments. The p-values were calculated using Student's t-test. ****: $p < 0.00001$.

Moreover, the smaller isoform Synpo2e (EGFP-Synpo2eWT/3xSA/3xSD) lacking the PDZ-domain, was transiently transfected into C2C12 cells, differentiated for six days, and analyzed before and after EPS. All analyzed constructs showed a strong localization to Z-discs, whereas only a slight association with lesions was observed without EPS (Figure 3.15 B-D, -EPS). Upon EPS they show localization at Z-discs and concomitantly a strong recruitment to lesions (Figure 3.15 B-D, +EPS). Lesion quantification of at least 25 images of transiently transfected EGFP-Synpo2eWT/3xSA/3xSD constructs showed a comparable amount of number of lesions per area (Figure 3.16 B). Small differences were obtained for the total lesion area, where Synpo2eWT seems to form more lesions compared to both phosphomimetic mutants (Figure 3.16 A). Taken together, these results imply the importance of a cyclic turnover between the phosphorylated and dephosphorylated state of Synpo2. To further understand the mechanism, specific analysis of the regulation by specific phosphatases and kinases would be necessary.

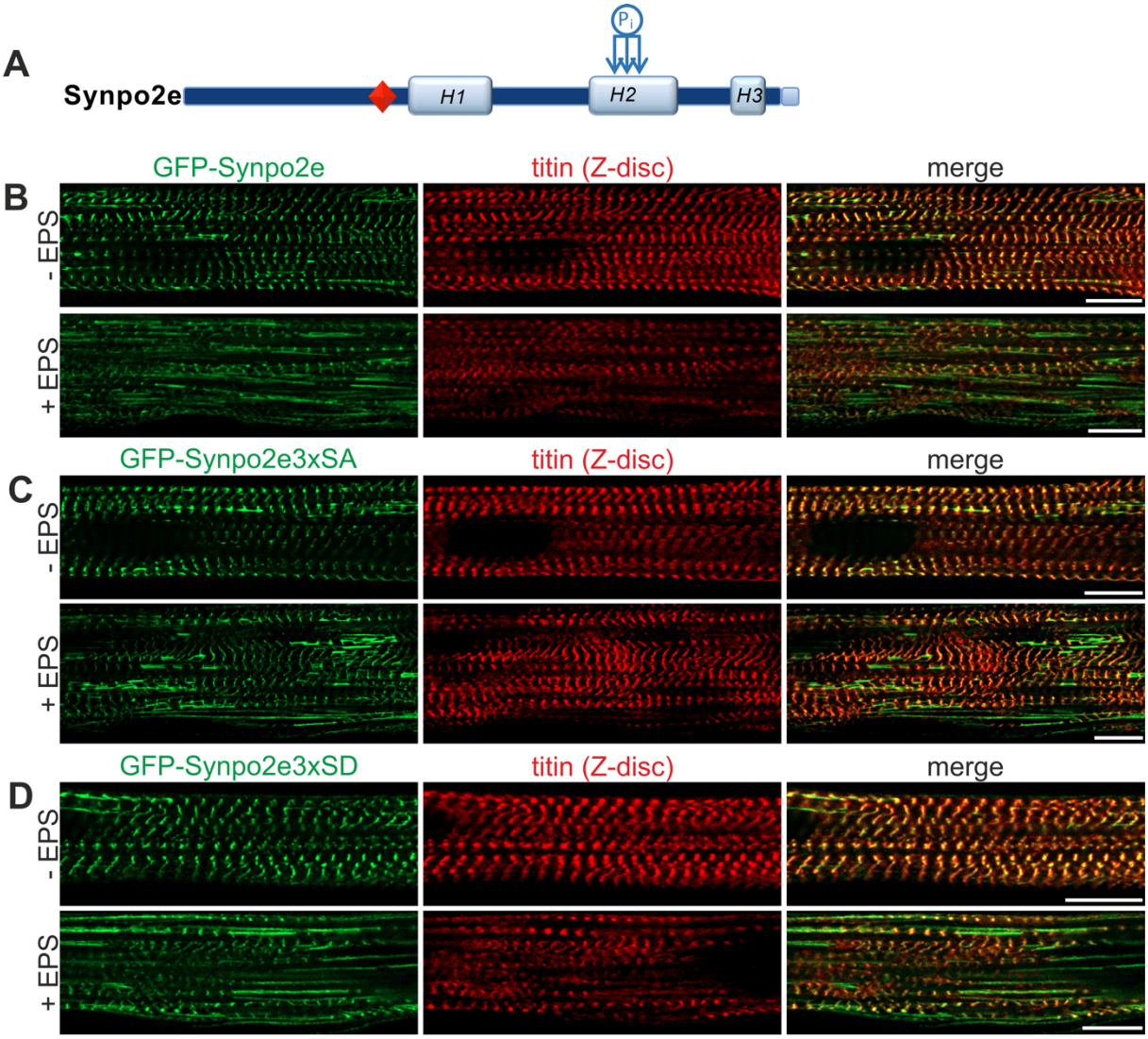

Figure 3.15: Triple phosphorylation in the H2 region has no impact in the localization of Synpo2e. (A) The triple phosphosite in the H2-region of Synpo2e is depicted in a schematic overview. (B-D) C2C12 myotubes transfected with EGFP-fusion proteins of Synpo2eWT, Synpo2e3xSA and Synpo2e3xSD and differentiated for six days. Cells were analyzed before and after 2 h of EPS. The WT as well as both phosphosite mutants were mainly localized at Z-discs and also in a few lesions (-EPS). Upon EPS Synpo2eWT/3xSA/3xSD were strongly redistributed to lesions (+EPS). Scale bars: 10 µm.

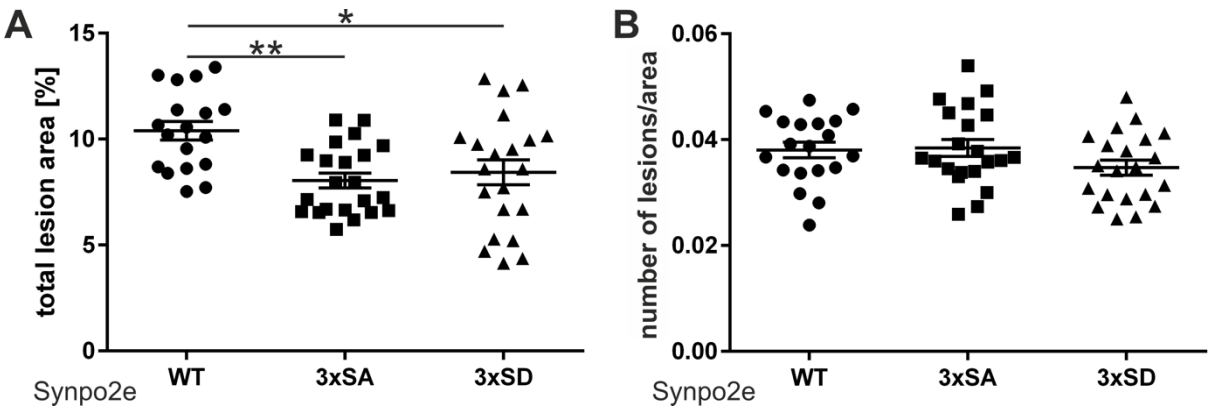

Figure 3.16: Quantitative analysis of phosphorylation state-dependent formation of mechanical stress-induced lesions in Synpo2e. C2C12 cells were transfected with EGFP-Synpo2eWT, EGFP-Synpo2e3xSA and EGFP-Synpo2e3xSD fusion proteins and differentiated for six days. Microscopic analysis was performed after 2 h of EPS (+EPS). (B) Quantitative analysis of the number of lesions per area showed no significant difference. (A) The total lesion area showed slight differences between Synpo2eWT and Synpo2e3xSA/3xSD. Error bars represent the standard deviation of at least 25 analyzed images of at least three different experiments. The p-values were calculated using Student's t-test. *: $p < 0.05$, **: $p < 0.001$.

3.6.3 Dynamics and mobility of Synpo2 are affected by phosphorylation in the H2

To further address the question how the triple phosphorylation in the H2 region impacts the biological function of Synpo2, I analyzed its influence on the mobility and dynamics of Synpo2b and Synpo2e. For this purpose, C2C12 cells were transiently transfected with EGFP-Synpo2b or EGFP-Synpo2e fusion constructs harboring the WT or the 3xSA or the 3xSD mutant. After six days of differentiation and an overnight EPS to achieve their mechanical adaptation (EPS setting: 10 V, 4 ms, 0.5 Hz), FRAP experiments were performed. All fusion proteins were found to be targeted to the Z-disc, with the Synpo2e fusion protein additionally located at myofibrillar lesions. Primarily defined Z-disc areas were bleached before the duration of fluorescence recovery was measured.

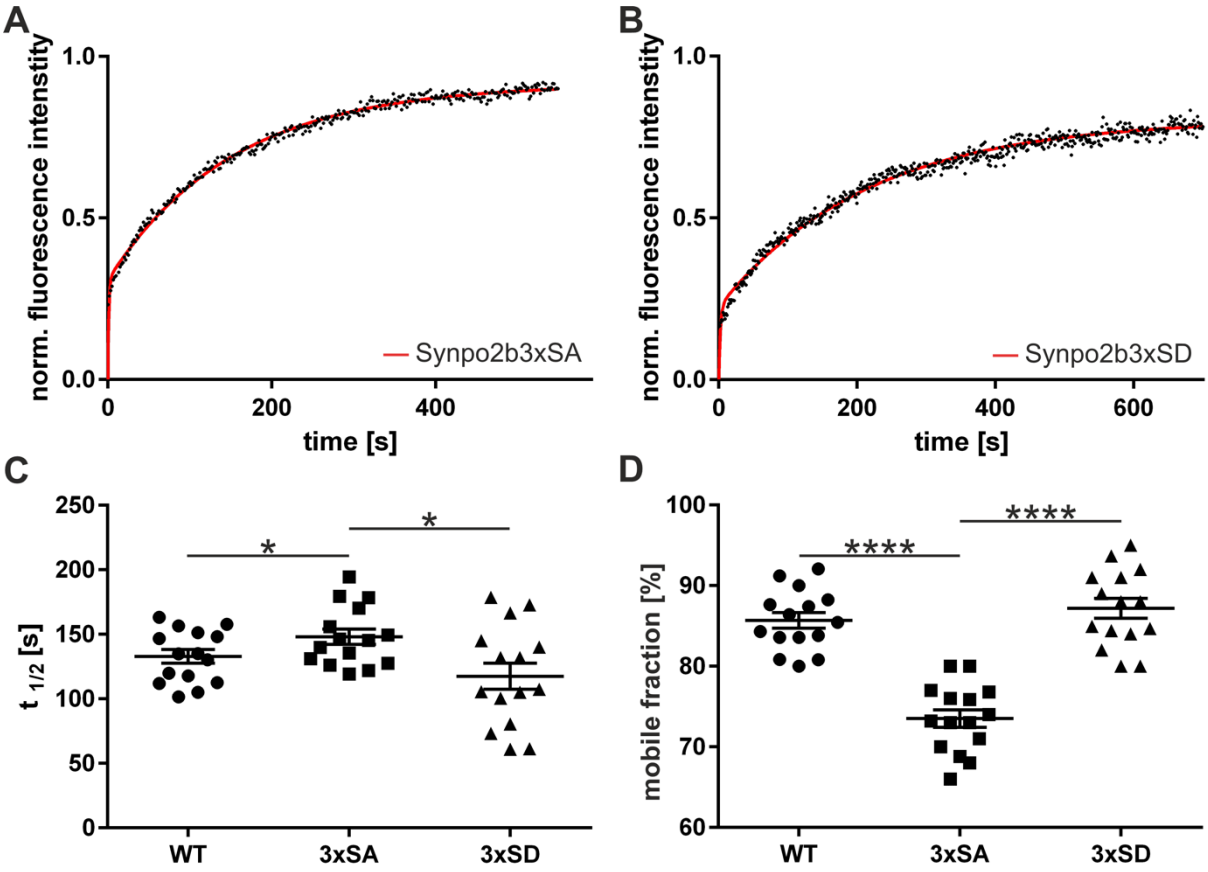

Figure 3.17: Synpo2b dynamics and mobility in Z-discs are altered in the absence of phosphorylation in the H2 region. Synpo2bWT, 3xSA mutant and 3xSD mutant were expressed as EGFP-fusion proteins in C2C12 cells, which were subsequently differentiated for six days. Recovery profiles followed a biphasic curve fit (A, B). FRAP measurements showed comparatively high dynamics and mobility of WT (128 s, 85 %) and 3xSD mutant (116 s, 87 %) Synpo2b in Z-discs. In contrast, significant differences were obtained for the dynamics and mobility of Synpo2b 3xSA (148 s, 73 %) compared to the WT (C, D). The error indicators show the standard deviation of at least four experiments each. The p-values were calculated using Student's t-test. *: $p < 0.05$, ****: $p < 0.00001$.

No significant differences in recovery times and mobile fractions were detected between Synpo2bWT and the Synpo2b3xSD mutant that mimics the phosphorylated state. I determined a half-life for the Z-disc regions of 128.1 s in Synpo2bWT-transfected cells and a comparable 116.5 s with the Synpo2b3xSD mutant. In contrast the half-life of Synpo2b3xSA, mimicking the dephosphorylated state, exhibited a significantly higher half-life with a mean of 148.7 s (Figure 3.17 A-C). Calculating the mobile fractions also revealed significant differences: The mobility of the Synpo2b3xSA mutants was found to be significantly reduced (73.5 %)

compared to the mobility of the Synpo2bWT (85.2 %) and Synpo2b3xSD (87.2 %) (Figure 3.17 D). Taken together, this data confirmed that the Synpo2b3xSA mutant is more stably anchored to the actin cytoskeleton compared to Synpo2b3xSD, which also showed a stronger redistribution to sarcomeric lesions (Figure 3.14 A, B).

FRAP experiments using the Synpo2e isoform, lacking the PDZ-domain, and its phosphosite mutants, also revealed significant differences. Here the half-life of the WT with a mean of 50 s was again similar to the Synpo2e3xSD mutant (mean: 48 s), whereas the Synpo2e3xSA mutant needed far longer times to recover (mean: 107.4 s). Conspicuous was also that the values of the half-life are very spread for the Synpo2e3xSA mutant, indicating that Synpo2e is more dynamic in the dephosphorylated state (Figure 3.18 A-C). No significant differences in mobile fractions could, however, be detected between WT and the two mutants (Figure 3.18 D).

As Synpo2e is also localized in lesions, FRAP studies were performed in lesions as well. Defined areas of lesions were bleached, and the regeneration time was measured. Again, the half-life values of the 3xSA mutant (160 s) showed a significantly longer regeneration time compared to the WT (75 s) and the 3xSD mutant (95 s) (Figure 3.19 A-C). Interestingly, the half-life values of Synpo2e3xSD in lesions were well grouped, compared to the values observed for Z-discs (compare Figure 3.18 C with Figure 3.19 C), indicating a reduced dynamic state in lesions.

Taken together, these results suggest that the Synpo2 3xSA mutant, mimicking the dephosphorylated state, has higher actin cytoskeleton binding affinity in both analyzed Synpo2 isoforms. Synpo2 3xSA has a significantly higher half-life value compared to the WT as well as the Synpo2 3xSD mutant (Figure 3.17 C, Figure 3.18 C). The mobile fraction of Synpo2e in the Z-discs is apparently not affected, indicating that the overall turnover rate remains the same, but is occurring more slowly in the dephosphorylated state. In reverse, this also suggests a reduced affinity to the cytoskeleton in the phosphorylated state of the investigated triple phosphosite in the H2 region.

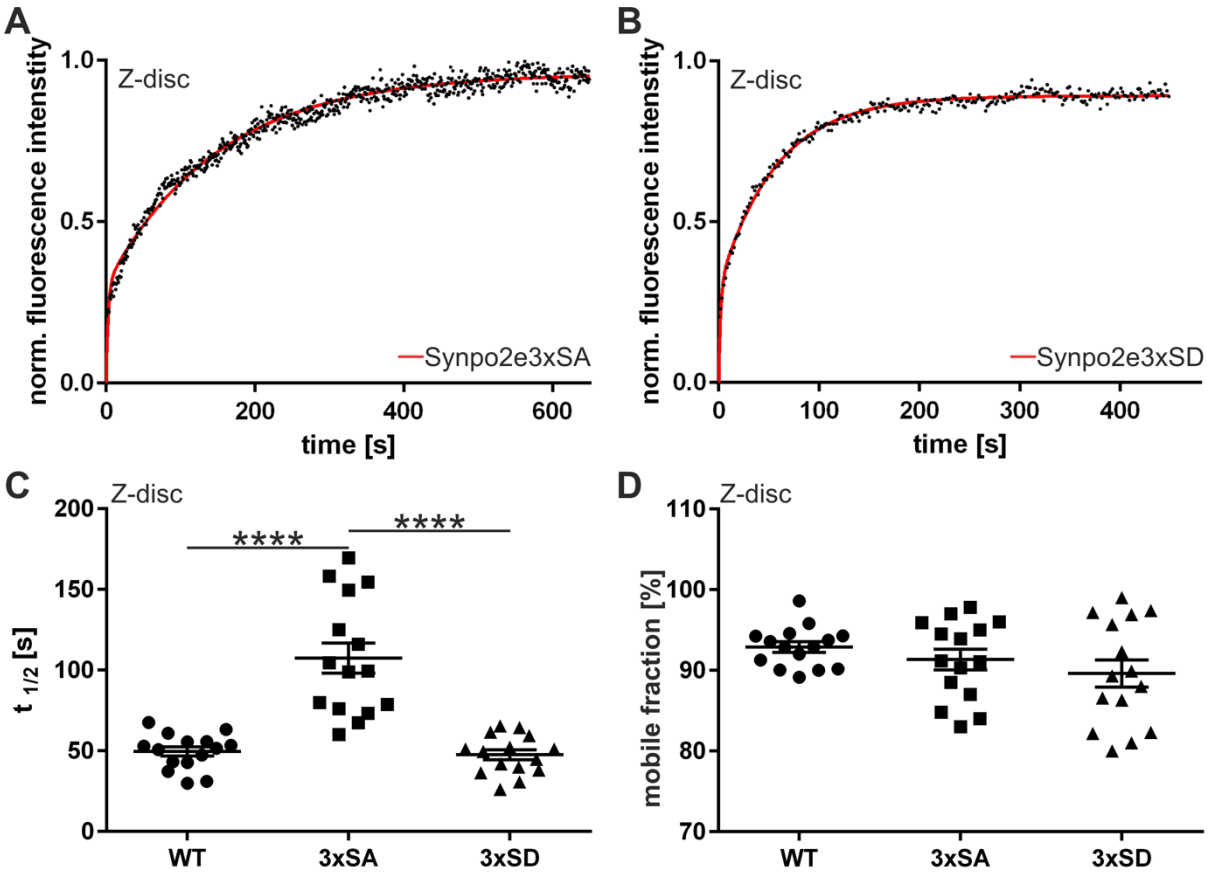

Figure 3.18: Phosphorylation in the H2 region impact the mobility and dynamics of Synpo2e in Z-discs. FRAP experiments in C2C12 cells transfected with Synpo2eWT, Synpo2e3xSA or Synpo2e3xSD mutants, respectively, and differentiated for six days. Recovery profiles followed a biphasic curve fit (A, B). (C) Analysis of the FRAP experiment with using GraphPad Prism showed a significantly higher recovery time for Synpo2e3xSA (107 s) compared to Synpo2eWT (50 s) and Synpo2e3xSD (48 s) in Z-disc. (D) No differences were obtained for the mobile fraction of the three constructs in the Z-disc. The error indicators show the standard deviation of 15 FRAP assays from at least four individual experiments each. The p-values were calculated using Student's t-test. ****: $p < 0.00001$.

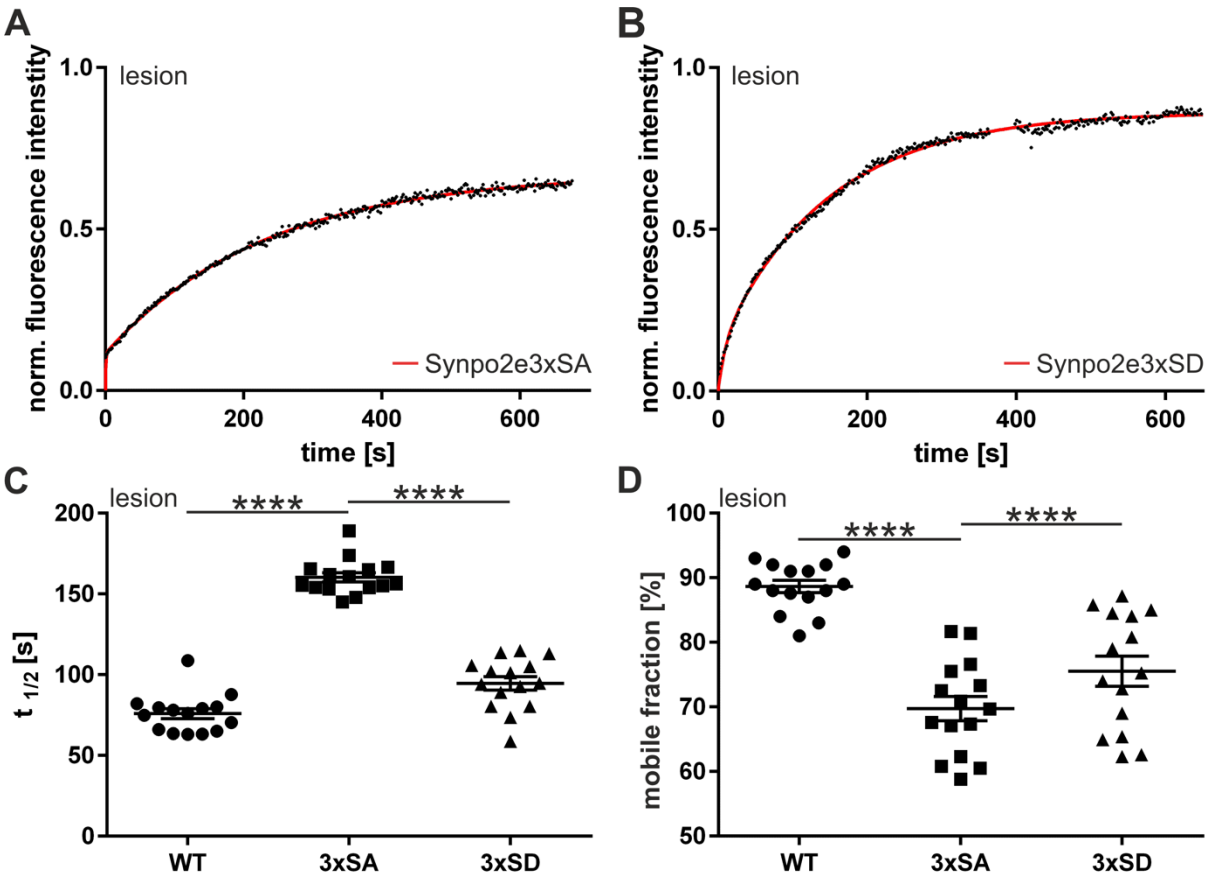

Figure 3.19: Phosphorylation in the H2 region impact the mobility and dynamics of Synpo2e in lesions. FRAP experiments in C2C12 cells transfected with Synpo2eWT, or Synpo2e3xSA or Synpo2e3xSD mutants, respectively, and differentiated for six days. Recovery profiles followed a biphasic curve fit (A, B). (C) Analysis of the FRAP experiment with using GraphPad Prism showed a significantly higher recovery time of Synpo2e3xSA (160 s) than in Synpo2eWT (75 s) and Synpo2e3xSD (95 s) in lesions. (D) The mobility of Synpo2e3xSA in the lesions is significantly lower. The error indicators show the standard deviation of 15 FRAP assays from at least four individual experiments each. The p-values were calculated using Student's t-test. ****: $p < 0.00001$.

3.7 Analysis of Synpo2 LC3-binding region (LIR)

The involvement of Synpo2 in autophagy prompted us to investigate if it might also directly interact with ATG8 family members, which are central proteins in autophagy. In mammals this protein family is encoded by 7 genes (LC3A – giving rise to two splice variants, LC3B, LC3B2 – with only one amino acid difference to LC3B, LC3C, GABARAP, GABARAPL1 and GABARAPL2), which can be grouped in the LC3 and GABARAP subfamilies (Jatana *et al.*, 2019). Both subfamily members, LC3 and GABARAP proteins, are associated to the phagophore membrane and upon association they serve as scaffold proteins to recruit diverse proteins. Most of those protein interactions with the ATG8 family members is mediated by a LIR motif. The canonical core LIR motif is $(W/F/Y)_0$-X_1-X_2-$(L/I/V)_3$ with an aromatic amino acid residue in position zero and a hydrophobic residue in position three. Furthermore, a high frequency of acidic residues (E or D) was described to be preferred in positions neighboring the core LIR motif (Johansen and Lamark, 2011). Interestingly, sometimes serine/threonine residues which can be phosphorylated are detected adjacent to the core sequence as well. These residues can affect the acidity depending on the phosphorylation state (Wild *et al.*, 2011).

Analysis of the Synpo2 sequence using iLIR, a web resource for prediction of Atg8-family interacting proteins (Kalvari et al., 2014; http://repeat.biol.ucy.ac.cy/iLIR/), revealed an interesting sequence motif (EDYLSL) fulfilling the LIR motif requirements (Synpo2b AA 733-738), with an aromatic amino acid at position zero (Y), a hydrophobic residue in position three (L), two acidic residues (E and D) at position minus one and minus two, as well as a serine residue which can be phosphorylated at position two of the core LIR motif. The latter described serine residue was also found in the Synpo2 phosphosite list of the previously described phosphoproteomic analysis received from B. Warscheid (unpublished work, University of Freiburg/ University of Würzburg, see Table.1.1). In addition, the program PONDR ("Predictor of Natural Disordered Regions", http://www.pondr.com) revealed an unstructured anchor sequence flanking the EDYLSL motif, which strengthened the probability of the LIR prediction. An NCBI BLAST search even showed that the sequence SGPEED**YLSL**GAEAC is 100 % conserved in Synpo2 sequences across all vertebrates (Figure 3.20). In contrast, a sequence alignment of the Synpo2 sequence with synaptopodin and Synpo2l sequences showed that the canonical tyrosine residue is not present in the latter two proteins, indicating a fundamental difference of the podin family proteins with respect to LIR binding (Figure 3.21).

```
Human (Homo sapiens)                SGPEEDYLSLGAEAC
Bovine (Bos taurus)                 SGPEEDYLSLGAEAC
Sheep (Ovis aries)                  SGPEEDYLSLGAEAC
Goat (Capra hircus)                 SGPEEDYLSLGAEAC
Dog (Canis familiaris)              SGPEEDYLSLGAEAC
Horse (Equus caballus)              SGPEEDYLSLGAEAC
Lion (Panthera leo)                 SGPEEDYLSLGAEAC
Mouse (Mus musculus)                SGPEEDYLSLGAEAC
Rat (Rattus norvegicus)             SGPEEDYLSLGAEAC
Guinea pig (Cavia porcellus)        SGPEEDYLSLGAEAC
Chicken (Gallus gallus)             SGPEEDYLSLGAEAC
Frog (Rana temporia)                SGPEEDYLSLGAEAC
Turbot (Scophthalmus maximus)       SGPEEDYLSLGAEAC
Fantail (Rhipidura dahli)           SGPEEDYLSLGAEAC
```

Figure 3.20: Sequence alignment of NCBI blast search of Synpo2 LIR motif. The NCBI blast search showed a 100 % conserved Synpo2 sequence SGPEED**YLSL**GAEAC across all vertebrates.

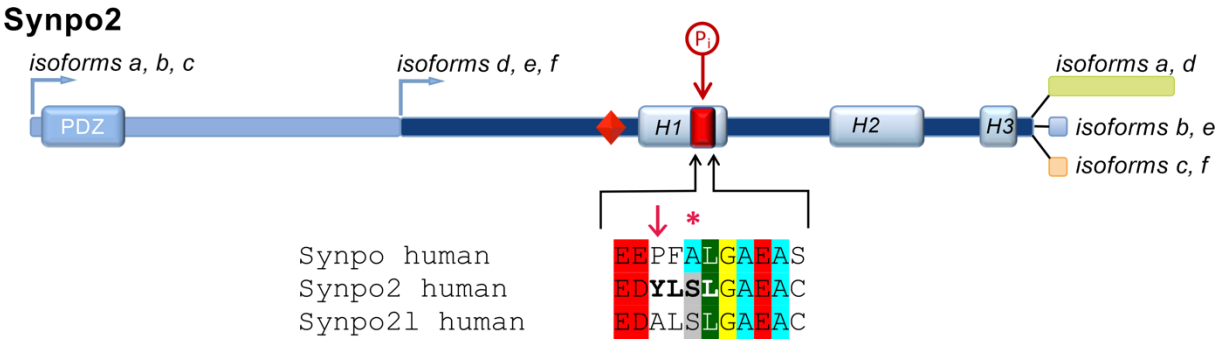

Figure 3.21: Sequence alignment of Synpo2 LIR sequence with Synpo and Synpo2l. The alignment depicts that the canonical tyrosine residue of the LIR core sequence is not present in Synpo and Synpo2l.

3.7.1 Phosphorylation-induced interaction of Synpo2 with LC3B

To functionally characterize the identified LIR motif in Synpo2, more specifically the phosphosite (Synpo2b: S737, Synpo2e: S342) found within this motif, peptide array analyses were performed. For this purpose, the following short synthetic peptide of Synpo2 containing the LIR motif attached to a cellulose membrane was used: GDSGPE**EDYLSL**GAEACN (Synpo2b AA 727-744; the core motif is emphasized by bold letters). To investigate the importance of each of the amino acids of the core motifs, peptides were synthesized, in which each of these amino acids was mutated to alanine. In addition, a peptide was made, in which

serine 737 (i.e., the residue identified in the EPS-dependent phosphoproteome study) was mutated to aspartic acid to mimic the phosphorylated state. Two further peptides served as positive controls: the peptide NCSGGDDDWTHLSSKEVD of sequestosome-1 (SQSTM1), a ubiquitin-binding protein, and AGVPPLEDFEVLDGVEDA from FKBP8. This peptide array was probed with recombinant GST-LC3B, and binding was detected with anti-GST antibodies. Both control peptides yielded strongly positive signals, assuring that the assay worked correctly. LC3B did, however, not bind to the Synpo2 WT peptide. Likewise, the point mutation of each AA of the core sequence to alanine did not show binding of LC3B. In contrast, strong binding of Synpo2 to LC3B was identified in the mutated peptide of the Synpo2, in which serine 737 (Synpo2b) was mutated to aspartic acid. The reaction was even considerably stronger than the one with the SQSTM-derived control peptide (Figure 3.22). This suggests an interaction of Synpo2 and LC3B that is induced by mechanical stress-dependent phosphorylation.

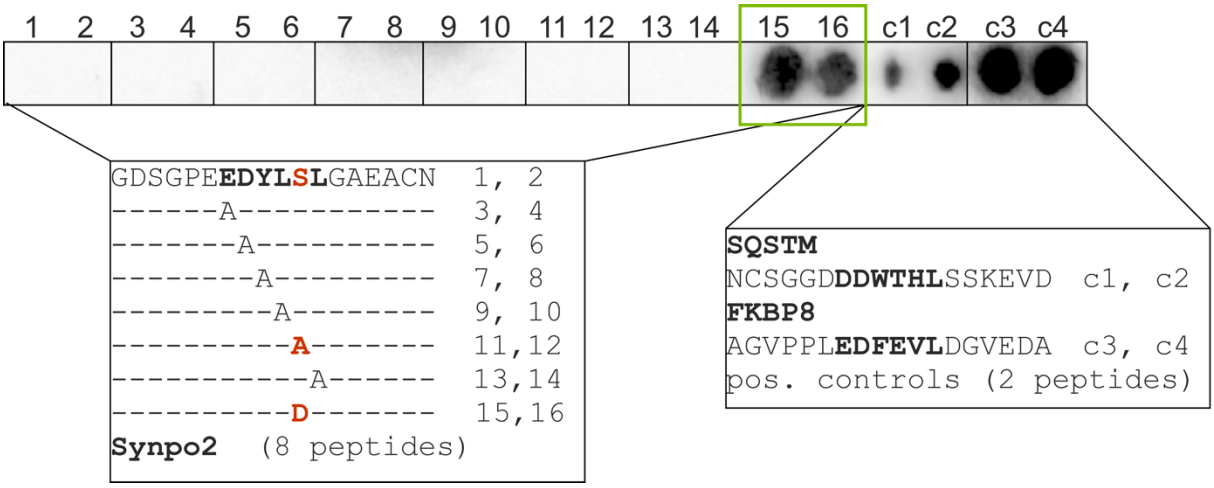

Figure 3.22: The interaction of Synpo2 with LC3B is induced by phosphorylation. An array was performed using a membrane spotted with 18 amino acids peptides covering the Synpo2 LIR motif, peptides containing point mutations of the six amino acids indicated to alanine, as well as a peptide containing a serine - aspartate point mutation mimicking the phosphorylated state of this residue. Two peptides covering documented LIR motifs from SQSTM and FKBP8 served as positive controls. Each peptide was attached twice to the cellulose membrane. Peptide positions are indicated above the array and peptide sequences are shown in the boxes. The array was overlayed with GST-LC3B, and binding was detected using an anti-GST antibody. Strong positive signals were obtained with both control peptides (spots c1 to c4), as well as with the Synpo2 peptide containing the serine to aspartic acid mutation within the LIR core motif (Ser737 in Synpo2b, Ser342 in Synpo2e) mimicking a phosphorylated state (spots 15, 16).

3.7.2 Confirmation of the binding of Synpo2 and LC3B using BiFC

To analyze the phosphosite that is required for the binding of Synpo2 to LC3B in a cell- based assay, two mutants were generated (LIRmut, Table 3.1). Serine 737 in Synpo2b was exchanged to alanine or to aspartate, respectively, to analyze either the dephosphorylated or a constitutively phosphorylated state. BiFC was used to investigate the interaction between LC3B and Synpo2 in contracting myotubes. For the implementation of this experiment, different BiFC combinations were cloned for a transient double transfection of C2C12 cells. Both proteins were fused to one of the two complementary non-fluorescent fragments of a fluorescent protein and only an interaction of both proteins should result in a microscopically detectable BiFC signal (Kerppola, 2006). The Venus1 construct (AA 1-154) and the Venus2 construct (AA 155-238) were expressed at both the N- and C-terminus of LC3B and Synpo2, resulting in eight different possible combinations.

C2C12 myotubes were transiently transfected with the different combinations, followed by differentiation for six days. Successful complementation was detected in both Venus1C-LC3B and Venus1N-LC3B in combination with Venus2N-Synpo2b and Venus2N-Synpo2e, confirming the binding of both Synpo2 isoforms to LC3B in cells. Since LC3B is a small protein with a predicted molecular mass of 14.6 kDa the observed signal with the vector on both sites of the protein is comprehensible.
The Synpo2b-LC3B complex showed a localization at Z-discs and in vesicular structures (Figure 3.23 -EPS). After EPS the complex remained localized at Z-discs, vesicular structures and in addition partially to lesions (Figure 3.23 +EPS). In a similar way, the Synpo2e-LC3B complex (i.e., with the Synpo2 isoform lacking the PDZ-domain) displayed a localization mainly at Z-discs and partially in lesions (arrow heads), as well as in vesicular structures (arrows) without EPS (Figure 3.24 -EPS). Upon EPS-induced contractions the Synpo2e-LC3B complex was most strongly detected in lesions and to a lower extent at Z-discs (Figure 3.24 +EPS).

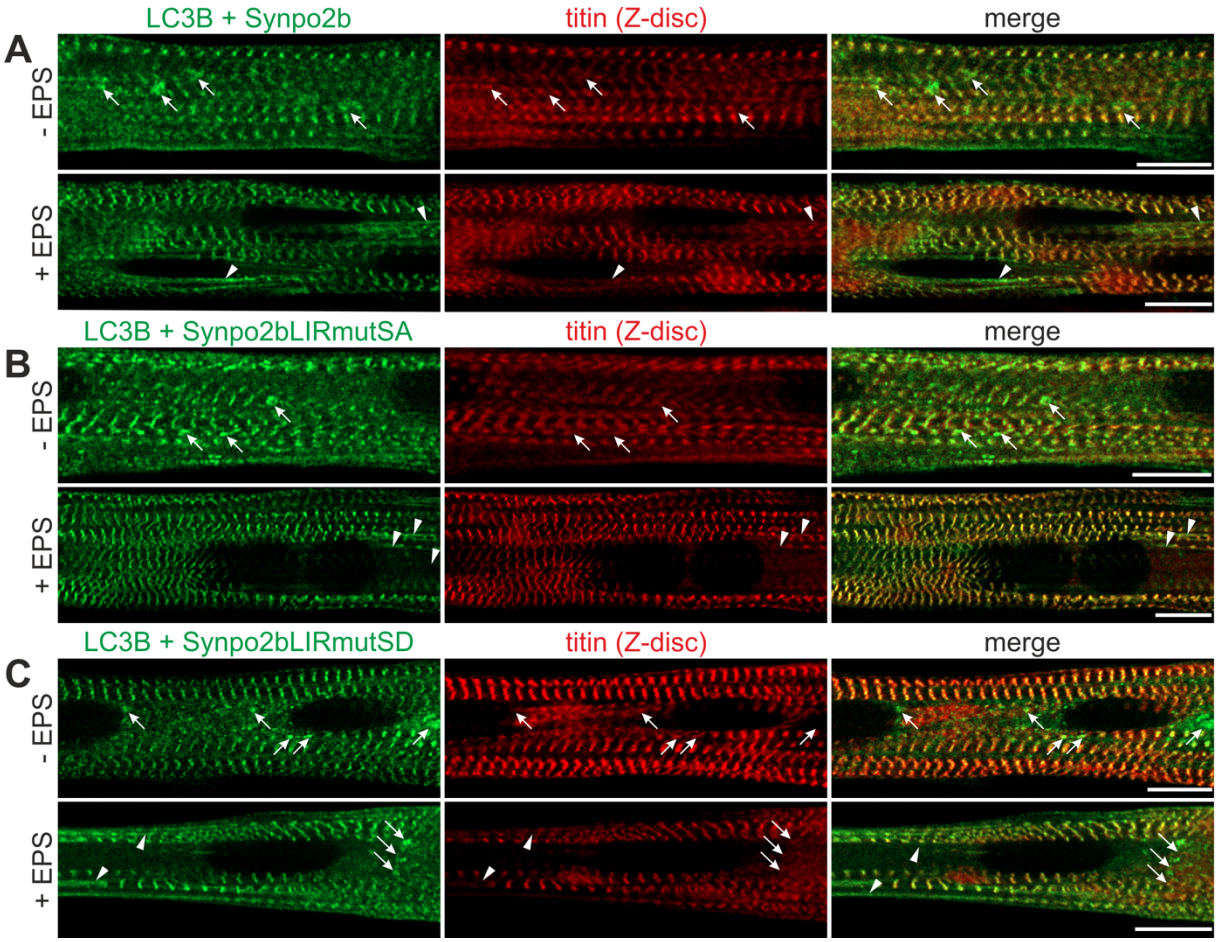

Figure 3.23: Confirmation of the interaction of LC3B with Synpo2b at the subcellular level. BiFC experiments in C2C12 myotubes, co-transfected with Venus1C-LC3B and (A) Venus2C-Synpo2bWT, (B) Venus2C-Synpo2bLIRmutSA, or (C) Venus2C-Synpo2bLIRmutSD, either untreated (panels labeled with -EPS) or after EPS (panels labeled with +EPS) indicate an interaction of LC3B and all Synpo2b constructs at Z-discs. Furthermore, a BiFC signal indicating the interaction of both proteins was detected in vesicular structures (arrows). In addition, a localization in lesions was detected in EPS-treated cells in all three combinations (arrow heads, +EPS). Scale bars: 10 µm.

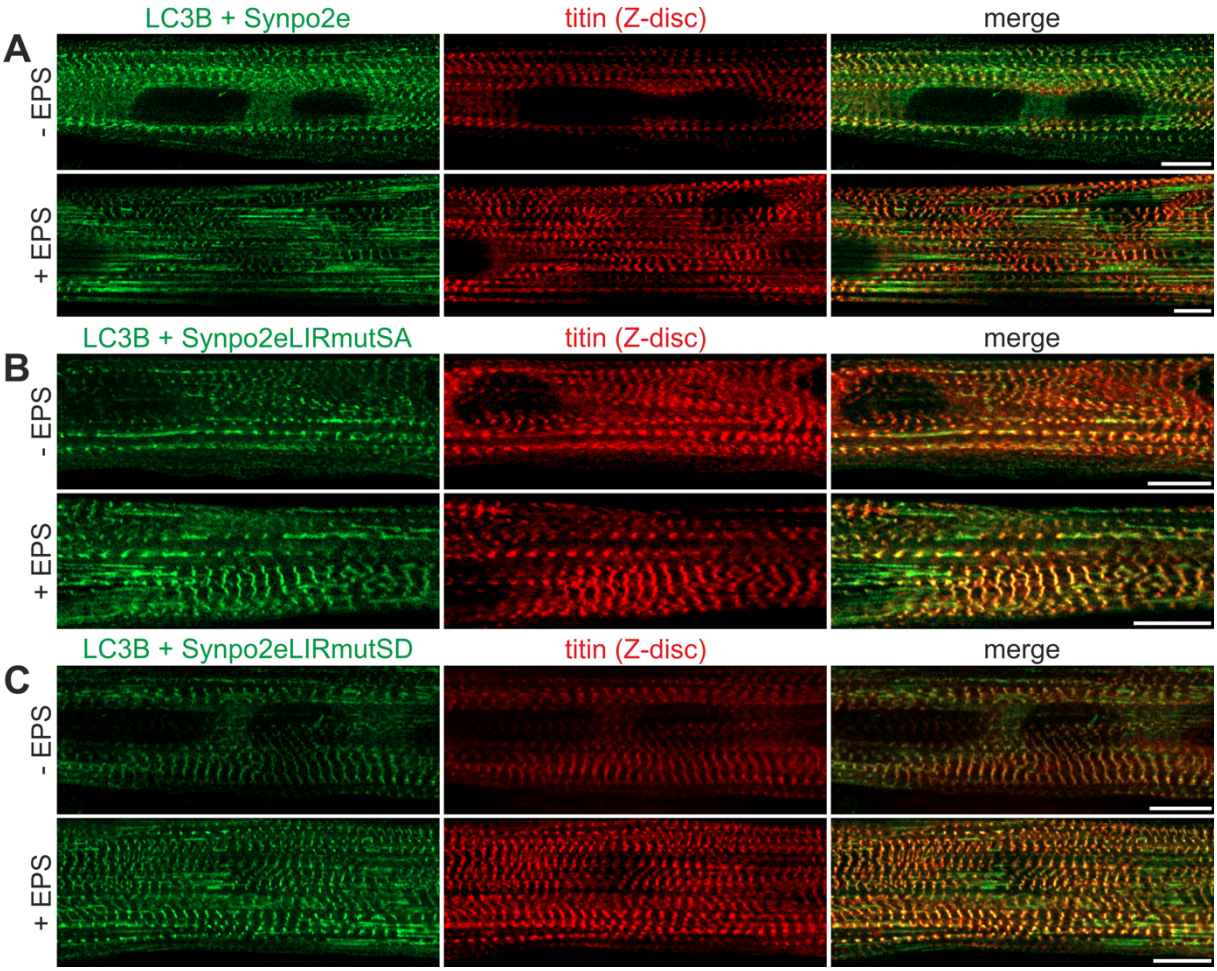

Figure 3.24: BiFC experiments confirming the interaction of Synpo2e with LC3B in skeletal muscle cells. C2C12 cells were double transfected with Venus1C-LC3B plus Venus2C-Synpo2e, or Venus2C-Synpo2eLIRmutSA or Venus2C-Synpo2eLIRmutSD and differentiated for six days. Fluorescent Synpo2e-LC3B complexes are clearly evident at Z-discs and to a lower degree in lesions (-EPS). Upon EPS, the complexes are more strikingly localized in sarcomeric lesions (+EPS). Scale bars: 10 μm.

3.7.3 Isoform-specific localization of LIR phosphomutants

The next set of experiments aimed at further investigating a potential impact of the phosphorylation state of the phosphosite in the LIR motif on the subcellular localization of Synpo2 alone, particularly upon mechanical stress induced by EPS. For this purpose, C2C12 cells were transiently transfected with EGFP-fusion proteins of Synpo2b LIR mutants, differentiated for six days and analyzed before and after EPS. The cells were microscopically analyzed without further treatment or after EPS-induced contractions. Here, the PDZ-containing Synpo2b isoform showed an association to Z-discs and vesicular structure with all constructs tested (EGFP-Synpo2bWT/LIRmutSA/LIRmutSD) in an untreated state (Figure 3.25 B-D, -EPS). Differences became evident upon EPS: the EGFP-Synpo2bWT protein remained localized at Z-discs, whereas both EGFP-Synpo2bLIRmutSA and EGFP-Synpo2bLIRmutSD in addition showed a clear association with vesicular structures (arrows) (Figure 3.25 B-D, +EPS).

Moreover, the smaller isoform Synpo2e (EGFP-Synpo2eWT/LIRmutSA/LIRmutSD) lacking the PDZ-domain, was also transiently transfected into C2C12 cells, and differentiated for six days. Microscopic investigations were performed with untreated as well as EPS-treated cells. In the untreated cells, transfected EGFP-Synpo2eWT and EGFP-Synpo2eLIRmutSA were detected mainly at Z-discs and partially in lesions. Interestingly, the EGFP-Synpo2eLIRmutSD was not only localized at Z-discs but also remarkably distinctly in vesicular structures (Figure 3.26 D, arrows). Upon EPS, all constructs showed a localization to Z-discs and a striking recruitment to lesions (Figure 3.26 B-D, +EPS).

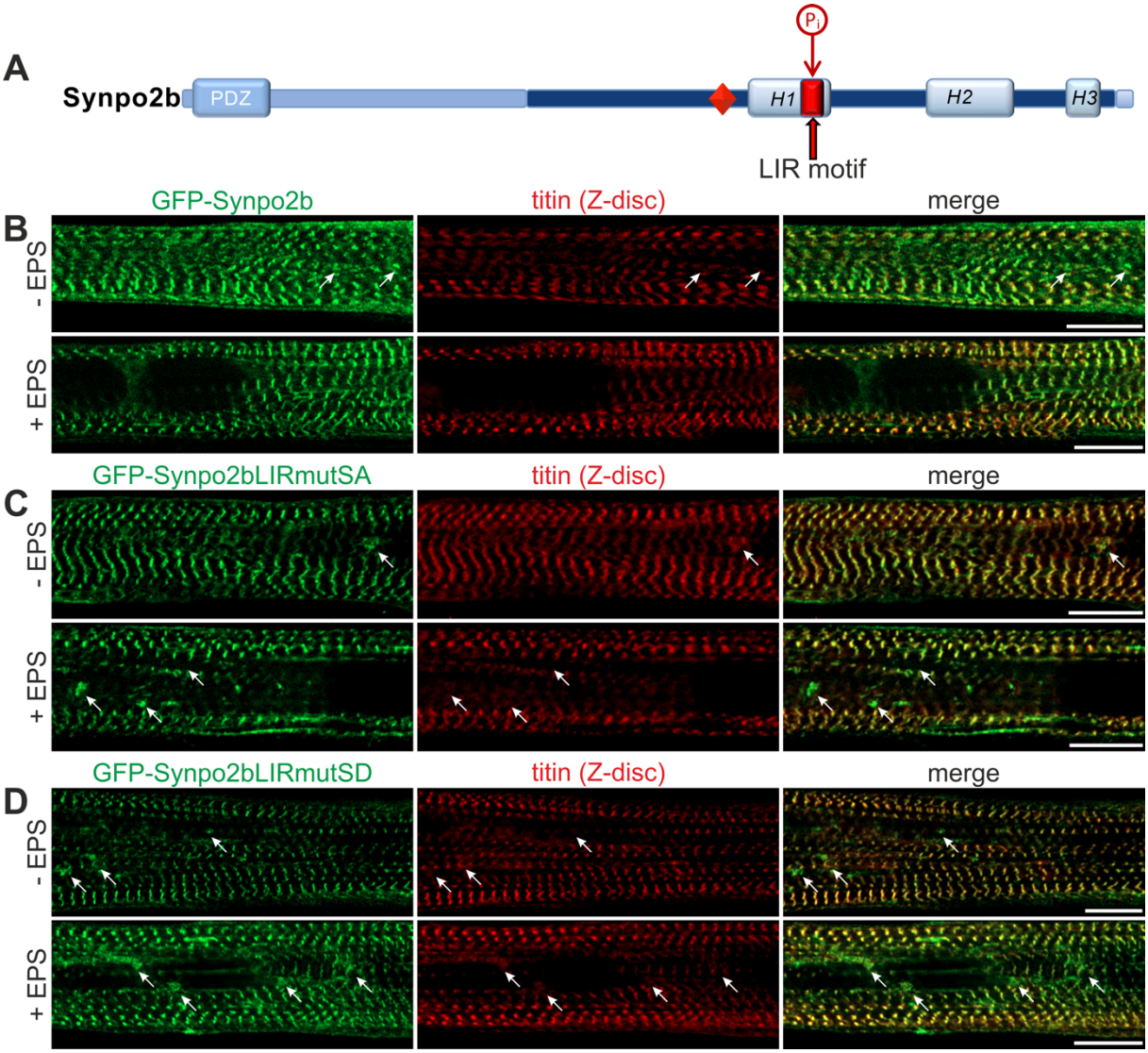

Figure 3.25: Subcellular localization of Synpo2b WT and LIR mutants before and after EPS. (A) Layout of Synpo2b with the LIR motif marked with the red rectangle. The serine residue (S737) mutated to alanine (LIRmutSA) or aspartic acid (LIRmutSD) is marked with a red arrow. (B-D) Both mutants localize to Z-disc and vesicular structures upon transient expression in C2C12 myotubes (-EPS). After 2h EPS of the transfected cells, all three contructs remained localized to Z-discs and in addition the two mutants localized to vesicular structures (+EPS). Scale bars: 10 µm.

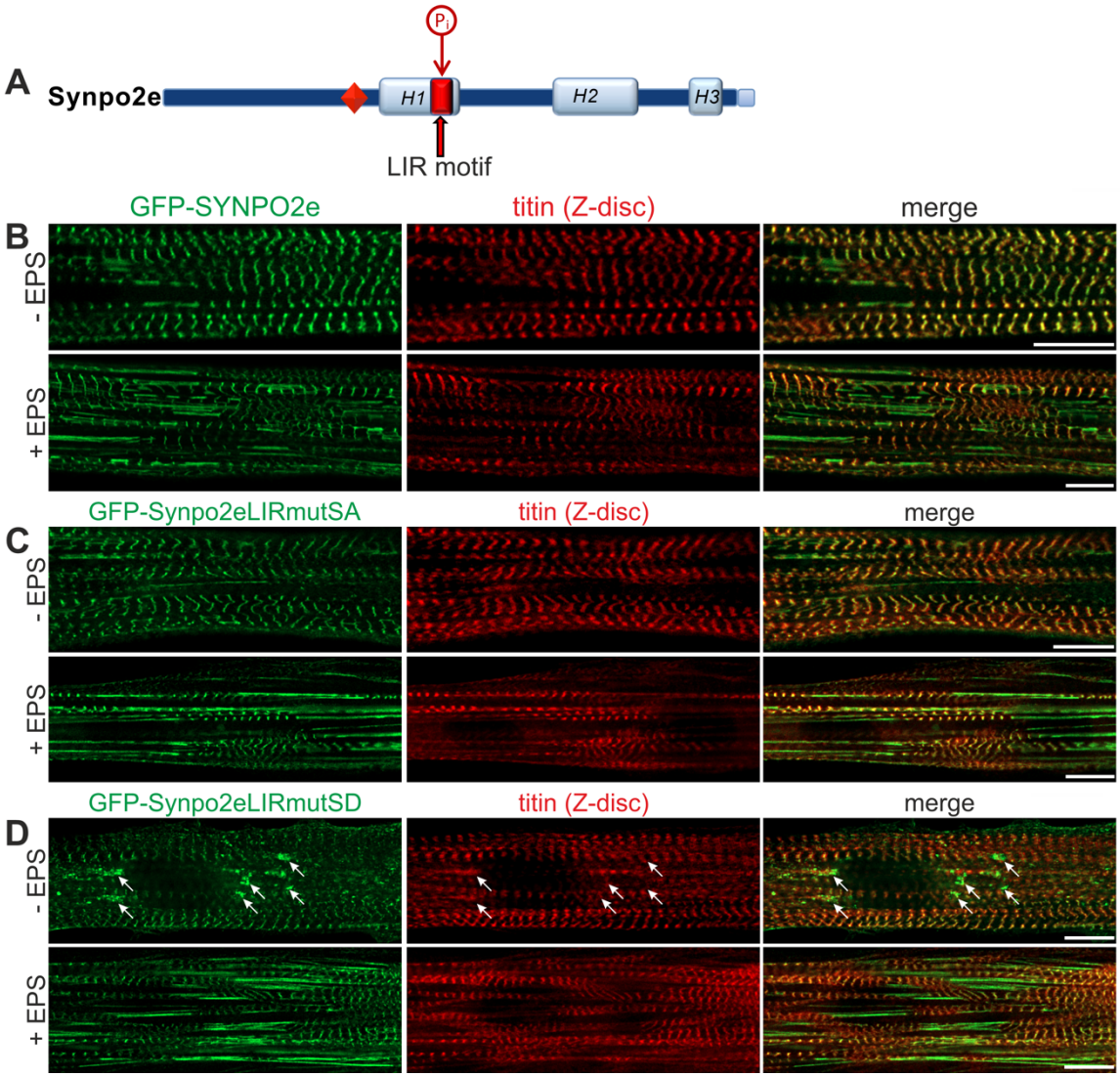

Figure 3.26: Subcellular localization of Synpo2e WT and LIR mutants before and after EPS. (A) Layout of Synpo2e with the LIR motif marked by a red rectangle. The serine residue (S342) mutated to either alanine (LIRmutSA) or aspartic acid (LIRmutSD) is denoted with a red arrow. After transient transfection into C2C12 cells, the WT construct and the LIRmutSA localize at Z-discs and partially in lesions (B, C, -EPS). In contrast, the LIRmutSD shows a noticeable localization in vesicular structures (arrows) in addition to its Z-disc localization (D, -EPS). Consecutive EPS of transfected cells induces efficiently higher localization to lesions in all three constructs (+EPS). Scale bars: 10 µm.

Further on it was interesting to see the localization of Synpo2 isoforms b and e and LC3B in myoblasts. For this purpose, C2C12 cells expressing mCherry-LC3B were transiently transfected with EGFP-fusion proteins of Synpo2b and Synpo2e and analyzed after reaching a confluency of 100 % without differentiation. Both Synpo2 isoforms as well as LC3B depicted a localization to vesicular structures in the C2C12 myoblasts (Figure 3.27, arrows).

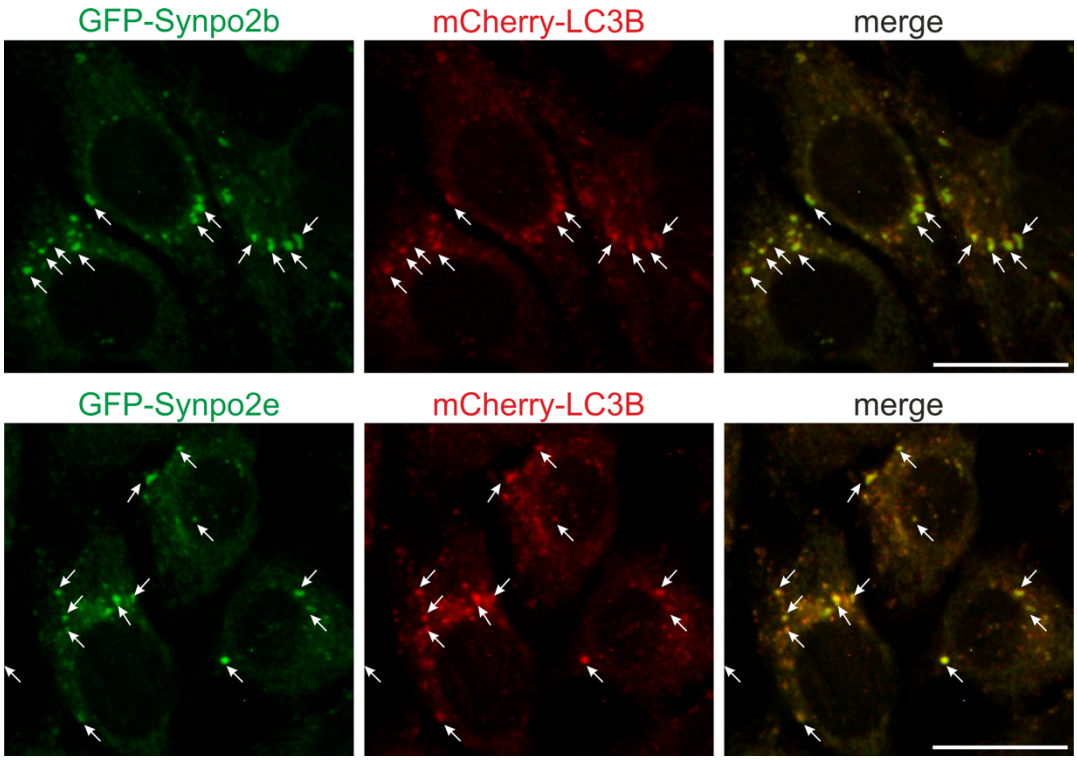

Figure 3.27: Localization of Synpo2 isoforms and LC3B in C2C12 myoblasts to vesicular structure. The C2C12 myoblasts expressing mCherry-LC3B transfected with EGFP-fusion proteins of Synpo2b and Synpo2e were analyzed after reaching a confluency of 100 %. Synpo2b, Synpo2e as well as LC3B depicted a localization to vesicular structure (arrows) in the myoblasts. Scale bars: 10 µm.

3.7.4 The phosphosite in the Synpo2b LIR motif influences protein mobility and dynamics

The findings that the phosphorylation in the LIR motif of Synpo2 regulates the binding to LC3 and influences its localization, demanded to further analyze whether the phosphosite in the LIR motif also has a direct impact on the molecular mobility and dynamics of Synpo2b and Synpo2e. For this purpose, C2C12 cells were transiently transfected with an EGFP-Synpo2b and EGFP-Synpo2e fusion constructs (WT, LIRmutSA and LIRmutSD), followed by differentiation for six days. FRAP experiments were performed after overnight EPS to achieve

mechanical adaptation of the cells (EPS setting: 10 V, 4 ms, 0.5 Hz). Defined Z-disc areas were bleached, and the duration of fluorescence regeneration was measured.

No significant differences in half-life and mobile fractions were detected between Synpo2bWT and the Synpo2bLIRmutSD that mimics the phosphorylated state. The half-lives were 129 s in cells transfected with the Synpo2bWT construct and 126 s in the cells transfected with the Synpo2bLIRmutSD construct, i.e., essentially identical. In contrast, the half-life of 93 s obtained in cells transfected with the Synpo2bLIRmutSA construct, mimicking the dephosphorylated state, was significantly lower (Figure 3.28 A-C). This data predicts slower turnover of Synpo2b upon dephosphorylation of the serine residue at amino acid position 737. No significant differences were obtained for the values of the mobile fractions, which indicates that the turnover rate of all three constructs remained the same (Figure 3.28 D).

In contrast to Synpo2b, the smaller isoform Synpo2e lacking the PDZ-domain did not show significant differences in mobility and dynamics in cells transfected with the three corresponding constructs (Synpo2eWT, Synpo2eLIRmutSA, Synpo2eLIRmutSD), both in Z-discs (Figure 3.29) and in lesions (Figure 3.30). This indicated that neither the mobility nor the dynamics of Synpo2e are influenced by the phosphorylation state of the phosphosite (S342) in the LIR motif.

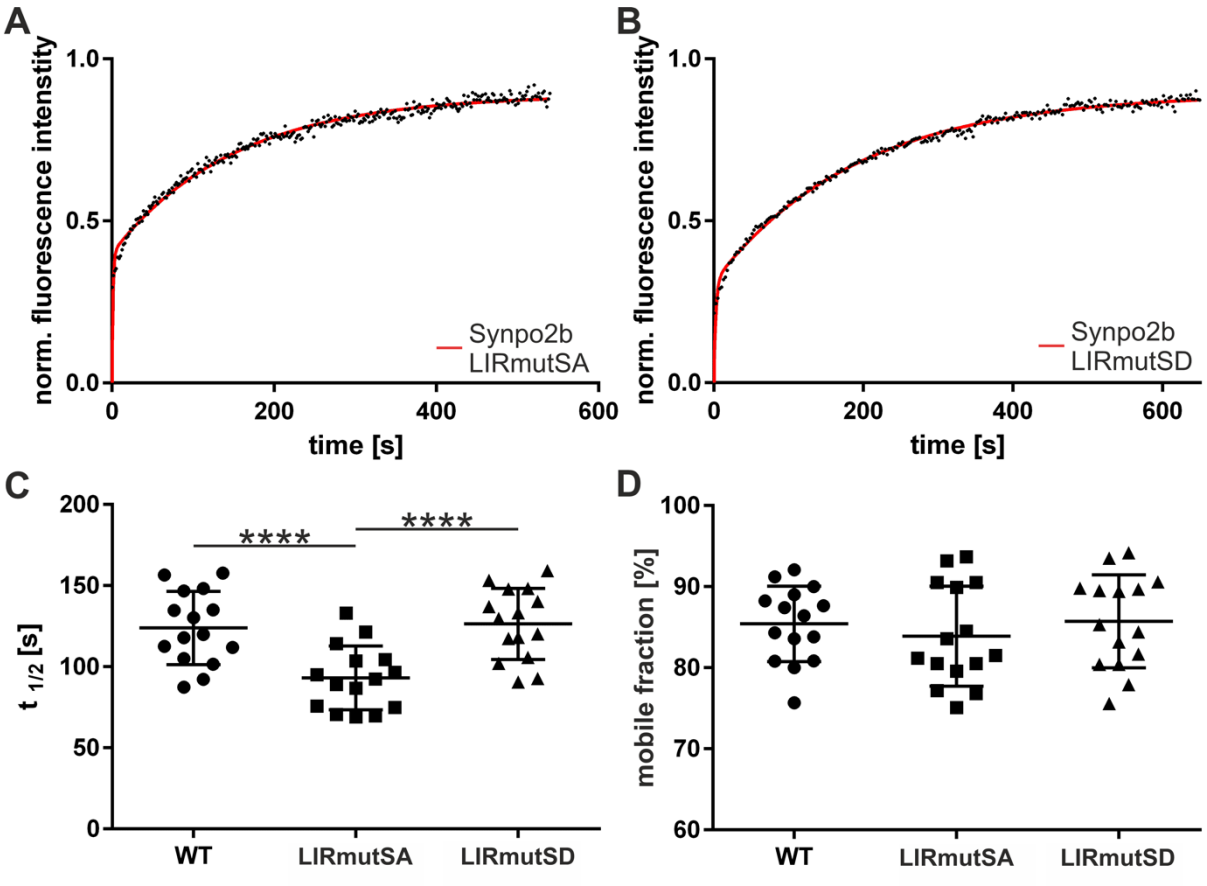

Figure 3.28: FRAP analysis of Synpo2b WT and LIR motif phosphosite mutants. FRAP experiments were performed in C2C12 myotubes overexpressing either EGFP-Synpo2bWT, EGFP-Synpo2bLIRmutSA (mimicking a constitutively unphosphorylated state) or EGFP-Synpo2bLIRmutSD (reflecting a constitutively phosphorylated state). Myotubes were differentiated for six days and mechano-adapted by EPS. The biphasic course of the curves (red line) shows a significantly shorter half-life for Synpo2b LIRmutSA (93 s) in bleached Z-discs (A, C) compared to both WT (129 s) and LIRmutSD (126 s) (B, C). The mobile fractions of all three construct do not differ (D). Error indicator shows the standard deviation of 15 FRAP assays from at least four individual experiments each. The p-values were calculated using Student's t-test. ****: $p < 0.00001$.

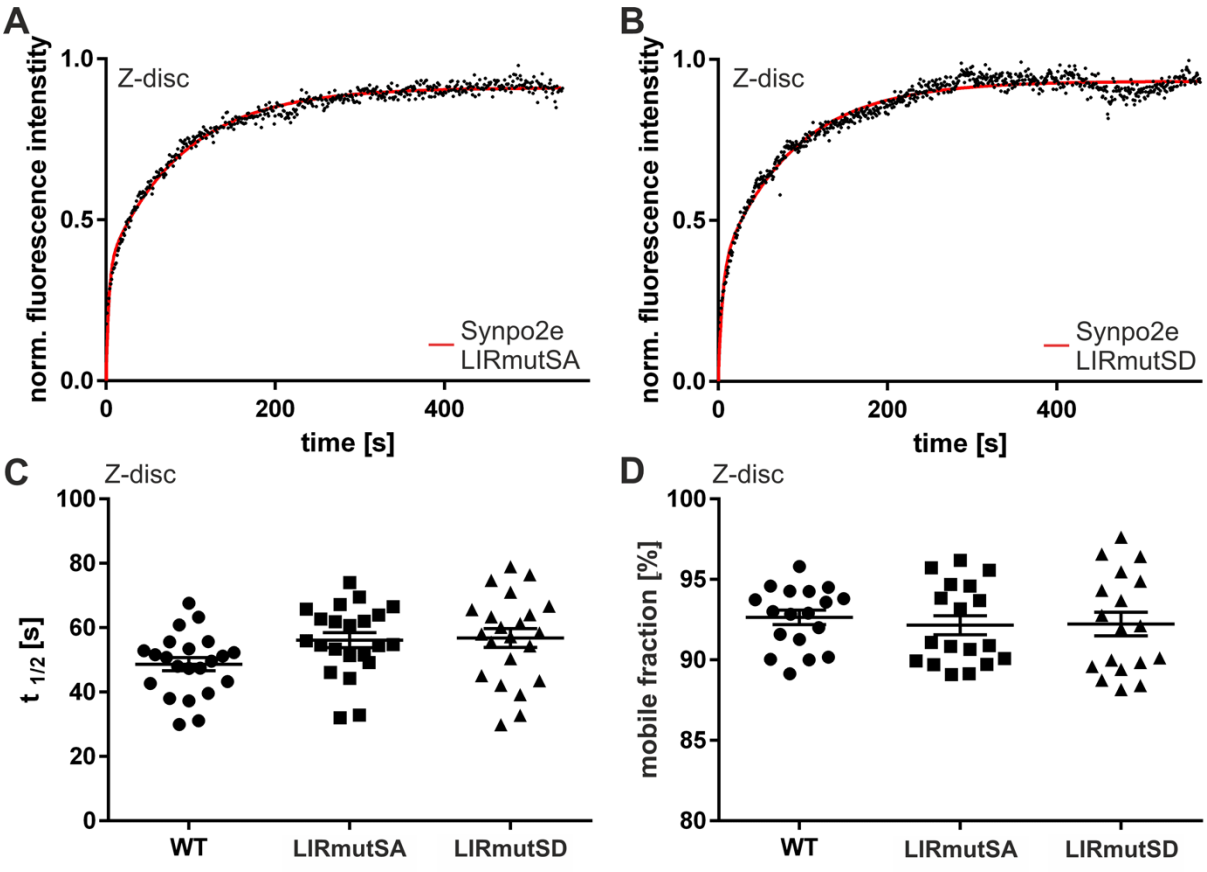

Figure 3.29: FRAP analysis of Synpo2e WT and LIR motif phosphosite mutants in Z-discs. FRAP experiments were performed in C2C12 myotubes overexpressing EGFP-Synpo2eWT, EGFP-Synpo2eLIRmutSA (mimicking a constitutively unphosphorylated state) or EGFP-Synpo2eLIRmutSD (reflecting a constitutively phosphorylated state). Myotubes were differentiated for six days and mechano-adapted by EPS. The biphasic course of the curve (red line) shows no significant difference in the regeneration time of all three analyzed constructs (A, B), which is also evident from the statistical analysis shown in C. Likewise, the mobile fraction of all tested constructs do not differ (D). Error indicators show the standard deviation of at least 15 values obtained from four experiments. The p-values were calculated using Student's t-test.

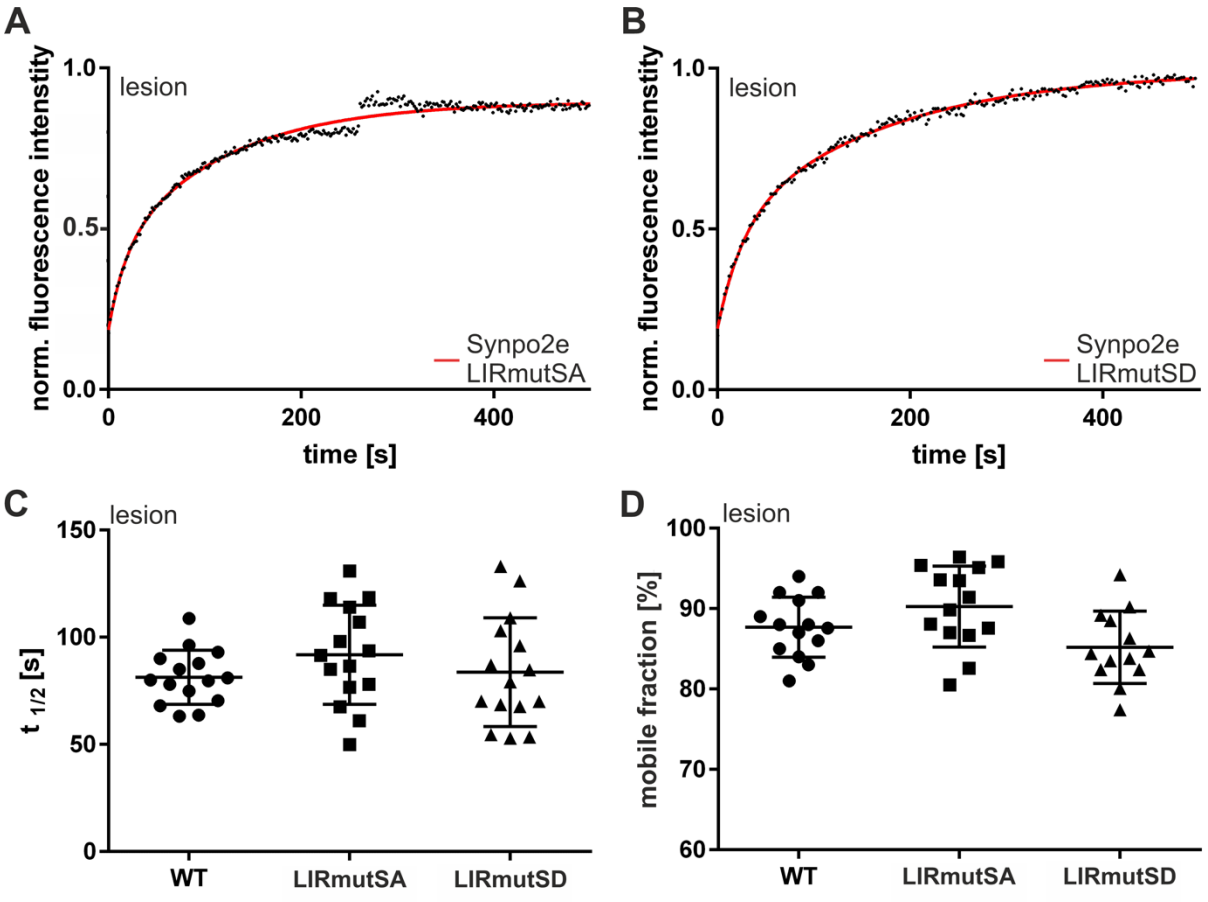

Figure 3.30: FRAP analysis of Synpo2e WT and LIR motif phosphosite mutants in sarcomeric lesions. C2C12 cells transiently transfected with EGFP-Synpo2eWT, or EGFP-Synpo2eLIRMutSA, or EGFP-Synpo2eLIRMutSD, differentiated for six days and treated with EPS overnight to achieve mechanic adaptation were used for FRAP analyses of lesions. Specific lesion areas were bleached and the duration of regeneration of the fluorescence signal was measured. The half-life (A-C) as well as the mobile fraction (D) do not show significant differences. The error indicator shows the standard deviation of at least 15 values obtained from four experiments. The p-values were calculated using Student's t-test.

3.8 Calsarcin-2 is a new interaction partner of Synpo2

Calsarcins (also known as myozenins or FATZ) are three similar, muscle-specific Z-disc-associated proteins, forming a family of calcineurin-binding and -regulating proteins (Frey *et al.*, 2000, Faulkner *et al.*, 2002, Takada *et al.*, 2002). The best studied calsarcin-2 is thought to be involved in tissue-specific regulation of the serine/threonine phosphatase calcineurin. The interaction of both proteins was shown to negatively regulate calcineurin/NFAT activity in skeletal muscle (Frey *et al.*, 2008). The phosphatase calcineurin was also shown to be involved in dephosphorylation of Synpo2, thereby regulating phosphorylation-dependent Synpo2 trafficking between the Z-disc and the nucleus (Faul *et al.*, 2007). In sections 3.6 and 3.7 of this work it was shown that the phosphorylation status of both Synpo2b and Synpo2e significantly influences protein interactions and dynamic behavior. It is therefore evident that both specific kinases and phosphatases are required to dynamically regulate the biological function of Synpo2. Based on these findings, we speculated that Synpo2 – calsarcin-2 – calcineurin might form a functional complex. To address this question, we began a systematic investigation of possible mutual interactions of these three proteins. The starting point was a yeast two-hybrid screen carried out by Norbert Frey (University of Heidelberg), in which calsarcin-2 was used as a bait protein against a universal cDNA library, yielding positive clones of Synpo2. To further investigate this potential interaction biochemically, co-IPs were performed using T7-tagged Synpo2 fragment H1+end (Figure 3.31 A, green outline) and EEF-tagged full-length calsarcin-2 constructs. This assay confirmed a strong and specific binding of calsarcin-2 with Synpo2 (Figure 3.31 B). To specify the binding region in Synpo2, another co-IP was performed with a fragment encompassing Synpo2 H1+H2 (Figure 3.31 A, red outline). The negative results of this assay (Figure 3.31 C) delineated the specific interaction of calsarcin-2 to the Synpo2 H2-end region.

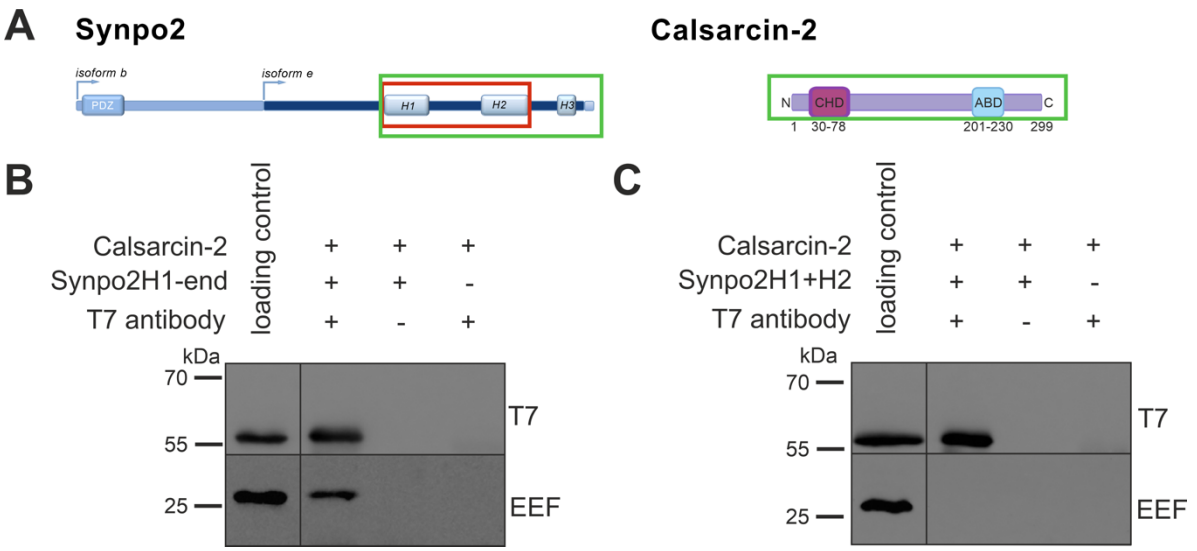

Figure 3.31: Co-IP confirming the interaction of Synpo2 with the Z-disc protein calsarcin-2. Schematic overview of the structure of Synpo2b/e (A) and calsarcin-2 (modified from Frey *et al.*, 2008, B). The fragments used for the Co-IPs are outlined in red and green, respectively (A, B). The co-IP of bacterially expressed Synpo2 H1-end fragment and calsarcin-2 shows strong binding of both proteins (C). The negative result of the co-IP of Synpo2 H1+H2 with calsarcin-2 delineated the binding region of calsarcin-2 and Synpo2 in the H2-end region. Antibodies against the T7-tag of the Synpo2 constructs and the EEF-tag of the calsarcin-2 were used for immunoprecipitations and immunodetections.

To further elucidate the interaction between Synpo2 and calsarcin-2 in contracting muscle at the subcellular level, a BiFC analysis was performed. Co-expression of Venus1C-calsarcin or Venus1N-calsarcin with Venus2N-Synpo2b or Venus2N-Synpo2e in C2C12 myotubes followed by EPS, gave a strong and specific BiFC signal, which confirms the binding of calsarcin-2 with the tested Synpo2 isoforms. Since calsarcin-2 is a very small protein with only 299 AA (Frey *et al.*, 2000), both tested Venus constructs were able to interact with their complementary half fused to Synpo2 (Figure 3.32 and 3.33). The BiFC signal of the Synpo2b + calsarcin-2 complex was located at Z-discs (Figure 3.32 B, C, -EPS). Upon EPS, the complex mainly remained localized at Z-discs, but in addition partial recruitment to lesions was evident (Figure 3.32 B, C, +EPS).

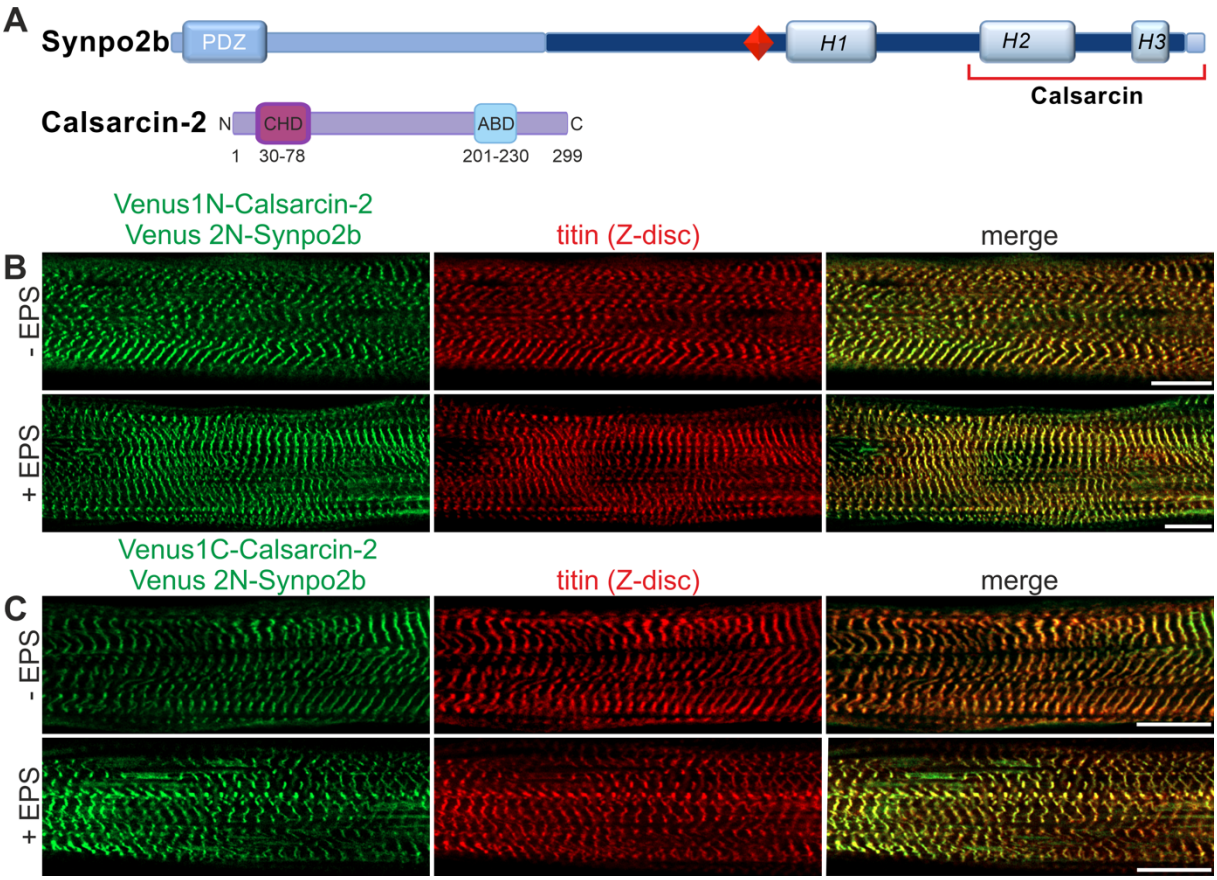

Figure 3.32: BiFC assay confirming and localizing the interaction of Synpo2b and calsarcin-2. (A) Schematic overview of Synpo2b with the H2-end region outlined in red and schematic layout of calsarcin-2 (modified from Frey *et al.*, 2008). Shown are C2C12 myotubes co-transfected with Venus1C-calsarcin-2 (B) or Venus1N-calsarcin-2 (C) and Venus2N-Synpo2b before and after EPS. Both calsarcin-2 constructs show a BiFC signal, which can only be detected when both proteins of interest are in proximity and interact. In the untreated state, the proteins showed a complex at Z-discs (B, C, -EPS), and upon EPS the Synpo2b + calsarcin-2 complex showed a partial localization in lesions as well (B, C, +EPS). Scale bars: 10 µm.

Next the Synpo2e + calsarcin-2 complex was analyzed by BiFC. Again, a strong and specific signal was obtained, which occurred mainly at Z-discs but also in lesions already without EPS (Fig. 3.33 B, C, -EPS). Upon EPS, the BiFC signal was observed in Z-discs and partially in lesions (Figure 3.33 B, C, +EPS). Taken together, the interaction between calsarcin-2 and Synpo2 isoforms e and b was verified both biochemically and *in vivo* in skeletal muscle cells.

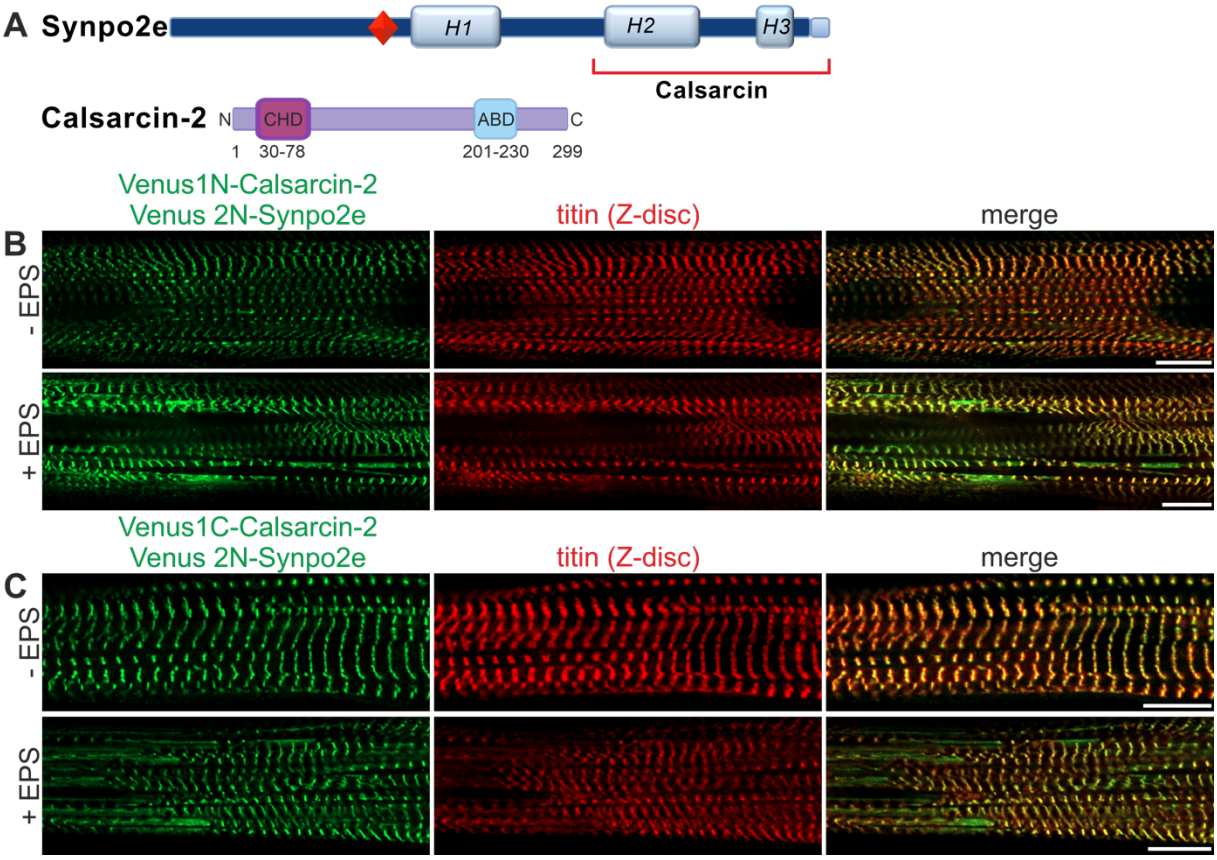

Figure 3.33: Confirmed interaction of Synpo2e on subcellular level through BiFC assay. (A) Layout of Synpo2e and calsarcin-2 (modified from Frey *et al.*, 2008). (B, C) C2C12 myotubes were co-transfected with Venus1C-calsarcin-2 or Venus1N-calsarcin-2 and Venus2N-Synpo2e before and after EPS. The complex of Synpo2e-calsarcin-2 showed a BiFC signal in the Z-discs (B, C, -EPS). The mechanical stress resulting from EPS induced a localization of Synpo2e-calsarcin-2 complex to Z-discs and partially to lesions (B, C, +EPS). Scale bars: 10 µm.

Calsarcin-2 was described as a Z-disc-associated protein (Frey *et al.*, 2000, Faulkner *et al.*, 2002, Takada *et al.*, 2002). Since our investigations had revealed the occurrence of several Z-disc-associated proteins, like filamin C (van der Ven *et al.*, 2006) and Synpo2 in sarcomeric lesions, we also wanted to ensure that calsarcin-2 alone (and not only in a BiFC-forced protein complex) is targeted to sarcomeric lesions. To analyze this question, the localization of this proteins was studied in C2C12 skeletal myotubes using a transfected EGFP-calsarcin-2 fusion protein. Microscopic analyses were performed before and after the induction of mechanical stress by applying EPS. The EGFP-calsarcin-2 fusion protein demonstrated the expected predominant localization at Z-discs (Figure 3.4, -EPS). In addition, it showed targeting to lesions that occurred in EPS treated cells (Figure 3.34, +EPS). It has to be noted, however, that

this redistribution was not as strong as it was evident with filamin C (van der Ven *et al.*, 2006) or Synpo2 (Lohanadan *et al.*, 2021).

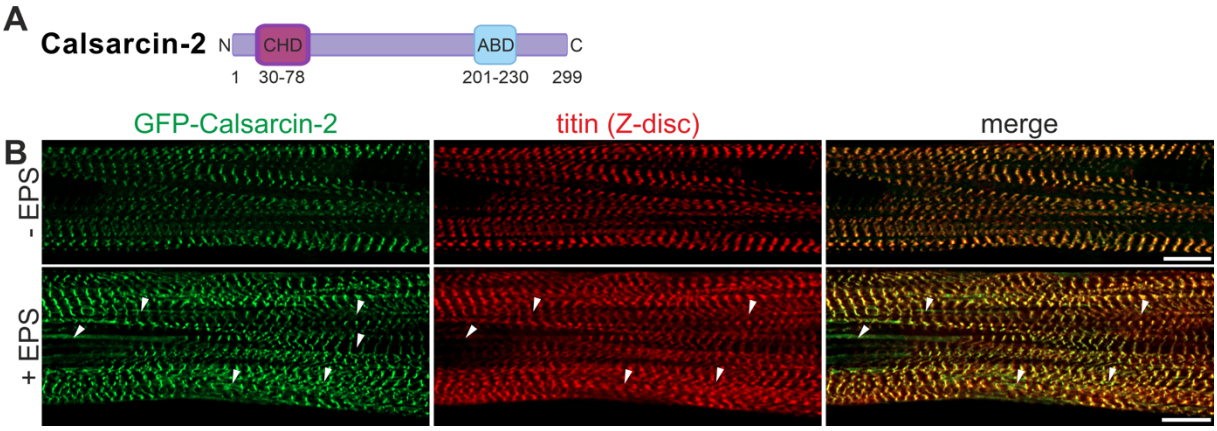

Figure 3.34: Localization of EGFP-calsarcin-2 in C2C12 cells. Myoblasts were transiently transfected with an EGFP-calsarcin-2 fusion construct and differentiated into myotubes for six days. (B) Fluorescent calsarcin-2 was mainly detected at Z-discs in untreated cells and upon EPS, treated cells showed a partial recruitment in lesions. Scale bars: 10 µm.

4.0 Discussion

4.1 Specific functions of Synpo2 isoforms in cytoskeleton stabilization and regulation of autophagy under mechanical stress

The muscle-specific protein Synpo2 was originally described to be related to synaptopodin as a member of the podin protein family (Weins *et al.*, 2001). Synpo2 is known to be expressed during early stages of myogenic differentiation and was suggested to be a regulator of muscle cell differentiation (Linnemann *et al.*, 2010; Weins *et al.*, 2001). Two alternative transcriptional promotors and alternatively spliced exons of the human SYNPO2 gene result in 6 isoforms with a distinction at both the N- and C-terminus. A major difference is the N-terminal PDZ-domain, which is only found in the long isoforms a to c but not in the short isoforms d to f (De Ganck *et al.*, 2008; Linnemann *et al.*, 2010; Kai *et al.*, 2012). As immunoblotting of skeletal muscle samples demonstrated that the long isoform Synpo2b and the short isoform Synpo2e are most highly expressed (Linnemann *et al.*, 2010), the study of this thesis is focused on these two proteins.

All available Synpo2 antibodies are directed against epitopes that are found in all protein variants, therefore recognizing all Synpo2 isoforms. Although this is sufficient for Western blotting, a different approach was necessary to answer the question whether different Synpo2 isoforms display distinct localizations in muscle cells. Transiently transfected EGFP fusion proteins expressed in cultured muscle cells demonstrated that both Synpo2b and Synpo2e in the "normal" working mode were associated mainly with Z-discs (Figure 3.1), whereas increased mechanical stress induced by EPS subsequently revealed a distinct behavior of the two proteins: while Synpo2b mainly remained associated with Z-discs, Synpo2e translocated mainly to sarcomeric lesions (Figure 3.1). These findings implied for the first time distinct biological functions for the long versus short Synpo2 protein variants.

Protein binding analyses have initially demonstrated that Synpo2 interacts with actin cytoskeleton proteins, in particular F-actin and the actin-crosslinking proteins filamin C and α-actinin-2 (Weins *et al.*, 2001; Linnemann *et al.*, 2010; Linnemann *et al.*, 2012). More recently, binding of Synpo2 to the co-chaperone BAG3 was demonstrated (Ulbricht et al., 2013). In the same work, the membrane fusion protein VPS18 was identified as the first specific ligand of the PDZ-domain (Ulbricht *et al.*, 2013). The interaction with the latter two binding partners

points to Synpo2 as a participant in the degradation of damaged cytoskeletal proteins through a selective autophagy pathway called CASA. Consequently, Synpo2 was proposed to operate at the intersection between signaling, cytoskeleton organization, and protein homeostasis.

To address the biological function of Synpo2, I used muscle cells in which Synpo2 expression was strongly reduced by shRNA-driven knockdown. Initial analyses demonstrated that the fusion of myoblasts into multinucleated myotubes and the mechanism of myofibril assembly as such were not altered in the absence of Synpo2. Nonetheless, cells with a deficiency for Synpo2 can apparently not sufficiently deal with the mechanical strain that is imposed by forced contractions elicited by EPS. Under these conditions, the lack of Synpo2 caused a fulminant augmentation of myofibrillar lesions, concomitant with a redistribution of filamin C to these lesions (Lohanadan *et al.*, 2021). These findings suggest that Synpo2 is a crucial adapter protein for the BAG3-associated cellular machinery dealing with increased mechanical stress. This is in line with the idea that effective autophagosome formation during CASA seems to require Synpo2 (Ulbricht *et al*., 2013; Kathage *et al.*, 2017). This concept was substantiated further by the finding that the conversion of LC3BI to LC3BII in contracting C2C12 mouse myotubes, in which the expression of Synpo2 was knocked down, occurred less efficiently (Lohanadan *et al.*, 2021).

Biochemical investigations identified a direct interaction of the WW-domain of the co-chaperone BAG3 with a PPPY motif that is part of all Synpo2 isoforms (Ulbricht *et al.*, 2013). In this investigation it had remained unclear, however, by which mechanism BAG3 is targeted to the Z-disc upon mechanical stress. Several lines of evidence have now shed light onto this question: First, a BAG3 construct in which the WW domain was made unfunctional by mutating the canonical tryptophane residues (BAG3 WAWA mutant), did no longer show the stress-dependent Z-disc translocation (see Figure 3.3). Second, in the Synpo2 knockdown cells, BAG3 could also not translocate to Z-discs (see Fig. 3.4). In addition, a direct interaction of BAG3 with both Synpo2 isoforms was shown in living muscle cells by using BiFC experiments (see Figure 3.5). Taken together, these data provide ample evidence that BAG3 forms functional complexes both with Synpo2b and Synpo2e. This interaction is required for specific targeting to Z-discs, sarcomeric lesions and vesicular structures in response to mechanical stress.

On top of that, these and subsequent experiments revealed a fundamentally diverse behavior and different functional properties of these two Synpo2 isoforms, particularly under conditions of increased mechanical stress induced by EPS. The complex of the Synpo2b isoform (containing the PDZ-domain) with BAG3 was primarily found localized to Z-disc and vesicular structures (see Figure 3.5). This is in accordance with the identified interaction of the PDZ-

domain with VPS18. FRAP experiments imply that the N-terminal portion containing the PDZ-domain stabilizes the association with the Z-disc and is more stably anchored to the actin cytoskeleton and considerably less dynamic compared to the smaller isoform Synpo2e lacking the PDZ-domain (see Figure 3.6). Furthermore, FRAP experiments demonstrated that Synpo2b directly responds to mechanical stress and autophagy, induced by EPS and rapamycin, respectively (Lohanadan *et al.*, 2021). The direct involvement of Synpo2b in autophagic processes also accounts for its strong dependence on protein synthesis in FRAP experiments. Accordingly, a blockade of protein synthesis by cycloheximide, resulting in a strongly reduced recovery of the fluorescence signal, suggests concomitant loss of Synpo2b by autophagic degradation and its involvement in autophagic clearance of damaged proteins at Z-discs (Lohanadan *et al.*, 2021). Summing it up, these data imply the functional theory that Synpo2b together with BAG3 and VPS18 is mainly involved in coupling the client processing CASA complex and the membrane tethering fusion machinery providing autophagosome membranes. In contrast, Synpo2e in conjunction with BAG3 was predominantly found in lesions, suggesting that the Synpo2e isoform lacking the PDZ-domain is involved in lesion-associated protein quality control upon mechanical stress (see Figure 3.5). In concomitance with these results, FRAP analyses reveal a remarkably higher molecular dynamic behavior of Synpo2e compared to Synpo2b (see Figure 3.6). The dynamics of Synpo2e is similar to that of filamin C, implying a direct involvement in the mechanosensory function of filamin C (Leber *et al.*, 2016). Synpo2e showed striking recruitment to lesions and a reduced mobility in lesions. In line with that, FRAP experiments performed after inducing autophagy and inhibiting protein synthesis by using rapamycin and cycloheximide, respectively, show that the lack of protein synthesis does not affect fluorescence recovery (Lohanadan *et al.*, 2021). These results indicate a functional switch of Synpo2e to a participation in stabilizing and protecting damaged myofibrils together with filamin C (Orfanos *et al.*, 2016; Leber *et al.*, 2016), which can exclusively be achieved by immediate recruitment of Synpo2e and filamin C from Z-discs to lesions. Taken together, these findings clearly imply the isoform-specific distinct functions in muscle protein homeostasis under mechanical stress, with Synpo2b being involved in autophagic degradation processes at the Z-discs, and Synpo2e performing functions in sarcomeric lesions independent from degradation.

These findings denote that Synpo2 isoforms are part of dynamic mechano-sensing protein complexes at Z-discs, which is under continuous threat due to the mechanical forces applied by contractile activity. Biophysical experiments have demonstrated that already piconewton forces (as exerted by myosin) are sufficient to unfold and thereby denature individual protein domains,

leading to an interruption and disturbance of their functions (Rief *et al.*, 1997; Pentikäinen *et al.*, 2009; Grison *et al.*, 2017). Constantly increased mechanical force may easily occur in contracting skeletal muscle cells. The resulting partial unfolding of critically important protein complexes may thus lead to impairment of the function and structure of myofibrils, possibly resulting in myofibril breakage. Events like these can already be observed in normally working muscle at a low incidence, but may be massively enhanced, e.g., by eccentric exercise. Such events were described as "sarcomeric lesions" and among other things they result in the well-known "delayed onset muscular soreness" (DOMS) and a reduction of contractile force of affected muscles (Yu *et al.*, 2002; Yu *et al.*, 2003; Yu *et al.*, 2004; Orfanos *et al.*, 2016). In addition to the structural damage observed microscopically, biochemical investigations performed on human test persons subjected to different exercise regimes revealed effects on the levels of proteins related to autophagy pathways (Ulbricht *et al.*, 2015).

Contraction-induced damage has the potential to lead first to the disruption of single myofibrils, which ultimately may sum up to complete fiber rupture. To avoid such harsh damage, muscle fibers must have the ability to immediately sense and rapidly react already to local myofibril destabilization. As an instant measure, the affected damaged area must be enforced and stabilized. Thus, Z-discs associated cytoskeletal proteins including filamin C and Xin actin-binding proteins (Xirps) are re-localized and recruited to such "weak" spots (Otten *et al.*, 2012; Orfanos *et al.*, 2016; Leber *et al.*, 2016). The data from this work imply that Synpo2e is a component of these lesions and is involved in the process of stabilization and enforcement. Interestingly, many Z-disc-associated proteins, including filamin C, Xin/Xirp1 as well as Synpo2, are highly phosphorylated proteins. Several of these phosphorylations appear to occur very early after mechanical stress induction through for example EPS and are highly regulated and/or regulate protein-protein interactions (Faul *et al.*, 2007; Chang *et al.*, 2013; Reimann *et al.*, 2017; Reimann *et al.*, 2020). This suggests that at least a fraction of these phosphorylations may represent a direct link between the observed differences in molecular dynamics upon induction of mechanical stress and the immediate and crucial need for protection against further damage of the contractile apparatus. The second step after the immediate stabilization is the initiation of repair processes of damaged areas. For this it is fundamental to coordinate on the one hand the removal of (mechanically) damaged proteins and on the other hand their resynthesis. Because of the capability of these damaged proteins to aggregate and thereby impede vital cellular activities, the degradation of these damaged proteins is necessary. The fundamental importance of this process is illustrated by a number of diseases, in which enhanced protein aggregation severely affects brain and muscle, resulting in cellular damage

and premature mortality (Aguzzi and O´Connor, 2010; Margeta, 2020). Therefore, autophagy and more specifically CASA is a critical cellular mechanism which is required for the repair of cellular damage and for the adaptation to mechanical force. Generally, damaged proteins are ubiquitylated, enclosed in autophagosomes and, after the fusion of the autophagosome with lysosomes, finally eliminated by proteolytic degradation (reviewed by Höhfeld *et al.*, 2021). Here the stress-inducible co-chaperone BAG3 in conjunction with HSF1 is critically involved in the regulation and balancing the autophagic removal and resynthesis of affected proteins (Franceschelli et al., 2008). Hence, CASA activity must be regulated and adjusted to the level of tension within the actin cytoskeleton (Ulbricht *et al.*, 2013a; Klimek *et al.*, 2017). BAG3 is fundamentally important as a protein homeostasis factor which is essential for muscle maintenance. This is illustrated by the rapid disintegration of the contractile apparatus in BAG3-deficient mice shortly after birth, which subsequently gives rise to progressively developing muscle weakness and leads to death by heart or lung failure already at the age of one month (Homma *et al.*, 2006). Another example for the key importance of BAG3 for muscle protein homeostasis is a point mutation in the human *BAG3* gene resulting in early onset severe cardiomyopathy, muscular dystrophy, respiratory insufficiency, and peripheral polyneuropathy, which subsequently leads to premature death already in the second decade of life (Selcen *et al.*, 2009). BAG3 is thought to exert its function in the context of CASA in muscle cells by recruiting heat shock proteins and through binding to mechanically damaged filamin directly and via Synpo2, which in this case seems to function as an essential adapter protein (Arndt *et al.*, 2010; Ulbricht *et al.*, 2013a).

Taken together, both the distinct subcellular localization and the diverse functionality of Synpo2 isoforms and their protein complexes begin to unravel isoform-specific roles of Synpo2 as spatial organizers and regulators of BAG3-containing protein homoeostasis systems. In future studies it will be interesting to investigate which additional factors and pathways regulate the precise composition of these complexes and their functions.

4.2 The triple phosphosite in the H2 region of Synpo2 has a regulatory function

A crucial step in myogenesis is the formation of the mature myofibrillar apparatus, including Z-discs. This assembly process seems to be augmented by contractile activity (Sanger *et al.*, 2005, Geach *et al.*, 2015). Previous studies showed that the abundance of proteins associated with sarcomere assembly as well as mitochondrial function are increased in differentiated skeletal muscle cells (Ong *et al.*, 2002, Cui *et al.*, 2009, Le Bihan *et al.*, 2015; Reimann *et al.*, 2017). However, proteomic analyses of cultured myotubes subjected to increased mechanical stress by applying EPS, revealed that these myotubes did not show an increased level of sarcomeric proteins (Reimann *et al.*, 2017). Hence, all necessary components for Z-disc maturation and full assembly of the contractile apparatus, as well as for myofibril maintenance are thought to be already expressed in unpaced myotubes (Reimann *et al.*, 2017). In EPS-treated myotubes, however, an increased level of ATP synthase was evident, suggesting a higher demand for energy-requiring processes, including myofibril contraction (Reimann *et al.*, 2017).

Subsequent phosphoproteome analyses of C2C12 cells after EPS provided a site-resolved map of contractility-induced protein phosphorylations. Quite striking was the fact that Z-disc-associated proteins, including the podin proteins, filamin C, the filamin-binding Xin-repeat proteins, the co-chaperone BAG3 and others, are particularly strongly phosphorylated (Reimann *et al.*, 2017 and unpublished work), underlining the view that the Z-disc is a signaling hub in the myofibrillar apparatus (Frank *et al.*, 2006). All of these experiments have revealed a large number of phosphosites in Synpo2, which were either up- or downregulated, including some sites regulated by mechanical activity (B. Warscheid, unpublished work; see table 1.1).
Previous work has already indicated some phosphorylation sites in Synpo2. The interaction of murine Synpo2 with 14-3-3 proteins, e.g., was described to be regulated by phosphorylation by PKA and CAMKII (Faul *et al.*, 2007). The significance of these findings has, however, remained rather elusive, as one of the two sites in Synpo2 that is required for 14-3-3 interaction is not even conserved between man and mouse. In addition, the function of this phosphorylation was implied in regulating cytoplasmic-nuclear transport of Synpo2, an effect that was not observed by other laboratories. In the non-muscle cell line PC3, an integrin-linked kinase-induced phosphorylation in the N-terminus of Synpo2 was described, which seems to be involved in Synpo2-mediated suppression of growth and migration (Yu and Luo, 2011).

In the list of Synpo2 phosphosites received from the Warscheid group, we identified a conspicuous cluster of three phosphosites (Synpo2b: S902 S906 S910, Synpo2e S507 S511 S515) in the H2 region (hence a sequence found in all Synpo2 isoforms, see Figure 3.10), which shows a high homology to the other podin protein family members synaptopodin and Synpo2l (Lin *et al.*, 2001, Linnemann *et al.*, 2010; B. Warscheid, unpublished work). This region of Synpo2 is involved in multiple protein interactions including the Ig-like domains 20-21 of filamin C (Linnemann *et al.*, 2010) and α-actinin-2 (Takada *et al.*, 2001; Pham and Chalovich, 2006; Faul *et al.*, 2007, Linnemann *et al.*, 2010). The potential significance of these interactions is emphasized by the key importance of these proteins for muscle cells: Filamin C was proposed to have a crucial role in early muscle development and in stabilizing myofibrillar Z-discs (van der Ven *et al.*, 2000a), and in the pathogenesis of muscular dystrophy (Thompson *et al.*, 2000). The fundamental importance of filamin C was reinforced by a mouse model carrying a deletion of *FLNC* exons 41-48, encoding the C-terminal portion of filamin C. The resulting low expression of the truncated protein leads to defects in primary myogenesis, and as a consequence the mice die shortly after birth due to respiratory failure (Dalkilic *et al.*, 2006). These data were interpreted as evidence that filamin C has a crucial role in muscle development and maintenance of structural integrity (Dalkilic et al., 2006). Similarly, mutations in α-actinin-2 were demonstrated to result in cardiomyopathies (Mohapatra *et al.*, 2003; Chiu *et al.*, 2009). In addition, the expression of truncated α-actinin in skeletal muscle causes hypertrophied Z-discs, suggesting a role of this protein in functional stabilization (Schultheiss *et al.*, 1992). Our own investigations showed that upon mechanical stress Synpo2 is recruited to areas of damage/lesion together with filamin C, and concomitantly the loss of Synpo2 results in increased instability of myofibrils under mechanical stress (Leber *et al.*, 2016, Lohanadan *et al.*, 2021).

The subsequent interaction studies described in this work yield better insight into how these interactions may be regulated. The Synpo2 mutants that mimic the constitutively phosphorylated state (3xSD) resulted in significantly weaker binding to both filamin C and α−actinin-2 (see Figures 3.11 and 3.12). Hence, one may conclude that the clustered triple phosphosite in the H2 region of Synpo2 (in Synpo2b S902 S906 S910, in Synpo2e S507 S511 S515) has a function in regulating protein-protein interaction, and the dephosphorylation of this phsophosite describes a stronger binding or higher affinity state of Synpo2. Synpo2 binds to the Ig-like domains 20-21 of filamin C, and thereby damaged or misfolded filamin C was proposed to be degraded through CASA (Arndt *et al.*, 2010, Ullbricht *et al.*, 2013, Kathage *et al.*, 2017). The reduced binding affinity of Synpo2 and filamin C in the phosphorylated state of the triple

phosphosite indicates that this CASA mediated degradation of filamin C is affected. This is in line with the results of the phosphoproteome studies including this phosphosite cluster in the Synpo2 H2 region, which showed downregulation upon enhanced mechanical stress in myotubes (B. Warscheid, unpublished work). Here, the phosphorylated state, in accordance with the less strongly binding state of Synpo2, is predominant in less active muscle. In contrast, upon enhanced contractility dephosphorylation will prevail, resulting in a stronger binding state. To understand the regulatory network, it will be very interesting to investigate which phosphatase is involved in this regulatory switch.

To address the effects of the triple phosphorylation on the subcellular localization of Synpo2 + filamin C complexes, BiFC and/or FRET experiments should be rewarding. In the constitutively phosphorylation-mimicking state Synpo2b (containing the PDZ-domain, which is thought to be involved in autophagy via the binding to VPS18) displays a striking redistribution from the Z-disc to lesions upon mechanical stress induction (Figure 3.13). The Synpo2b 3xSD mutant, which mimics a constitutively phosphorylated state, lacks the elemental turnover, which is achieved through regulated phosphorylation and dephosphorylation reactions. Hence, the Synpo2b mutant, mimicking the phosphorylated state (Synpo2b3xSD) features less stable interactions with the actin cytoskeleton, which leads to the striking damage observed, articulating in increased lesion formation, followed by a considerable recruitment of Synpo2b to these lesions (Figure 3.14). This confirms an impact of the investigated phosphosite on the activity and localization of Synpo2b upon mechanical stress.

In addition to studying the localization of the Synpo2 phosphosite mutants, the dynamics were directly investigated using FRAP experiments in living skeletal muscle cells. Most importantly, the Synpo2b variant mimicking the dephosphorylated state depicted a significant increase of the mean half-life and a significant decrease of the mobile fraction in Z-discs (Figure 3.17). These findings indicate an increased stability of the constitutively dephosphorylated Synpo2b. In addition, the decreased mobile fraction of the constitutively dephosphorylated variant, suggests an effect of the phosphorylation state on the turnover rate of the protein. Taken together, these data - in accordance with the reduced binding of the constitutively phosphorylated Synpo2 to filamin C as well as α-actinin-2 - indicate a highly regulatory function of the serine residues (Synpo2b: S902 S906 S910) in the H2 region, which may be interpreted as a kind of gain of function of the Synpo2b in dephosphorylated state.

Complementary FRAP data obtained for the constitutively dephosphorylated variant of Synpo2e serine residues (Synpo2e S507 S511 S515) revealed a highly significant increase in the mean half-life both in Z-discs and in lesions, indicating a higher affinity of Synpo2e to the

Z-disc in the dephosphorylated state (Figure 3.18 A-C and Figure 3.19 A-C). The mobile fraction of all Synpo2e variants remained unchanged, illustrating a sustained turnover of the protein independent of its phosphorylation state (Figure 3.18 D).

As a result of the denoted difference in protein affinities and dynamics, we observed that the lesion area of constitutively phosphorylated and dephosphorylated Synpo2e isoforms (lacking the PDZ-domain and thus lacking the binding to VPS18) significantly differs from the lesion area obtained for the WT protein (Figure 3.16 A). These findings indicate that continuous cycles of phosphorylation and dephosphorylation are crucial for maintenance of the turnover of Z-disc proteins and sarcomeric structure. We can therefore state that the dynamics of the Synpo2e isoform, which is suggested to have an important role in lesion-associated protein quality control, is, at least in part, regulated through phosphorylation and dephosphorylation of the serine residues (Synpo2e S507, S511, S515) in the H2 region.

Taken together, it is evident that these clustered phosphorylation sites have strong regulatory roles for the localization, mobility, dynamics, and protein-protein interactions of both investigated Synpo2 isoforms. Hence, further analysis to denominate precisely the kinases and phosphatases involved in this process are of great interest to identify signaling pathways that regulate this post-translational modification in the context of myofibrillar damage and maintenance. This knowledge may be helpful to manage and/or support the numerous conditions in which the balance of assembling and degrading mechanisms is disturbed, including patients suffering from muscular dystrophies, immobilization-induced muscular atrophy or cachexia (reviewed by: Fanzani *et al.*, 2012; Bonaldo and Sandri, 2013; Schmidt *et al.*, 2018).

Previously performed radiographic experiments, performed with a Synpo2 fragment (Synpo2b AA 405-916) containing these three serine residues, had suggested that this sequence includes phosphorylation sites for PKA as well as for PKC and MAPK (Linnemann, 2010). However, the analyzed fragment contained numerous other potential phosphorylation sites and therefore such assays have to be performed with shorter and more defined fragments down to specific peptides to identify the kinases and phosphatases responsible for the phosphorylation of these triple phosphosites. In order to reduce the number of the kinases to be considered, predictions can be made with the help of databases in which the consensus recognition sites of the kinases are stored. Kinase prediction analysis can be performed by numerous *in silico* methods like for example NetPhosK (Hjerrild *et al.*, 2004, Blom *et al.*, 2004), NetworkKIN (Linding *et al.*, 2007), Scansite (4), KinasePhos (Wong *et al.*, 2007), PredPhospho (Kim *et al.*, 2004), which predict kinase specific protein phosphorylation. As an example, NetworkKIN provides kinase-

substrate predictions based on the latest human phosphoproteome and protein association network from PhosphoSite (Hornbeck *et al.*, 2004), Phospho-ELM (Diella *et al.*, 2008) and STRING (von Mering *et al.*, 2007) databases. Preliminary analyses indicate a more complex regulation, involving – amongst others – SP-directed ERK/MAP kinases and the basophilic PKB/Akt. A combination of single point mutations and specific inhibitors may help to solve this question. Finally, since the investigated serine residues in the H2 region are essentially conserved in all podins (see Figure 3.10), it also remains to be clarified whether their functions are similar or even the same.

4.3 The calcineurin-binding and -regulating protein calsarcin-2 binds to Synpo2

The results from the analyzed conserved triple phosphosite in H2 show a phosphorylation state dependency of Synpo2b dynamics and mobility (Figure 3.17), protein-protein interactions (Figure 3.11, 3.12) and localization (Figure 3.13, 3.14). To analyze in detail the signaling pathways involved in regulating the function of the phosphosites in Synpo2, it is important to identify both the kinases and phosphatases which are responsible for the precise phosphorylation state of the respective site(s). A serine/threonine phosphatase which has already been implied to be involved in Synpo2 phosphorylation is calcineurin (Faul *et al.*, 2007). Calcineurin is activated by calcium-dependent binding to the calcium-sensing protein calmodulin (reviewed in Parra & Rothermel, 2017). This phosphatase was described as a key factor regulating the activity of a number of transcription factors (Hogan *et al.*, 2005, Tremblay *et al.*, 2008, Sakuma *et al.*, 2010), thereby activating diverse transcriptional programs involved in autophagy (Parra and Rothermel, 2017), cardiac function (Sakuma *et al.*, 2010, Dewenter *et al.*, 2017, Parra and Rothermel, 2017) or T-cell activation (Hogan *et al.*, 2005). The muscle-specific protein calsarcin-2 was shown to interact with calcineurin and thereby inhibit the transcriptional activity of NFAT in skeletal muscle. Calsarcin was therefore proposed to be involved in the tissue-specific regulation of calcineurin (Frey *et al.*, 2000, Frey *et al.*, 2008). Calsarcin-2 is localized to myofibrillar Z-discs, and it interacts with the Z-disc proteins α-actinin, ZASP and myotilin. Recently a yeast two-hybrid screen carried out by Norbert Frey (University of Heidelberg, unpublished work), in which calsarcin-2 was used as a bait protein against a universal cDNA library, provided an indication of an interaction between calsarcin-2 and Synpo2. This proposed interaction between calsarcin-2 and Synpo2 has now been verified

by biochemical protein interaction studies in this work (Figure 3.31). More specifically, the binding site was localized in a portion between the H2 region and the C-Terminus of Synpo2b/Synpo2e. In addition to these biochemical data, the subcellular localization of complexes of Synpo2 b and e with calsarcin-2 was demonstrated in Z-discs and lesions (Figures 3.32, 3.33). These findings raise the interesting question, whether Synpo2 is only passively regulated by calcineurin as previously proposed (Faul *et al.*, 2007), or whether there is an impact of calsarcin-2 together with Synpo2 in the regulation of calcineurin activity. In order to investigate this more specifically, binding assays of specific phosphosite-containing Synpo2 fragments with calsarcin-2 and calcineurin have to be performed and effects on established downstream effector proteins of calcineurin have to be analyzed (e.g., by measuring effects on NFAT activity).

4.4 Phosphorylation-dependent binding of LC3B to Synpo2

LC3B is commonly used as the autophagosomal marker in mammals and belongs to the LC3 subfamily (together with LC3A and LC3C), which is alongside with GABARAP (and GABARAPL) a member of the ATG8 family (Lazova *et al.*, 2012; Jatana *et al.*, 2019). Both the LC3 and GABARAP subfamilies are conjugated to the growing phagophore membrane and upon lipid conjugation they operate as scaffolds to recruit numerous diverse proteins to the phagophore (Weidberg *et al.*, 2011; Thukral *et al.*, 2015). The interaction with most of the proteins is mediated by a LIR peptide motif. This motif was initially identified in p62 (Pankiv *et al.*, 2007, Ichimura *et al.*, 2008) but later found in a growing list of proteins from yeast to mammals. It is a short linear peptide sequence with the minimal consensus for an aromatic amino acid residue in position zero and a hydrophobic residue in position three $(W/F/Y)_0$-X_1-X_2-$(L/I/V)_3$. In addition, it was reported that a high frequency of acidic residues (E or D), and occasionally serine/threonine residues which can be phosphorylated, are located in proximity to the LIR core sequence (Johansen and Lamark, 2020). As described in chapter 3.7, a database search revealed strong indications for the presence of a LIR motif (EDYLSL) in the multi-adapter protein Synpo2b at AA positions 733 to 738. Interestingly, the LIR sequence includes a serine residue, which was found to be phosphorylated at position two of the core sequence upon EPS-induced twitching (B. Warscheid, unpublished work, Figure 3.21).

A peptide array, which is a highly efficient and very accurate method for the identification of LIR motifs within a given full-length protein, was performed for detailed mapping of the extent

of the binding motifs using two-dimensional substitution mutagenesis probing each position of the binding motif. Surprisingly, only the Synpo2 LIR motif containing peptide with a point mutation of the serine residue at position two of the core motif (Synpo2b: S737, Synpo2e: S342) to aspartate (i.e., a phosphorylation mimicking mutation) resulted in binding to LC3B (Figure 3.22), indicating a phosphorylation dependent interaction of LC3B with Synpo2. A similar, phosphorylation-dependent binding of LC3B to a LIR was described for optineurin (Wild *et al.*, 2011) and Bnip3 (Zhu *et al.*, 2013). Moreover, the Synpo2 LIR core sequence is flanked by two acidic residues located N-terminally to the core sequence (E = position -2, D = position -1). Here, Johansen and Lamark suggested that surrounding acidic residues located N-terminally to the core motif are part of the consensus LIR sequence and are important for LIR-mediated interactions (Johansen and Lamark, 2020).

Phosphoproteome analyses had identified an upregulation of the described Synpo2 phosphosite in the core sequence of the LIR motif under EPS conditions, i.e., in a situation of increased mechanical stress (B. Warscheid, unpublished work). BiFC was then used as an *in vivo* assay to investigate possible effects of mutations mimicking distinct phosphorylation states of the LIR of Synpo2 isoforms on the formation of complexes with LC3B. Here, not only the wildtype and the serine to aspartic acid mutant, but also the serine to alanine mutant, yielded positive signals, both in Z-discs, vesicular structures, and lesions (Figures 3.23 and 3.24). Nevertheless, the preference of Synpo2b for vesicular structures and of Synpo2e for lesions was not affected by their association with LC3. Control transfections using only Synpo2b and e, respectively, harboring either the LIR SD or the LIR SA mutant, did not display significant differences in their subcellular targeting in comparison to the wildtype proteins, irrespective of the application of EPS (Figures 3.25 and 3.26). These data can be interpreted in the following way: Since the BiFC assay is a manifestation of a binding through the reconstitution of a fluorescence protein, the complex is virtually "frozen" and as a consequence shows less dynamics. It will subsequently most likely be drawn to the structure to which one of the binding partners of the complex displays the highest affinity. In this case, the complex localizes predominantly to the preferred localization areas of Synpo2, which is particularly evident with the Synpo2e isoform and its predominant lesion targeting. Synpo2b-LC3 complexes in turn are found in vesicular structures, implying their enclosure in autophagosomes and subsequent elimination in lysosomes (Ulbricht *et al.*, 2013a; Ulbricht *et al.*, 2013b; Arndt *et al.*, 2010). Interestingly the SA mutant of Synpo2b has a significantly shorter half-life in FRAP assays in comparison to both wildtype and the phosphorylation mimicking LIR SD mutant (see Figure 3.28). This difference reflects a similar behavior of the wildtype and the Synpo2b protein phosphorylated

at this site. The longer half-life of these two indicates stronger attachment to their sarcomeric binding partners filamin C and α-actinin-2. This may also mean that the Synpo2b LIRmutSA variant is more resistant to autophagic degradation, and resynthesis of the wildtype and Synpo2 LIRmut SD proteins is required for complete recovery. Solely the phosphorylation mimicking Synpo2eLIRmutSD variant showed, in addition to its "normal" localization at Z-discs, a notable localization to vesicular structure (Figure 3.26). This isoform, lacking the PDZ-domain is usually associated with lesions and responsible for lesion-associated protein quality control upon mechanical stress (Lohanadan *et al.*, 2021). These results suggest that the localization and function of this isoform appear to be partially altered by the LIR motif phosphorylation, which can be interpreted as a dominant effect. The application of mechanical stress, however, reverses or overrides this dominant effect, since the Synpo2eLIRmutSD is strikingly recruited to lesions alike the WT and the Synpo2eLIRmutSA (Figure 3.26).

Global proteomics screens performed by the Behrends lab suggested a higher specificity of LIR mediated interactions *in vivo* compared to *in vitro* binding assays (Behrends *et al.*, 2010). This is partially in accordance with the *in vivo* binding of all Synpo2 variants to LC3B, independent of the phosphorylation state of the Synpo2 LIR motif, whereas in the *in vitro* performed peptide array binding was very selectively only detected upon phosphorylation of the LIR motif. Generally, BiFC is a suitable method to validate the binding of two proteins of interest, but it has to be taken into consideration that the binding affinity is not reflected in this assay. A positive signal may already result from the reconstitution of the fluorescence proteins coupled to relatively weakly interacting proteins, resulting in a persistent strong attachment, followed by decreased dynamics. Hence, the binding of Synpo2 and LC3B is very likely of relatively low affinity, rendering the peptide array negative for the wildtype protein. Recent studies have revealed that phosphorylation of a serine residue in the protein optineurin by the S/T-kinase TBK1 (tank binding kinase 1) resulted in a higher affinity for ATG8 proteins (Wild *et al.*, 2011; Richter *et al.*, 2016). Therefore, it can be hypothesized, that the phosphorylation in Synpo2 LIR motif (Synpo2b S737) increases the binding affinity to LC3B, and hence to a visualization of the binding *in vitro*, whereas the dephosphorylated state of the LIR-motif has a too low binding affinity to detect the interaction *in vitro*. To evaluate this further, direct affinity measurements using, e.g., surface acoustic wave (SAW) measurement (Perpeet *et al.*, 2006) or isothermic titration calorimetry (ITC) (Cliff *et al.*, 2004) will have to be performed in the future.

Altogether, these investigations have unraveled substantial novel insight into the facets of Synpo2 functions and their isoform-specific regulation. This is of particular interest in the context of how muscle cells deal with mechanical stress and how protein homeostasis is

maintained under these conditions. A deeper understanding of these processes may help to manage patients suffering from conditions in which proteostasis is beyond control, e.g., in muscular dystrophies or immobilization-induced autophagy.

5.0 References

Aguzzi A, O'Connor T. Protein aggregation diseases: pathogenicity and therapeutic perspectives. *Nat Rev Drug Discov*. (2010) 9:237-48. doi: 10.1038/nrd3050.

Alberts B, Johnson A, Lewis J, Raff M, Roberts K, and Walter P. Molecular Biology of the Cell. (2007) *Garland Science Textbooks*.

Michael McKinley, Valerie O'Loughlin, Elizabeth Pennefather-O'Brie. ISE Human Anatomy. (2009) *McGraw-Hill Education.*

Al Tanoury Z, Schaffner-Reckinger E, Halavatyi A, Hoffmann C, Moes M, Hadzic E, Catillon M, Yatskou M, Friederich E. Quantitative kinetic study of the actin-bundling protein L-plastin and of its impact on actin turn-over. *PLoS One.* (2010) Feb 5:e9210. doi: 10.1371/journal.pone.0009210.

Aramburu J, Rao A, Klee CB. Calcineurin: from structure to function. *Curr Top Cell Regul*. (2000) 36:237-95. doi: 10.1016/s0070-2137(01)80011-x.

Arimura T, Ishikawa T, Nunoda S, Kawai S, Kimura A. Dilated cardiomyopathy-associated BAG3 mutations impair Z-disc assembly and enhance sensitivity to apoptosis in cardiomyocytes. *Hum Mutat.* (2011) 32:1481-91. doi: 10.1002/humu.21603.

Arndt V, Dick N, Tawo R, Dreiseidler M, Wenzel D, Hesse M, Fürst DO, Saftig P, Saint R, Fleischmann BK, Hoch M, Höhfeld J. Chaperone-assisted selective autophagy is essential for muscle maintenance. *Curr Biol.* (2010) 20:143-8. doi: 10.1016/j.cub.2009.11.022.

Beere HM. Death versus survival: functional interaction between the apoptotic and stress-inducible heat shock protein pathways. *J Clin Invest.* (2005) 115:2633-9. doi: 10.1172/JCI26471.

Behrends C, Sowa ME, Gygi SP, Harper JW. Network organization of the human autophagy system. *Nature.* (2010) 466:68-76. doi: 10.1038/nature09204.

Berthier C, Blaineau S. Supramolecular organization of the subsarcolemmal cytoskeleton of adult skeletal muscle fibers. A review. *Biol Cell.* (1997) 89:413.

Blanchard A, Ohanian V, Critchley D. The structure and function of alpha-actinin. *J Muscle Res Cell Motil.* (1989) 10:280-9. doi: 10.1007/BF01758424.

Blom N, Sicheritz-Pontén T, Gupta R, Gammeltoft S, Brunak S. Prediction of post-translational glycosylation and phosphorylation of proteins from the amino acid sequence. *Proteomics.* (2004) 4:1633-49. doi: 10.1002/pmic.200300771.

Bonaldo P, Sandri M. Cellular and molecular mechanisms of muscle atrophy. *Dis Model Mech*. (2013) 6:25-39. doi: 10.1242/dmm.010389.

Bröcker C, Kuhlee A, Gatsogiannis C, Balderhaar HJ, Hönscher C, Engelbrecht-Vandré S, Ungermann C, Raunser S. Molecular architecture of the multisubunit homotypic fusion and vacuole protein sorting (HOPS) tethering complex. *Proc Natl Acad Sci USA*. (2012) 109:1991-6. doi: 10.1073/pnas.1117797109.

Burch N, Arnold AS, Item F, Summermatter S, Brochmann Santana Santos G, Christe M, Boutellier U, Toigo M, Handschin C. Electric pulse stimulation of cultured murine muscle cells reproduces gene expression changes of trained mouse muscle. *PLoS One.* (2010) 5:e10970. doi: 10.1371/journal.pone.0010970.

Castresana J, Saraste M. Does Vav bind to F-actin through a CH domain? *FEBS Lett.* (1995) 374:149-51. doi: 10.1016/0014-5793(95)01098-y.

Chang YW, Chang YT, Wang Q, Lin JJ, Chen YJ, Chen CC. Quantitative phosphoproteomic study of pressure-overloaded mouse heart reveals dynamin-related protein 1 as a modulator of cardiac hypertrophy. *Mol Cell Proteomics.* (2013) 12:3094-107. doi: 10.1074/mcp.M113.027649.

Chen H, Zhu X, Cong P, Sheetz MP, Nakamura F, Yan J. Differential mechanical stability of filamin A rod segments. *Biophys J.* (2011) 101:1231-7. doi: 10.1016/j.bpj.2011.07.028.

Chiang W, Greaser ML. Binding of filamin isoforms to myofibrils. *J Muscle Res Cell Motil.* (2000) 21:321-33. doi: 10.1023/a:1005650706464.

Chiu C, Bagnall RD, Ingles J, Yeates L, Kennerson M, Donald JA, Jormakka M, Lind JM, Semsarian C. Mutations in alpha-actinin-2 cause hypertrophic cardiomyopathy: a genome-wide analysis. *J Am Coll Cardiol.* (2010) 55:1127-35. doi: 10.1016/j.jacc.2009.11.016.

Clark KA, McElhinny AS, Beckerle MC, Gregorio CC. Striated muscle cytoarchitecture: an intricate web of form and function. *Annu Rev Cell Dev Biol.* (2002) 18:637-706. doi: 10.1146/annurev.cellbio.18.012502.105840.

Cliff MJ, Gutierrez A, Ladbury JE. A survey of the year 2003 literature on applications of isothermal titration calorimetry. *J Mol Recognit*. (2004) 17:513-23. doi: 10.1002/jmr.714.

Cohen P. The origins of protein phosphorylation. *Nat Cell Biol.* (2002) 4:127-30. doi: 10.1038/ncb0502-e127.

Cui Z, Chen X, Lu B, Park SK, Xu T, Xie Z, Xue P, Hou J, Hang H, Yates JR 3rd, Yang F. Preliminary quantitative profile of differential protein expression between rat L6 myoblasts and myotubes by stable isotope labeling with amino acids in cell culture. *Proteomics.* (2009) 9:1274-92. doi: 10.1002/pmic.200800354.

Dalkilic I, Schienda J, Thompson TG, Kunkel LM. Loss of FilaminC (FLNc) results in severe defects in myogenesis and myotube structure. *Mol Cell Biol.* (2006) 26:6522-34. doi: 10.1128/MCB.00243-06.

Davison MD, Critchley DR. alpha-Actinins and the DMD protein contain spectrin-like repeats. *Cell.* (1988) 52:159-60. doi: 10.1016/0092-8674(88)90503-x.

De Ganck A, De Corte V, Staes A, Gevaert K, Vandekerckhove J, Gettemans J. Multiple isoforms of the tumor suppressor myopodin are simultaneously transcribed in cancer cells. *Biochem Biophys Res Commun.* (2008) 370:269-73. doi: 10.1016/j.bbrc.2008.03.086.

Dewenter M, von der Lieth A, Katus HA, Backs J. Calcium Signaling and Transcriptional Regulation in Cardiomyocytes. *Circ Res.* (2017) 121:1000-1020. doi: 10.1161/CIRCRESAHA.117.310355.

Diella F, Gould CM, Chica C, Via A, Gibson TJ. Phospho.ELM: a database of phosphorylation sites--update 2008. *Nucleic Acids Res.* (2008) 36:240-4. doi: 10.1093/nar/gkm772.

Djinović-Carugo K, Young P, Gautel M, Saraste M. Structure of the alpha-actinin rod: molecular basis for cross-linking of actin filaments. *Cell.* (1999) 98:537-46. doi: 10.1016/s0092-8674(00)81981-9.

Dolmetsch RE, Lewis RS, Goodnow CC, Healy JI. Differential activation of transcription factors induced by Ca2+ response amplitude and duration. *Nature.* (1997) 386:855-8. doi: 10.1038/386855a0.

Doong H, Rizzo K, Fang S, Kulpa V, Weissman AM, Kohn EC. CAIR-1/BAG-3 abrogates heat shock protein-70 chaperone complex-mediated protein degradation: accumulation of poly-ubiquitinated Hsp90 client proteins. *J Biol Chem.* (2003) 278:28490-500. doi: 10.1074/jbc.M209682200.

Du A, Sanger JM, Linask KK, Sanger JW. Myofibrillogenesis in the first cardiomyocytes formed from isolated quail precardiac mesoderm. *Dev Biol.* (2003) 257:382-94. doi: 10.1016/s0012-1606(03)00104-0.

Duff RM, Tay V, Hackman P, Ravenscroft G, McLean C, Kennedy P, Steinbach A, Schöffler W, van der Ven PFM, Fürst DO, Song J, Djinović-Carugo K, Penttilä S, Raheem O, Reardon K, Malandrini A, Gambelli S, Villanova M, Nowak KJ, Williams DR, Landers JE, Brown RH Jr, Udd B, Laing NG. Mutations in the N-terminal actin-binding domain of filamin C cause a distal myopathy. *Am J Hum Genet.* (2011) 88:729-740. doi: 10.1016/j.ajhg.2011.04.021.

Ehrlicher AJ, Nakamura F, Hartwig JH, Weitz DA, Stossel TP. Mechanical strain in actin networks regulates FilGAP and integrin binding to filamin A. *Nature.* (2011) 478:260-3. doi: 10.1038/nature10430.

Epp N, Rethmeier R, Krämer L, Ungermann C. Membrane dynamics and fusion at late endosomes and vacuoles-Rab regulation, multisubunit tethering complexes and SNAREs. *Eur J Cell Biol.* (2011) 90:779-85. doi: 10.1016/j.ejcb.2011.04.007.

Eulitz S, Sauer F, Pelissier MC, Boisguerin P, Molt S, Schuld J, Orfanos Z, Kley RA, Volkmer R, Wilmanns M, Kirfel G, van der Ven PF, Fürst DO. Identification of Xin-repeat proteins as novel ligands of the SH3 domains of nebulin and nebulette and analysis of their interaction during myofibril formation and remodeling. *Mol Biol Cell.* (2013) 24:3215-26. doi: 10.1091/mbc.E13-04-0202.

Fanzani A, Conraads VM, Penna F, Martinet W. Molecular and cellular mechanisms of skeletal muscle atrophy: an update. *J Cachexia Sarcopenia Muscle*. (2012) 3:163-79. doi: 10.1007/s13539-012-0074-6

Faul C, Dhume A, Schecter AD, Mundel P. Protein kinase A, Ca2+/calmodulin-dependent kinase II, and calcineurin regulate the intracellular trafficking of myopodin between the Z-disc and the nucleus of cardiac myocytes. *Mol Cell Biol.* (2007) 27:8215-27. doi: 10.1128/MCB.00950-07.

Faul C, Hüttelmaier S, Oh J, Hachet V, Singer RH, Mundel P. Promotion of importin alpha-mediated nuclear import by the phosphorylation-dependent binding of cargo protein to 14-3-3. *J Cell Biol*. (2005) 169:415-24. doi: 10.1083/jcb.200411169.

Faulkner G, Pallavicini A, Comelli A, Salamon M, Bortoletto G, Ievolella C, Trevisan S, Kojic' S, Dalla Vecchia F, Laveder P, Valle G, Lanfranchi G. FATZ, a filamin-, actinin-, and telethonin-binding protein of the Z-disc of skeletal muscle. *J Biol Chem.* (2000) 275:41234-42. doi: 10.1074/jbc.M007493200.

Feldman AM, Begay RL, Knezevic T, Myers VD, Slavov DB, Zhu W, Gowan K, Graw SL, Jones KL, Tilley DG, Coleman RC, Walinsky P, Cheung JY, Mestroni L, Khalili K, Taylor MR. Decreased levels of BAG3 in a family with a rare variant and in idiopathic dilated cardiomyopathy. *J Cell Physiol.* (2014) 229:1697-702. doi: 10.1002/jcp.24615.

Feldman AM, Gordon J, Wang J, Song J, Zhang XQ, Myers VD, Tilley DG, Gao E, Hoffman NE, Tomar D, Madesh M, Rabinowitz J, Koch WJ, Su F, Khalili K, Cheung JY. BAG3 regulates contractility and Ca(2+) homeostasis in adult mouse ventricular myocytes. *J Mol Cell Cardiol.* (2016) 92:10-20. doi: 10.1016/j.yjmcc.2016.01.015.

Fraley TS, Tran TC, Corgan AM, Nash CA, Hao J, Critchley DR, Greenwood JA. Phosphoinositide binding inhibits alpha-actinin bundling activity. *J Biol Chem.* (2003) 278:24039-45. doi: 10.1074/jbc.M213288200.

Franaszczyk M, Bilinska ZT, Sobieszczańska-Małek M, Michalak E, Sleszycka J, Sioma A, Małek ŁA, Kaczmarska D, Walczak E, Włodarski P, Hutnik Ł, Milanowska B, Dzielinska Z, Religa G, Grzybowski J, Zieliński T, Ploski R. The BAG3 gene variants in Polish patients with dilated cardiomyopathy: four novel mutations and a genotype-phenotype correlation. *J Transl Med.* (2014) 12:192. doi: 10.1186/1479-5876-12-192.

Franceschelli S, Rosati A, Lerose R, De Nicola S, Turco MC, Pascale M. Bag3 gene expression is regulated by heat shock factor 1. *J Cell Physiol.* (2008) 215:575-7. doi: 10.1002/jcp.21397.

Frank D, Kuhn C, Katus HA, Frey N. The sarcomeric Z-disc: a nodal point in signalling and disease. *J Mol Med (Berl).* (2006) 84:446-68. doi: 10.1007/s00109-005-0033-1.

Frey N, Frank D, Lippl S, Kuhn C, Kögler H, Barrientos T, Rohr C, Will R, Müller OJ, Weiler H, Bassel-Duby R, Katus HA, Olson EN. Calsarcin-2 deficiency increases exercise capacity in mice through calcineurin/NFAT activation. *J Clin Invest.* (2008) 118:3598-608. doi: 10.1172/JCI36277.

Frey N, Olson EN. Calsarcin-3, a novel skeletal muscle-specific member of the calsarcin family, interacts with multiple Z-disc proteins. *J Biol Chem.* (2002) 277:13998-4004. doi: 10.1074/jbc.M200712200.

Frey N, Richardson JA, Olson EN. Calsarcins, a novel family of sarcomeric calcineurin-binding proteins. *Proc Natl Acad Sci USA.* (2000) 97:14632-7. doi: 10.1073/pnas.260501097.

Fucini P, Renner C, Herberhold C, Noegel AA, Holak TA. The repeating segments of the F-actin cross-linking gelation factor (ABP-120) have an immunoglobulin-like fold. *Nat Struct Biol.* (1997) 4:223-30. doi: 10.1038/nsb0397-223.

Fujita H, Nedachi T, Kanzaki M. Accelerated de novo sarcomere assembly by electric pulse stimulation in C2C12 myotubes. *Exp Cell Res.* (2007) 313:1853-65. doi: 10.1016/j.yexcr.2007.03.002.

Fürst DO, Goldfarb LG, Kley RA, Vorgerd M, Olivé M, van der Ven PF. Filamin C-related myopathies: pathology and mechanisms. *Acta Neuropathol.* (2013) 125:33-46. doi: 10.1007/s00401-012-1054-9.

Fürst DO, Osborn M, Nave R, Weber K. The organization of titin filaments in the half-sarcomere revealed by monoclonal antibodies in immunoelectron microscopy: a map of ten nonrepetitive epitopes starting at the Z line extends close to the M line. *J Cell Biol.* (1988) 106:1563-72. doi: 10.1083/jcb.106.5.1563.

Gamerdinger M, Hajieva P, Kaya AM, Wolfrum U, Hartl FU, Behl C. Protein quality control during aging involves recruitment of the macroautophagy pathway by BAG3. *EMBO J.* (2009) 28:889-901. doi: 10.1038/emboj.2009.29.

Gamerdinger M, Kaya AM, Wolfrum U, Clement AM, Behl C. BAG3 mediates chaperone-based aggresome-targeting and selective autophagy of misfolded proteins. *EMBO Rep.* (2011) 12:149-56. doi: 10.1038/embor.2010.203.

Gautel M. The sarcomere and the nucleus: functional links to hypertrophy, atrophy and sarcopenia. *Adv Exp Med Biol.* (2008) 642:176-91. doi: 10.1007/978-0-387-84847-1_13.

Geach TJ, Hirst EM, Zimmerman LB. Contractile activity is required for Z-disc sarcomere maturation in vivo. *Genesis.* (2015) 53:299-307. doi: 10.1002/dvg.22851.

Ghosh SR, Hope IA. Determination of the mobility of novel and established Caenorhabditis elegans sarcomeric proteins in vivo. *Eur J Cell Biol.* (2010) 89:437-48. doi: 10.1016/j.ejcb.2009.11.027.

Gorlin JB, Yamin R, Egan S, Stewart M, Stossel TP, Kwiatkowski DJ, Hartwig JH. Human endothelial actin-binding protein (ABP-280, nonmuscle filamin): a molecular leaf spring. *J Cell Biol.* (1990) 111:1089-105. doi: 10.1083/jcb.111.3.1089.

Grison M, Merkel U, Kostan J, Djinović-Carugo K, Rief M. α-Actinin/titin interaction: A dynamic and mechanically stable cluster of bonds in the muscle Z-disk. *Proc Natl Acad Sci USA.* (2017) 114:1015-1020. doi: 10.1073/pnas.1612681114.

Hannigan GE, McDonald PC, Walsh MP, Dedhar S. Integrin-linked kinase: not so 'pseudo' after all. Oncogene. (2011) 30:4375-85. doi: 10.1038/onc.2011.177.

Hartl FU, Bracher A, Hayer-Hartl M. Molecular chaperones in protein folding and proteostasis. *Nature.* (2011) 475:324-32. doi: 10.1038/nature10317.

Haslbeck M, Franzmann T, Weinfurtner D, Buchner J. Some like it hot: the structure and function of small heat-shock proteins. *Nat Struct Mol Biol.* (2005) 12:842-6. doi: 10.1038/nsmb993.

Haq S, Choukroun G, Lim H, Tymitz KM, del Monte F, Gwathmey J, Grazette L, Michael A, Hajjar R, Force T, Molkentin JD. Differential activation of signal transduction pathways in human hearts with hypertrophy versus advanced heart failure. *Circulation.* (2001) 103:670-7. doi: 10.1161/01.cir.103.5.670.

Heikkinen O, Permi P, Koskela H, Ylänne J, Kilpeläinen I. 1H, 13C and 15N resonance assignments of the human filamin A tandem immunoglobulin-like domains 16-17 and 18-19. *Biomol NMR Assign.* (2009) 3:53-6. doi: 10.1007/s12104-008-9140-6.

Himmel M, Van Der Ven PF, Stöcklein W, Fürst DO. The limits of promiscuity: isoform-specific dimerization of filamins. *Biochemistry.* (2003) 42:430-9. doi: 10.1021/bi026501+.

Hjerrild M, Stensballe A, Rasmussen TE, Kofoed CB, Blom N, Sicheritz-Ponten T, Larsen MR, Brunak S, Jensen ON, Gammeltoft S. Identification of phosphorylation sites in protein kinase A substrates using artificial neural networks and mass spectrometry. *J Proteome Res.* (2004) 3:426-33. doi: 10.1021/pr0341033.

Hogan PG, Li H. Calcineurin. *Curr Biol.* (2005) 15:R442-3. doi: 10.1016/j.cub.2005.06.006.

Homma S, Iwasaki M, Shelton GD, Engvall E, Reed JC, Takayama S. BAG3 deficiency results in fulminant myopathy and early lethality. *Am J Pathol.* (2006) 169:761-73. doi: 10.2353/ajpath.2006.060250.

Hornbeck PV, Chabra I, Kornhauser JM, Skrzypek E, Zhang B. PhosphoSite: A bioinformatics resource dedicated to physiological protein phosphorylation. *Proteomics.* (2004) 4:1551-61. doi: 10.1002/pmic.200300772.

Hoshijima M. Mechanical stress-strain sensors embedded in cardiac cytoskeleton: Z disk, titin, and associated structures. *Am J Physiol Heart Circ Physiol.* (2006) 290:H1313-25. doi: 10.1152/ajpheart.00816.2005.

Hu CD, Chinenov Y, Kerppola TK. Visualization of interactions among bZIP and Rel family proteins in living cells using bimolecular fluorescence complementation. *Mol Cell.* (2002) 9:789-98. doi: 10.1016/s1097-2765(02)00496-3.

Huxley H, Hanson J. Changes in the cross-striations of muscle during contraction and stretch and their structural interpretation. *Nature.* (1954) ;173:973-6. doi: 10.1038/173973a0.

Ichimura Y, Kumanomidou T, Sou YS, Mizushima T, Ezaki J, Ueno T, Kominami E, Yamane T, Tanaka K, Komatsu M. Structural basis for sorting mechanism of p62 in selective autophagy. *J Biol Chem.* (2008) 283:22847-57. doi: 10.1074/jbc.M802182200.

Inoue H, Nojima H, Okayama H. High efficiency transformation of Escherichia coli with plasmids. *Gene.* (1990) 96:23-8. doi: 10.1016/0378-1119(90)90336-p.

Jackson MJ. Reactive oxygen species and redox-regulation of skeletal muscle adaptations to exercise. *Philos Trans R Soc Lond B Biol Sci.* (2005) 360:2285-91. doi: 10.1098/rstb.2005.1773.

Jatana N, Ascher DB, Pires DEV, Gokhale RS, Thukral L. Human LC3 and GABARAP subfamily members achieve functional specificity via specific structural modulations. *Autophagy.* (2020) 16:239-255. doi: 10.1080/15548627.2019.1606636.

Johansen T, Lamark T. Selective autophagy mediated by autophagic adapter proteins. *Autophagy.* (2011) 7:279-96. doi: 10.4161/auto.7.3.14487.

Johansen T, Lamark T. Selective Autophagy: ATG8 Family Proteins, LIR Motifs and Cargo Receptors. *J Mol Biol.* (2020) 432:80-103. doi: 10.1016/j.jmb.2019.07.016.

Kai F, Tanner K, King C, Duncan R. Myopodin isoforms alter the chemokinetic response of PC3 cells in response to different migration stimuli via differential effects on Rho-ROCK signaling pathways. *Carcinogenesis.* (2012) 33:2100-7. doi: 10.1093/carcin/bgs268.

Kakalis LT, Kennedy M, Sikkink R, Rusnak F, Armitage IM. Characterization of the calcium-binding sites of calcineurin B. *FEBS Lett.* (1995) 362:55-8. doi: 10.1016/0014-5793(95)00207-p.

Kathage B, Gehlert S, Ulbricht A, Lüdecke L, Tapia VE, Orfanos Z, Wenzel D, Bloch W, Volkmer R, Fleischmann BK, Fürst DO, Höhfeld J. The cochaperone BAG3 coordinates protein synthesis and autophagy under mechanical strain through spatial regulation of mTORC1. *Biochim Biophys Acta Mol Cell Res.* (2017) 1864:62-75. doi: 10.1016/j.bbamcr.2016.10.007.
Kerppola TK. Design and implementation of bimolecular fluorescence complementation (BiFC) assays for the visualization of protein interactions in living cells. *Nat Protoc.* (2006) 1:1278-86. doi: 10.1038/nprot.2006.201.

Khaymina SS, Kenney JM, Schroeter MM, Chalovich JM. Fesselin is a natively unfolded protein. *J Proteome Res.* (2007) 6:3648-54. doi: 10.1021/pr070237v.

Kim H, McCulloch CA. Filamin A mediates interactions between cytoskeletal proteins that control cell adhesion. *FEBS Lett.* (2011) 585:18-22. doi: 10.1016/j.febslet.2010.11.033.

Kim JH, Lee J, Oh B, Kimm K, Koh I. Prediction of phosphorylation sites using SVMs. *Bioinformatics.* (2004) 20:3179-84. doi: 10.1093/bioinformatics/bth382.

Kinoshita E, Kinoshita-Kikuta E, Ujihara H, Koike T. Mobility shift detection of phosphorylation on large proteins using a Phos-tag SDS-PAGE gel strengthened with agarose. *Proteomics.* (2009) 9:4098-101. doi: 10.1002/pmic.200900020.

Klee CB, Ren H, Wang X. Regulation of the calmodulin-stimulated protein phosphatase, calcineurin. *J Biol Chem*. (1998) 273:13367-70. doi: 10.1074/jbc.273.22.13367.

Kley RA, Maerkens A, Leber Y, Theis V, Schreiner A, van der Ven PF, Uszkoreit J, Stephan C, Eulitz S, Euler N, Kirschner J, Müller K, Meyer HE, Tegenthoff M, Fürst DO, Vorgerd M, Müller T, Marcus K. A combined laser microdissection and mass spectrometry approach reveals new disease relevant proteins accumulating in aggregates of filaminopathy patients. *Mol Cell Proteomics.* (2013) 12:215-27. doi: 10.1074/mcp.M112.023176.

Klimek C, Kathage B, Wördehoff J, Höhfeld J. BAG3-mediated proteostasis at a glance. *J Cell Sci.* (2017) 130:2781-2788. doi: 10.1242/jcs.203679.

Kołakowski J, Wrzosek A, Dabrowska R. Fesselin is a target protein for calmodulin in a calcium-dependent manner. *Biochem Biophys Res Commun.* (2004) 323:1251-6. doi: 10.1016/j.bbrc.2004.08.224.

Lad Y, Kiema T, Jiang P, Pentikäinen OT, Coles CH, Campbell ID, Calderwood DA, Ylänne J. Structure of three tandem filamin domains reveals auto-inhibition of ligand binding. *EMBO J.* (2007) 26:3993-4004. doi: 10.1038/sj.emboj.7601827.

Laemmli UK. Cleavage of structural proteins during the assembly of the head of bacteriophage T4. *Nature.* (1970) 227:680-5. doi: 10.1038/227680a0.

Lapierre LR, Kumsta C, Sandri M, Ballabio A, Hansen M. Transcriptional and epigenetic regulation of autophagy in aging. *Autophagy.* (2015) 11:867-80. doi: 10.1080/15548627.2015.1034410.

Lazova R, Camp RL, Klump V, Siddiqui SF, Amaravadi RK, Pawelek JM. Punctate LC3B expression is a common feature of solid tumors and associated with proliferation, metastasis, and poor outcome. *Clin Cancer Res.* (2012) 18:370-9. doi: 10.1158/1078-0432.CCR-11-1282.

Leber Y, Ruparelia AA, Kirfel G, van der Ven PF, Hoffmann B, Merkel R, Bryson-Richardson RJ, Fürst DO. Filamin C is a highly dynamic protein associated with fast repair of myofibrillar microdamage. *Hum Mol Genet.* (2016) 25:2776-2788. doi: 10.1093/hmg/ddw135.

Le Bihan MC, Barrio-Hernandez I, Mortensen TP, Henningsen J, Jensen SS, Bigot A, Blagoev B, Butler-Browne G, Kratchmarova I. Cellular Proteome Dynamics during Differentiation of Human Primary Myoblasts. *J Proteome Res.* (2015) 14:3348-61. doi: 10.1021/acs.jproteome.5b00397.

Lee HC, Cherk SW, Chan SK, Wong S, Tong TW, Ho WS, Chan AY, Lee KC, Mak CM. BAG3-related myofibrillar myopathy in a Chinese family. *Clin Genet.* (2012) 81:394-8. doi: 10.1111/j.1399-0004.2011.01659.x.

Leinweber BD, Fredricksen RS, Hoffman DR, Chalovich JM. Fesselin: a novel synaptopodin-like actin binding protein from muscle tissue. *J Muscle Res Cell Motil.* (1999) 20:539-45. doi: 10.1023/a:1005597306671.

Levine B, Kroemer G. Autophagy in the pathogenesis of disease. *Cell.* (2008) 132:27-42. doi: 10.1016/j.cell.2007.12.018.

Levine B, Kroemer G. Biological Functions of Autophagy Genes: A Disease Perspective. *Cell.* (2019) 176:11-42. doi: 10.1016/j.cell.2018.09.048.

Lewis YE, Moskovitz A, Mutlak M, Heineke J, Caspi LH, Kehat I. Localization of transcripts, translation, and degradation for spatiotemporal sarcomere maintenance. J *Mol Cell Cardiol.* (2018) 116:16-28. doi: 10.1016/j.yjmcc.2018.01.012.

Li H, Rao A, Hogan PG. Interaction of calcineurin with substrates and targeting proteins. *Trends Cell Biol.* (2011) 21:91-103. doi: 10.1016/j.tcb.2010.09.011.

Lin F, Yu YP, Woods J, Cieply K, Gooding B, Finkelstein P, Dhir R, Krill D, Becich MJ, Michalopoulos G, Finkelstein S, Luo JH. Myopodin, a synaptopodin homologue, is frequently deleted in invasive prostate cancers. *Am J Pathol.* (2001) 159:1603-12. doi: 10.1016/S0002-9440(10)63006-4.

Linding R, Jensen LJ, Ostheimer GJ, van Vugt MA, Jørgensen C, Miron IM, Diella F, Colwill K, Taylor L, Elder K, Metalnikov P, Nguyen V, Pasculescu A, Jin J, Park JG, Samson LD, Woodgett JR, Russell RB, Bork P, Yaffe MB, Pawson T. Systematic discovery of in vivo phosphorylation networks. *Cell.* (2007a) 129:1415-26. doi: 10.1016/j.cell.2007.05.052.

Linding R, Jensen LJ, Pasculescu A, Olhovsky M, Colwill K, Bork P, Yaffe MB, Pawson T. NetworKIN: a resource for exploring cellular phosphorylation networks. *Nucleic Acids Res*. (2008) 36:D695-9. doi: 10.1093/nar/gkm902.

Linnemann A, van der Ven PF, Vakeel P, Albinus B, Simonis D, Bendas G, Schenk JA, Micheel B, Kley RA, Fürst DO. The sarcomeric Z-disc component myopodin is a multiadapter protein that interacts with filamin and alpha-actinin. *Eur J Cell Biol.* (2010) 89:681-92. doi: 10.1016/j.ejcb.2010.04.004.

Linnemann A, Vakeel P, Bezerra E, Orfanos Z, Djinović-Carugo K, van der Ven PF, Kirfel G, Fürst DO. Myopodin is an F-actin bundling protein with multiple independent actin-binding regions. *J Muscle Res Cell Motil.* (2013) 34:61-9. doi: 10.1007/s10974-012-9334-5.

Liu F, Grundke-Iqbal I, Iqbal K, Oda Y, Tomizawa K, Gong CX. Truncation and activation of calcineurin A by calpain I in Alzheimer disease brain. *J Biol Chem.* (2005) 280:37755-62. doi: 10.1074/jbc.M507475200.

Liu K, Czaja MJ. Regulation of lipid stores and metabolism by lipophagy. *Cell Death Differ.* (2013) 20:3-11. doi: 10.1038/cdd.2012.63.

Lohanadan K, Molt S, Dierck F, van der Ven PFM, Frey N, Höhfeld J, Fürst DO. Isoform-specific functions of synaptopodin-2 variants in cytoskeleton stabilization and autophagy regulation in muscle under mechanical stress. *Exp Cell Res.* (2021) 408:112865. doi: 10.1016/j.yexcr.2021.112865.

Lottspeich, F. and Engels, J. W.: *Bioanalytik 2. Auflage*. Elsevier, Spektrum Akademis- cher Verlag (cit. on p.12) (2005).

Manabe Y, Miyatake S, Takagi M, Nakamura M, Okeda A, Nakano T, Hirshman MF, Goodyear LJ, Fujii NL. Characterization of an acute muscle contraction model using cultured C2C12 myotubes. *PLoS One.* (2012) 7:e52592. doi: 10.1371/journal.pone.0052592.

Manning G, Whyte DB, Martinez R, Hunter T, Sudarsanam S. The protein kinase complement of the human genome. *Science.* (2002) 298:1912-34. doi: 10.1126/science.1075762.

Margeta M. Autophagy Defects in Skeletal Myopathies. *Annu Rev Pathol.* (2020) 15:261-285. doi: 10.1146/annurev-pathmechdis-012419-032618.

Mizushima N, Levine B, Cuervo AM, Klionsky DJ. Autophagy fights disease through cellular self-digestion. *Nature.* (2008) 451:1069-75. doi: 10.1038/nature06639.

Mizushima N, Yoshimori T, Levine B. Methods in mammalian autophagy research. *Cell.* (2010) 140:313-26. doi: 10.1016/j.cell.2010.01.028.

Mizushima N, Yoshimori T, Ohsumi Y. The role of Atg proteins in autophagosome formation. *Annu Rev Cell Dev Biol.* (2011) 27:107-32. doi: 10.1146/annurev-cellbio-092910-154005.

Mohapatra B, Jimenez S, Lin JH, Bowles KR, Coveler KJ, Marx JG, Chrisco MA, Murphy RT, Lurie PR, Schwartz RJ, Elliott PM, Vatta M, McKenna W, Towbin JA, Bowles NE. Mutations in the muscle LIM protein and alpha-actinin-2 genes in dilated cardiomyopathy and endocardial fibroelastosis. *Mol Genet Metab.* (2003) 80:207-15. doi: 10.1016/s1096-7192(03)00142-2.

Molkentin JD, Lu JR, Antos CL, Markham B, Richardson J, Robbins J, Grant SR, Olson EN. A calcineurin-dependent transcriptional pathway for cardiac hypertrophy. *Cell.* (1998) 93:215-28. doi: 10.1016/s0092-8674(00)81573-1.

Molt S, Bührdel JB, Yakovlev S, Schein P, Orfanos Z, Kirfel G, Winter L, Wiche G, van der Ven PF, Rottbauer W, Just S, Belkin AM, Fürst DO. Aciculin interacts with filamin C and Xin and is essential for myofibril assembly, remodeling and maintenance. *J Cell Sci.* (2014) 127:3578-92. doi: 10.1242/jcs.152157.

Moreau K, Rubinsztein DC. The plasma membrane as a control center for autophagy. *Autophagy.* (2012) 8:861-3. doi: 10.4161/auto.20060.

Mullis K, Faloona F, Scharf S, Saiki R, Horn G, Erlich H. Specific enzymatic amplification of DNA in vitro: the polymerase chain reaction. 1986. *Biotechnology.* (1992) 24:17-27.

Mundel P, Heid HW, Mundel TM, Krüger M, Reiser J, Kriz W. Synaptopodin: an actin-associated protein in telencephalic dendrites and renal podocytes. *J Cell Biol.* (1997) 139:193-204. doi: 10.1083/jcb.139.1.193.
Moser H. Duchenne muscular dystrophy: pathogenetic aspects and genetic prevention. *Hum Genet.* (1984) 66:17-40. doi: 10.1007/BF00275183.

Nakamura F, Stossel TP, Hartwig JH. The filamins: organizers of cell structure and function. *Cell Adh Migr.* (2011) 5:160-9. doi: 10.4161/cam.5.2.14401.

Nave R, Fürst DO, Weber K. Interaction of alpha-actinin and nebulin in vitro. Support for the existence of a fourth filament system in skeletal muscle. *FEBS Lett.* (1990) 269:163-6. doi: 10.1016/0014-5793(90)81144-d.

Nedachi T, Fujita H, Kanzaki M. Contractile C2C12 myotube model for studying exercise-inducible responses in skeletal muscle. *Am J Physiol Endocrinol Metab.* (2008) 295:1191-204. doi: 10.1152/ajpendo.90280.2008.

Nascimbeni AC, Fanin M, Masiero E, Angelini C, Sandri M. Impaired autophagy contributes to muscle atrophy in glycogen storage disease type II patients. *Autophagy.* (2012a) 8:1697-700. doi: 10.4161/auto.21691.

Nascimbeni AC, Fanin M, Masiero E, Angelini C, Sandri M. The role of autophagy in the pathogenesis of glycogen storage disease type II (GSDII). *Cell Death Differ.* (2012b) 19:1698-708. doi: 10.1038/cdd.2012.52.

Norton N, Li D, Rieder MJ, Siegfried JD, Rampersaud E, Züchner S, Mangos S, Gonzalez-Quintana J, Wang L, McGee S, Reiser J, Martin E, Nickerson DA, Hershberger RE. Genome-wide studies of copy number variation and exome sequencing identify rare variants in BAG3 as a cause of dilated cardiomyopathy. *Am J Hum Genet.* (2011) 88:273-82. doi: 10.1016/j.ajhg.2011.01.016.

Ohta Y, Suzuki N, Nakamura S, Hartwig JH, Stossel TP. The small GTPase RalA targets filamin to induce filopodia. *Proc Natl Acad Sci USA.* (1999) 96:2122-8. doi: 10.1073/pnas.96.5.2122.

Ohtsuka H, Yajima H, Maruyama K, Kimura S. The N-terminal Z repeat 5 of connectin/titin binds to the C-terminal region of alpha-actinin. *Biochem Biophys Res Commun.* (1997) 235:1-3. doi: 10.1006/bbrc.1997.6534.

Oka T, Dai YS, Molkentin JD. Regulation of calcineurin through transcriptional induction of the calcineurin A beta promoter in vitro and in vivo. *Mol Cell Biol.* (2005) 25:6649-59. doi: 10.1128/MCB.25.15.6649-6659.2005.

Ong SE, Blagoev B, Kratchmarova I, Kristensen DB, Steen H, Pandey A, Mann M. Stable isotope labeling by amino acids in cell culture, SILAC, as a simple and accurate approach to expression proteomics. *Mol Cell Proteomics.* (2002) 1:376-86. doi: 10.1074/mcp.m200025-mcp200.

Ono S. Dynamic regulation of sarcomeric actin filaments in striated muscle. *Cytoskeleton (Hoboken)*. (2010) 67:677-92. doi: 10.1002/cm.20476.

Otten C, van der Ven PF, Lewrenz I, Paul S, Steinhagen A, Busch-Nentwich E, Eichhorst J, Wiesner B, Stemple D, Strähle U, Fürst DO, Abdelilah-Seyfried S. Xirp proteins mark injured skeletal muscle in zebrafish. *PLoS One.* (2012) 7:e31041. doi: 10.1371/journal.pone.0031041.

Orfanos Z, Gödderz MP, Soroka E, Gödderz T, Rumyantseva A, van der Ven PF, Hawke TJ, Fürst DO. Breaking sarcomeres by in vitro exercise. *Sci Rep.* (2016) 6:19614. doi: 10.1038/srep19614.

Pankiv S, Clausen TH, Lamark T, Brech A, Bruun JA, Outzen H, Øvervatn A, Bjørkøy G, Johansen T. p62/SQSTM1 binds directly to Atg8/LC3 to facilitate degradation of ubiquitinated protein aggregates by autophagy. *J Biol Chem.* (2007) 282:24131-45. doi: 10.1074/jbc.M702824200.

Papa I, Astier C, Kwiatek O, Raynaud F, Bonnal C, Lebart MC, Roustan C, Benyamin Y. Alpha actinin-CapZ, an anchoring complex for thin filaments in Z-line. *J Muscle Res Cell Motil.* (1999) 20:187-97. doi: 10.1023/a:1005489319058.

Parra V, Rothermel BA. Calcineurin signaling in the heart: The importance of time and place. *J Mol Cell Cardiol.* (2017) 103:121-136. doi: 10.1016/j.yjmcc.2016.12.006.

Patel TJ, Lieber RL. Force transmission in skeletal muscle: from actomyosin to external tendons. *Exerc Sport Sci Rev.* (1997) 25:321-63.

Pentikäinen U, Ylänne J. The regulation mechanism for the auto-inhibition of binding of human filamin A to integrin. *J Mol Biol.* (2009) 393:644-57. doi: 10.1016/j.jmb.2009.08.035.

Perpeet M, Glass S, Gronewold T, Kiwitz A, Malavé A, Stoyanov I, Tewes M, Quandt E. SAW sensor system for marker-free molecular interaction analysis. (2006) *Anal. Lett. 39*, 1747-1757.

Pham M, Chalovich JM. Smooth muscle alpha-actinin binds tightly to fesselin and attenuates its activity toward actin polymerization. *J Muscle Res Cell Motil.* (2006) 27:45-51. doi: 10.1007/s10974-005-9053-2.

Pudas R, Kiema TR, Butler PJ, Stewart M, Ylänne J. Structural basis for vertebrate filamin dimerization. *Structure.* (2005) 13:111-9. doi: 10.1016/j.str.2004.10.014.

Purslow PP. The structure and functional significance of variations in the connective tissue within muscle. *Comp Biochem Physiol A Mol Integr Physiol.* (2002) 133:947-66. doi: 10.1016/s1095-6433(02)00141-1.

Pyle WG, Solaro RJ. At the crossroads of myocardial signaling: the role of Z-discs in intracellular signaling and cardiac function. *Circ Res.* (2004) 94:296-305. doi: 10.1161/01.

Reimann L, Schwäble AN, Fricke AL, Mühlhäuser WWD, Leber Y, Lohanadan K, Puchinger MG, Schäuble S, Faessler E, Wiese H, Reichenbach C, Knapp B, Peikert CD, Drepper F, Hahn U, Kreutz C, van der Ven PFM, Radziwill G, Djinović-Carugo K, Fürst DO, Warscheid B. Phosphoproteomics identifies dual-site phosphorylation in an extended basophilic motif regulating FILIP1-mediated degradation of filamin-C. *Commun Biol.* (2020) 3:253. doi: 10.1038/s42003-020-0982-5.

Reimann L, Wiese H, Leber Y, Schwäble AN, Fricke AL, Rohland A, Knapp B, Peikert CD, Drepper F, van der Ven PF, Radziwill G, Fürst DO, Warscheid B. Myofibrillar Z-discs Are a Protein Phosphorylation Hot Spot with Protein Kinase C (PKCα) Modulating Protein Dynamics. *Mol Cell Proteomics.* (2017) 16:346-367. doi: 10.1074/mcp.M116.065425.

Renegar RH, Chalovich JM, Leinweber BD, Zary JT, Schroeter MM. Localization of the actin-binding protein fesselin in chicken smooth muscle. *Histochem Cell Biol.* (2009) 131:191-6. doi: 10.1007/s00418-008-0508-6.

Rhee D, Sanger JM, Sanger JW. The premyofibril: evidence for its role in myofibrillogenesis. *Cell Motil Cytoskeleton.* (1994) 28:1-24. doi: 10.1002/cm.970280102.

Ribeiro Ede A Jr, Pinotsis N, Ghisleni A, Salmazo A, Konarev PV, Kostan J, Sjöblom B, Schreiner C, Polyansky AA, Gkougkoulia EA, Holt MR, Aachmann FL, Zagrović B, Bordignon E, Pirker KF, Svergun DI, Gautel M, Djinović-Carugo K. The structure and regulation of human muscle α-actinin. *Cell.* (2014) 159:1447-60. doi: 10.1016/j.cell.2014.10.056.

Richter B, Sliter DA, Herhaus L, Stolz A, Wang C, Beli P, Zaffagnini G, Wild P, Martens S, Wagner SA, Youle RJ, Dikic I. Phosphorylation of OPTN by TBK1 enhances its binding to Ub chains and promotes selective autophagy of damaged mitochondria. *Proc Natl Acad Sci USA.* (2016) 113:4039-44. doi: 10.1073/pnas.1523926113.

Rief M, Gautel M, Oesterhelt F, Fernandez JM, Gaub HE. Reversible unfolding of individual titin immunoglobulin domains by AFM. *Science.* (1997) 276:1109-12. doi: 10.1126/science.276.5315.1109.

Rognoni L, Stigler J, Pelz B, Ylänne J, Rief M. Dynamic force sensing of filamin revealed in single-molecule experiments. *Proc Natl Acad Sci USA.* (2012) 109:19679-84. doi: 10.1073/pnas.1211274109.

Rudolph F, Hüttemeister J, da Silva Lopes K, Jüttner R, Yu L, Bergmann N, Friedrich D, Preibisch S, Wagner E, Lehnart SE, Gregorio CC, Gotthardt M. Resolving titin's lifecycle and the spatial organization of protein turnover in mouse cardiomyocytes. *Proc Natl Acad Sci USA.* (2019) 116:25126-25136. doi: 10.1073/pnas.1904385116.

Rusnak F, Mertz P. Calcineurin: form and function. *Physiol Rev.* (2000) 80:1483-521. doi: 10.1152/physrev.2000.80.4.1483.

Sakuma K, Yamaguchi A. The functional role of calcineurin in hypertrophy, regeneration, and disorders of skeletal muscle. *J Biomed Biotechnol.* (2010) 2010:721219. doi: 10.1155/2010/721219.

Salmikangas P, Mykkänen OM, Grönholm M, Heiska L, Kere J, Carpén O. Myotilin, a novel sarcomeric protein with two Ig-like domains, is encoded by a candidate gene for limb-girdle muscular dystrophy. *Hum Mol Genet.* (1999) 8:1329-36. doi: 10.1093/hmg/8.7.1329.

Sanger JW, Ayoob JC, Chowrashi P, Zurawski D, Sanger JM. Assembly of myofibrils in cardiac muscle cells. *Adv Exp Med Biol.* (2000) 481:89-102; discussion 103-5. doi: 10.1007/978-1-4615-4267-4_6.

Sanger JW, Chowrashi P, Shaner NC, Spalthoff S, Wang J, Freeman NL, Sanger JM. Myofibrillogenesis in skeletal muscle cells. *Clin Orthop Relat Res.* (2002) (403 Suppl):S153-62. doi: 10.1097/00003086-200210001-00018.

Sanger JW, Kang S, Siebrands CC, Freeman N, Du A, Wang J, Stout AL, Sanger JM. How to build a myofibril. *J Muscle Res Cell Motil.* (2005) 26:343-54. doi: 10.1007/s10974-005-9016-7.

Sarparanta J, Jonson PH, Golzio C, Sandell S, Luque H, Screen M, McDonald K, Stajich JM, Mahjneh I, Vihola A, Raheem O, Penttilä S, Lehtinen S, Huovinen S, Palmio J, Tasca G, Ricci E, Hackman P, Hauser M, Katsanis N, Udd B. Mutations affecting the cytoplasmic functions of the co-chaperone DNAJB6 cause limb-girdle muscular dystrophy. *Nat Genet.* (2012) 44:450-5, S1-2. doi: 10.1038/ng.1103.

Schmidt SF, Rohm M, Herzig S, Berriel Diaz M. Cancer Cachexia: More Than Skeletal Muscle Wasting. *Trends Cancer*. (2018) 4:849-860. doi: 10.1016/j.trecan.2018.10.001.

Schneider CA, Rasband WS, Eliceiri KW. NIH Image to ImageJ: 25 years of image analysis. Nat Methods. 2012 Jul;9(7):671-5. doi: 10.1038/nmeth.2089. PMID: 22930834; PMCID: PMC5554542.

Schultheiss T, Choi J, Lin ZX, DiLullo C, Cohen-Gould L, Fischman D, Holtzer H. A sarcomeric alpha-actinin truncated at the carboxyl end induces the breakdown of stress fibers in PtK2 cells and the formation of nemaline-like bodies and breakdown of myofibrils in myotubes. *Proc Natl Acad Sci USA.* (1992) 89:9282-6. doi: 10.1073/pnas.89.19.9282.

Schwartz D, Gygi SP. An iterative statistical approach to the identification of protein phosphorylation motifs from large-scale data sets. *Nat Biotechnol.* (2005) 23:1391-8. doi: 10.1038/nbt1146.

Schroeter MM, Chalovich JM. Fesselin binds to actin and myosin and inhibits actin-activated ATPase activity. *J Muscle Res Cell Motil.* (2005) 26:183-9. doi: 10.1007/s10974-005-9009-6.

Schünke M. Topographie und Funktion des Bewegungssystems. *Thieme Verlag* (2000).

Selcen D, Muntoni F, Burton BK, Pegoraro E, Sewry C, Bite AV, Engel AG. Mutation in BAG3 causes severe dominant childhood muscular dystrophy. *Ann Neurol.* (2009) 65:83-9. doi: 10.1002/ana.21553.

Seo MD, Seok SH, Im H, Kwon AR, Lee SJ, Kim HR, Cho Y, Park D, Lee BJ. Crystal structure of the dimerization domain of human filamin A. *Proteins.* (2009) 75:258-63. doi: 10.1002/prot.22336.

Shaid S, Brandts CH, Serve H, Dikic I. Ubiquitination and selective autophagy. *Cell Death Differ.* (2013) 20:21-30. doi: 10.1038/cdd.2012.72.

Sievers F, Wilm A, Dineen D, Gibson TJ, Karplus K, Li W, Lopez R, McWilliam H, Remmert M, Söding J, Thompson JD, Higgins DG. Fast, scalable generation of high-quality protein multiple sequence alignments using Clustal Omega. Mol Syst Biol. 2011 Oct 11;7:539. doi: 10.1038/msb.2011.75. PMID: 21988835; PMCID: PMC3261699.

Sjöblom B, Salmazo A, Djinović-Carugo K. Alpha-actinin structure and regulation. *Cell Mol Life Sci.* (2008) 65:2688-701. doi: 10.1007/s00018-008-8080-8.

Taigen T, De Windt LJ, Lim HW, Molkentin JD. Targeted inhibition of calcineurin prevents agonist-induced cardiomyocyte hypertrophy. *Proc Natl Acad Sci USA.* (2000) 97:1196-201. doi: 10.1073/pnas.97.3.1196.

Takada F, Vander Woude DL, Tong HQ, Thompson TG, Watkins SC, Kunkel LM, Beggs AH. Myozenin: an alpha-actinin- and gamma-filamin-binding protein of skeletal muscle Z lines. *Proc Natl Acad Sci USA.* (2001) 98:1595-600. doi: 10.1073/pnas.98.4.1595.

Takayama S, Xie Z, Reed JC. An evolutionarily conserved family of Hsp70/Hsc70 molecular chaperone regulators. *J Biol Chem.* (1999) 274:781-6. doi: 10.1074/jbc.274.2.781.

Thelen MH, Simonides WS, van Hardeveld C. Electrical stimulation of C2C12 myotubes induces contractions and represses thyroid-hormone-dependent transcription of the fast-type sarcoplasmic-reticulum Ca2+-ATPase gene. *Biochem J.* (1997) 321:845-8. doi: 10.1042/bj3210845.

Thompson TG, Chan YM, Hack AA, Brosius M, Rajala M, Lidov HG, McNally EM, Watkins S, Kunkel LM. Filamin 2 (FLN2): A muscle-specific sarcoglycan interacting protein. *J Cell Biol.* (2000) 148:115-26. doi: 10.1083/jcb.148.1.115.

Thukral L, Sengupta D, Ramkumar A, Murthy D, Agrawal N, Gokhale RS. The Molecular Mechanism Underlying Recruitment and Insertion of Lipid-Anchored LC3 Protein into Membranes. *Biophys J*. (2015) 109:2067-78. doi: 10.1016/j.bpj.2015.09.022.

Ten Broek RW, Grefte S, Von den Hoff JW. Regulatory factors and cell populations involved in skeletal muscle regeneration. *J Cell Physiol.* (2010) 224:7-16. doi: 10.1002/jcp.22127.

Towbin H, Staehelin T, Gordon J. Electrophoretic transfer of proteins from polyacrylamide gels to nitrocellulose sheets: procedure and some applications. *Proc Natl Acad Sci USA.* (1979) 76:4350-4. doi: 10.1073/pnas.76.9.4350.

Travé G, Pastore A, Hyvönen M, Saraste M. The C-terminal domain of alpha-spectrin is structurally related to calmodulin. *Eur J Biochem.* (1995) 227:35-42. doi: 10.1111/j.1432-1033.1995.tb20357.x.

Tremblay ML, Giguère V. Phosphatases at the heart of FoxO metabolic control. *Cell Metab.* (2008) 7:101-3. doi: 10.1016/j.cmet.2008.01.004.

Tskhovrebova L, Trinick J. Roles of titin in the structure and elasticity of the sarcomere. *J Biomed Biotechnol.* (2010) 2010:612482. doi: 10.1155/2010/612482.

Ulbricht A, Eppler FJ, Tapia VE, van der Ven PF, Hampe N, Hersch N, Vakeel P, Stadel D, Haas A, Saftig P, Behrends C, Fürst DO, Volkmer R, Hoffmann B, Kolanus W, Höhfeld J. Cellular mechanotransduction relies on tension-induced and chaperone-assisted autophagy. *Curr Biol.* (2013a) 23:430-5. doi: 10.1016/j.cub.2013.01.064.

Ulbricht A, Gehlert S, Leciejewski B, Schiffer T, Bloch W, Höhfeld J. Induction and adaptation of chaperone-assisted selective autophagy CASA in response to resistance exercise in human skeletal muscle. *Autophagy.* (2015) 11:538-46. doi: 10.1080/15548627.2015.1017186.

Ulbricht A, Höhfeld J. Tension-induced autophagy: may the chaperone be with you. *Autophagy.* (2013b) 9:920-2. doi: 10.4161/auto.24213.

Van der Ven PF, Ehler E, Vakeel P, Eulitz S, Schenk JA, Milting H, Micheel B, Fürst DO. Unusual splicing events result in distinct Xin isoforms that associate differentially with filamin c and Mena/VASP. *Exp Cell Res.* (2006) 312:2154-67. doi: 10.1016/j.yexcr.2006.03.015.

Van der Ven PF, Obermann WM, Lemke B, Gautel M, Weber K, Fürst DO. Characterization of muscle filamin isoforms suggests a possible role of gamma-filamin/ABP-L in sarcomeric Z-disc formation. *Cell Motil Cytoskeleton.* (2000a) 45:149-62. doi: 10.1002/(SICI)1097-0169(200002)45:2<149::AID-CM6>3.0.CO;2-G.

Van der Ven PF, Wiesner S, Salmikangas P, Auerbach D, Himmel M, Kempa S, Hayess K, Pacholsky D, Taivainen A, Schröder R, Carpén O, Fürst DO. Indications for a novel muscular dystrophy pathway. gamma-filamin, the muscle-specific filamin isoform, interacts with myotilin. *J Cell Biol.* (2000b) 151:235-48. doi: 10.1083/jcb.151.2.235.

Van Troys M, Vandekerckhove J, Ampe C. Structural modules in actin-binding proteins: towards a new classification. *Biochim Biophys Acta.* (1999) 1448:323-48. doi: 10.1016/s0167-4889(98)00152-9.

Vijayan K, Thompson JL, Norenberg KM, Fitts RH, Riley DA. Fiber-type susceptibility to eccentric contraction-induced damage of hindlimb-unloaded rat AL muscles. *J Appl Physiol (1985).* (2001) 90:770-6. doi: 10.1152/jappl.2001.90.3.770.

Vijayan K, Thompson JL, Riley DA. Sarcomere lesion damage occurs mainly in slow fibers of reloaded rat adductor longus muscles. *J Appl Physiol (1985).* (1998) 85:1017-23. doi: 10.1152/jappl.1998.85.3.1017.

Von Mering C, Jensen LJ, Kuhn M, Chaffron S, Doerks T, Krüger B, Snel B, Bork P. STRING 7--recent developments in the integration and prediction of protein interactions. *Nucleic Acids Res.* (2007) 35:D358-62. doi: 10.1093/nar/gkl825.

Vorgerd M, van der Ven PF, Bruchertseifer V, Löwe T, Kley RA, Schröder R, Lochmüller H, Himmel M, Koehler K, Fürst DO, Huebner A. A mutation in the dimerization domain of filamin c causes a novel type of autosomal dominant myofibrillar myopathy. *Am J Hum Genet.* (2005) 77:297-304. doi: 10.1086/431959.

Wagers AJ, Conboy IM. Cellular and molecular signatures of muscle regeneration: current concepts and controversies in adult myogenesis. *Cell.* (2005) 122:659-67. doi: 10.1016/j.cell.2005.08.021.

Wang K, Singer SJ. Interaction of filamin with f-actin in solution. *Proc Natl Acad Sci USA.* (1977) 74:2021-5. doi: 10.1073/pnas.74.5.2021.

Weidberg H, Shpilka T, Shvets E, Abada A, Shimron F, Elazar Z. LC3 and GATE-16 N termini mediate membrane fusion processes required for autophagosome biogenesis. *Dev Cell.* (2011) 20:444-54. doi: 10.1016/j.devcel.2011.02.006.

Weins A, Schwarz K, Faul C, Barisoni L, Linke WA, Mundel P. Differentiation- and stress-dependent nuclear cytoplasmic redistribution of myopodin, a novel actin-bundling protein. *J Cell Biol.* (2001) 155:393-404. doi: 10.1083/jcb.200012039.

Wickner W. Membrane fusion: five lipids, four SNAREs, three chaperones, two nucleotides, and a Rab, all dancing in a ring on yeast vacuoles. *Annu Rev Cell Dev Biol.* (2010) 26:115-36. doi: 10.1146/annurev-cellbio-100109-104131.

Wild P, Farhan H, McEwan DG, Wagner S, Rogov VV, Brady NR, Richter B, Korac J, Waidmann O, Choudhary C, Dötsch V, Bumann D, Dikic I. Phosphorylation of the autophagy receptor optineurin restricts Salmonella growth. *Science.* (2011) 333:228-33. doi: 10.1126/science.1205405.

Wilkins MR, Sanchez JC, Gooley AA, Appel RD, Humphery-Smith I, Hochstrasser DF, Williams KL. Progress with proteome projects: why all proteins expressed by a genome should be identified and how to do it. *Biotechnol Genet Eng Rev.* (1996) 13:19-50. doi: 10.1080/02648725.1996.10647923.

Willis MS, Schisler JC, Portbury AL, Patterson C. Build it up-Tear it down: protein quality control in the cardiac sarcomere. *Cardiovasc Res.* (2009) 81:439-48. doi: 10.1093/cvr/cvn289.

Winter L, Staszewska I, Mihailovska E, Fischer I, Goldmann WH, Schröder R, Wiche G. Chemical chaperone ameliorates pathological protein aggregation in plectin-deficient muscle. *J Clin Invest.* (2014) 124:1144-57. doi: 10.1172/JCI71919.

Wong YH, Lee TY, Liang HK, Huang CM, Wang TY, Yang YH, Chu CH, Huang HD, Ko MT, Hwang JK. KinasePhos 2.0: a web server for identifying protein kinase-specific phosphorylation sites based on sequences and coupling patterns. *Nucleic Acids Res.* (2007) 35:W588-94. doi: 10.1093/nar/gkm322.

Xie Z, Xu W, Davie EW, Chung DW. Molecular cloning of human ABPL, an actin-binding protein homologue. *Biochem Biophys Res Commun.* (1998) 251:914-9. doi: 10.1006/bbrc.1998.9506.

Yaffe D, Saxel O. A myogenic cell line with altered serum requirements for differentiation. Differentiation. (1977) 7:159-66. doi: 10.1111/j.1432-0436.1977.tb01507.x.

Yamazaki M, Furuike S, Ito T. Mechanical response of single filamin A (ABP-280) molecules and its role in the actin cytoskeleton. *J Muscle Res Cell Motil.* (2002) 23:525-34. doi: 10.1023/a:1023418725001.

Young P, Gautel M. The interaction of titin and alpha-actinin is controlled by a phospholipid-regulated intramolecular pseudoligand mechanism. *EMBO J.* (2000) 19:6331-40. doi: 10.1093/emboj/19.23.6331.

Yu JG, Carlsson L, Thornell LE. Evidence for myofibril remodeling as opposed to myofibril damage in human muscles with DOMS: an ultrastructural and immunoelectron microscopic study. *Histochem Cell Biol.* (2004) 121:219-27. doi: 10.1007/s00418-004-0625-9.

Yu JG, Thornell LE. Desmin and actin alterations in human muscles affected by delayed onset muscle soreness: a high resolution immunocytochemical study. *Histochem Cell Biol.* (2002) 118:171-9. doi: 10.1007/s00418-002-0427-x.

Yu JG, Fürst DO, Thornell LE. The mode of myofibril remodelling in human skeletal muscle affected by DOMS induced by eccentric contractions. *Histochem Cell Biol.* (2003) 119:383-93. doi: 10.1007/s00418-003-0522-7.

Yu YP, Luo JH. Myopodin-mediated suppression of prostate cancer cell migration involves interaction with zyxin. *Cancer Res.* (2006) 66:7414-9. doi: 10.1158/0008-5472.CAN-06-0227.

Yu YP, Luo JH. Phosphorylation and interaction of myopodin by integrin-link kinase lead to suppression of cell growth and motility in prostate cancer cells. *Oncogene.* (2011) 30:4855-63. doi: 10.1038/onc.2011.200.

Zhou AX, Hartwig JH, Akyürek LM. Filamins in cell signaling, transcription and organ development. *Trends Cell Biol.* (2010) 20:113-23. doi: 10.1016/j.tcb.2009.12.001.

Zhu Y, Massen S, Terenzio M, Lang V, Chen-Lindner S, Eils R, Novak I, Dikic I, Hamacher-Brady A, Brady NR. Modulation of serines 17 and 24 in the LC3-interacting region of Bnip3 determines pro-survival mitophagy versus apoptosis. *J Biol Chem*. (2013) 288:1099-113. doi: 10.1074/jbc.M112.399345.

Zoncu R, Bar-Peled L, Efeyan A, Wang S, Sancak Y, Sabatini DM. mTORC1 senses lysosomal amino acids through an inside-out mechanism that requires the vacuolar H (+)-ATPase. *Science.* (2011) 334:678-83. doi: 10.1126/science.1207056.

Appendix

A. Abbreviations

A	alanine
ABD	actin-binding domain
ATP	adenosine triphosphate
ADP	adenosine diphosphate
APS	ammonium persulfate
BiFC	bimolecular fluorescence complementation
bp	base pair
BSA	bovine serum albumin
°C	Celsius
cDNA	complementary DNA
CaM	calmodulin-like calcium-binding domain
CASA	chaperone assisted selective autophagy
CH	calponin homology
CO_2	carbon dioxide
CoIP	co-immunoprecipitation
d	domain
D	aspartic acid
ddH_2O	double distilled water
DMEM	Dulbecco´s modified eagle medium
DMSO	dimethyl sulfoxide
DNA	desoxyribonucleic acid
dNTP	deoxy nucleoside triphosphate
DTT	dithiothreitol
E. coli	Escherichia Coli
ECL	enhanced chemiluminescence
EDTA	ethylenediaminetetraacetic acid
EGFP	enhanced green fluorescence protein
EYFP	enhanced yellow fluorescence protein
EGS	ethylene glycol bis[sulfosuccinimidylsuccinate]
FCS	fetal calf serum
FRAP	fluorescence recovery after photobleaching
GAPDH	glyceraldehyde-3-phophate-dehydrogenase

h	hour
His6	hexa-histidine
HRP	horseradish peroxidase
IF	immunofluorescence
Ig	immunoglobulin
IPTG	isopropyl-β-D-1-thiogalactopyranoside
kDa	kilodalton
kd	knockdown
l	liter
MDa	megadalton
min	minute
MFM	myofibrillar myopathy
MTJ	myotendinous junction
mRNA	messenger RNA
NEAA	nonessential amino acids
NGS	normal goat serum
NTA	nitrilotriacetate acid
OD	optical density
PAA	poly acrylic acid
PAGE	polyacrylamide gel electrophoresis
PBS	phosphate buffered saline
PEG	polyethylene glycol
PFA	paraformaldehyde
PKA	protein kinase A
PCR	polymerase chain reaction
RNA	ribonucleic acid
ROI	region of interest
rpm	rounds per minute
RT-PCR	reverse transcriptase PCR
s	seconds
S	serine
SDS	sodium dodecyl sulfate
SEM	scanning electron microscopy
Synpo2	synaptopodin-2

TAE	tris acetate EDTA
TBST	tris buffered saline plus Triton X-100
TE	tris EDTA
TEMED	tetramethyl ethylenediamine
Tris	Tris-(hydroxymethyl)-aminomethane
RT	room temperature
U	units
UV	ultraviolet
V	volt
WB	western blot
WT	wild type
XIRP	Xin-repeat proteins

B. Index of figures

C. Index of tables

D. Vector Maps

pET23aEEF

Length: 3.6 kb
Origin: Novagen (pET23a)

T7 promotor
His_6-tag
EEF-tag
F1 origin
ampicillin resistance

```
                          T7 Promotor
BglII                     ---------->
AGATCTCGATCCCGCGAAATTAATACGACTCACTATAGGGAGACCACAACGGTTTCCC

XbaI                              rbs          NdeI  MluI      SalI
TCTAGAAATAATTTTGTTTAACTTTAAGAAGGAGATATACATATGACGCGTTTTGTCGAC

     His6-Tag      Immuno-Tag    XhoI
CACCACCACCACCACCACGAGGAGTTCTGACTCGAGCACCACCACCACCACCACTGAGAT
 H   H   H   H   H   H  E   E   F  Stop

CCGGCTGCTAACAAAGCCCGAAAGGAAGCTGAGTTGGCTGCTGCCACCGCTGAGCAATAA

                 T7-Terminator
CTAGCATAACCCCTTGGGGCCTCTAAACGGGTCTTGAGGGGT
```

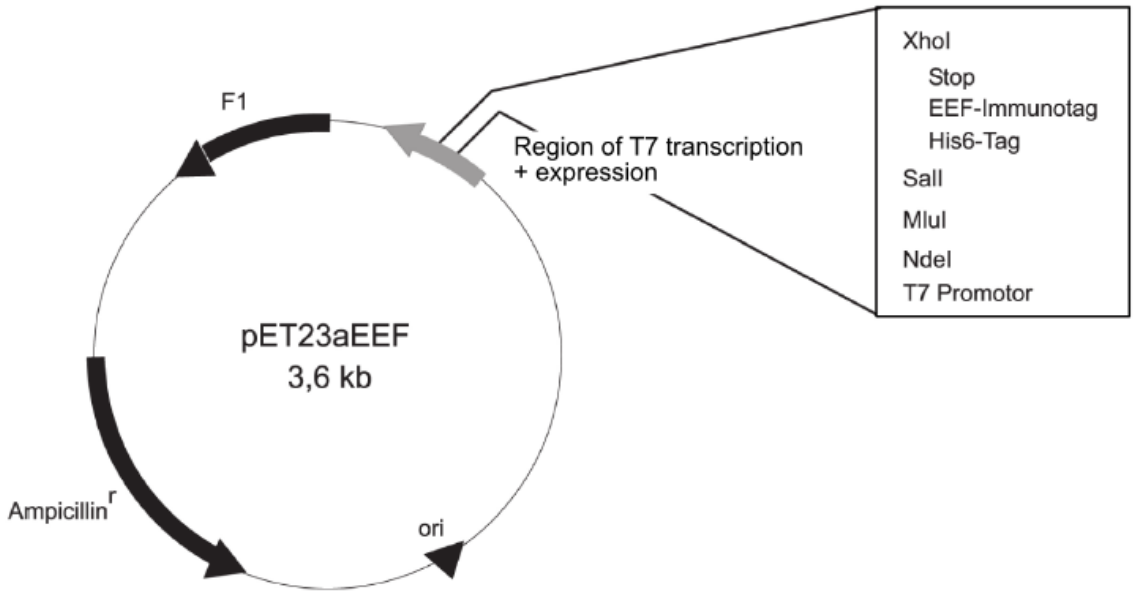

pET23aT7

Length: 3.6 kb
Origin: Novagen (pET23a)

T7 promotor
His_6-tag
EEF-tag
F1 origin
ampicillin resistance

```
                                T7 Promotor
BglII                          ------------>
AGATCTCGATCCCGCGAAATTAATACGACTCACTATAGGGAGACCACAACGGTTTCCC

XbaI                                rbs          NdeI  NheI
TCTAGAAATAATTTTGTTTAACTTTAAGAAGGAGATATACATATGGCTAGCATGACT
                                                  M  A  S  M  T

    T7-Immunotag       BamHI MluI                              SalI
GGTGGACAGCAAATGGGTCGCGGATCCACGCGT  [        Insert        ] GTCGAC
 G  G  Q  Q  M  G  R  G  S  T  R                              V  D

 XhoI      His6-Tag
CTCGAGCACCACCACCACCACCACTGAGATCCGGCTGCTAACAAAGCCCGAAAGGAAG
 L  E  H  H  H  H  H  H Stop

                                                  T7-Terminator
CTGAGTTGGCTGCTGCCACCGCTGAGCAATAACTAGCATAACCCCTTGGGGCCTCTAA

ACGGGTCTTGAGGGGT
```

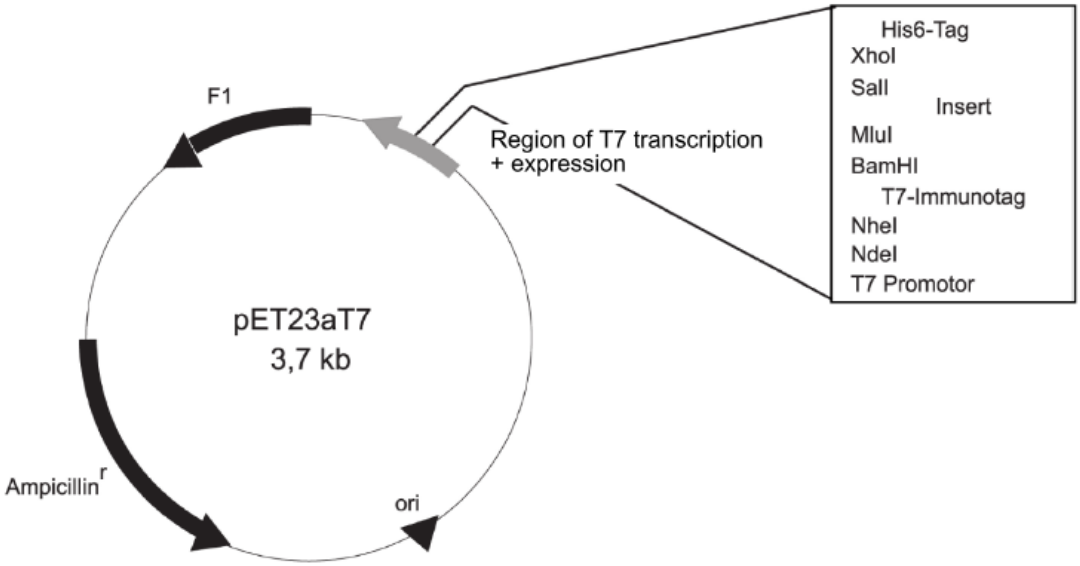

pDEST15

Length: 7.0 kb

T7 promotor
GST-tag
pBR322 origin
ampicillin resistance

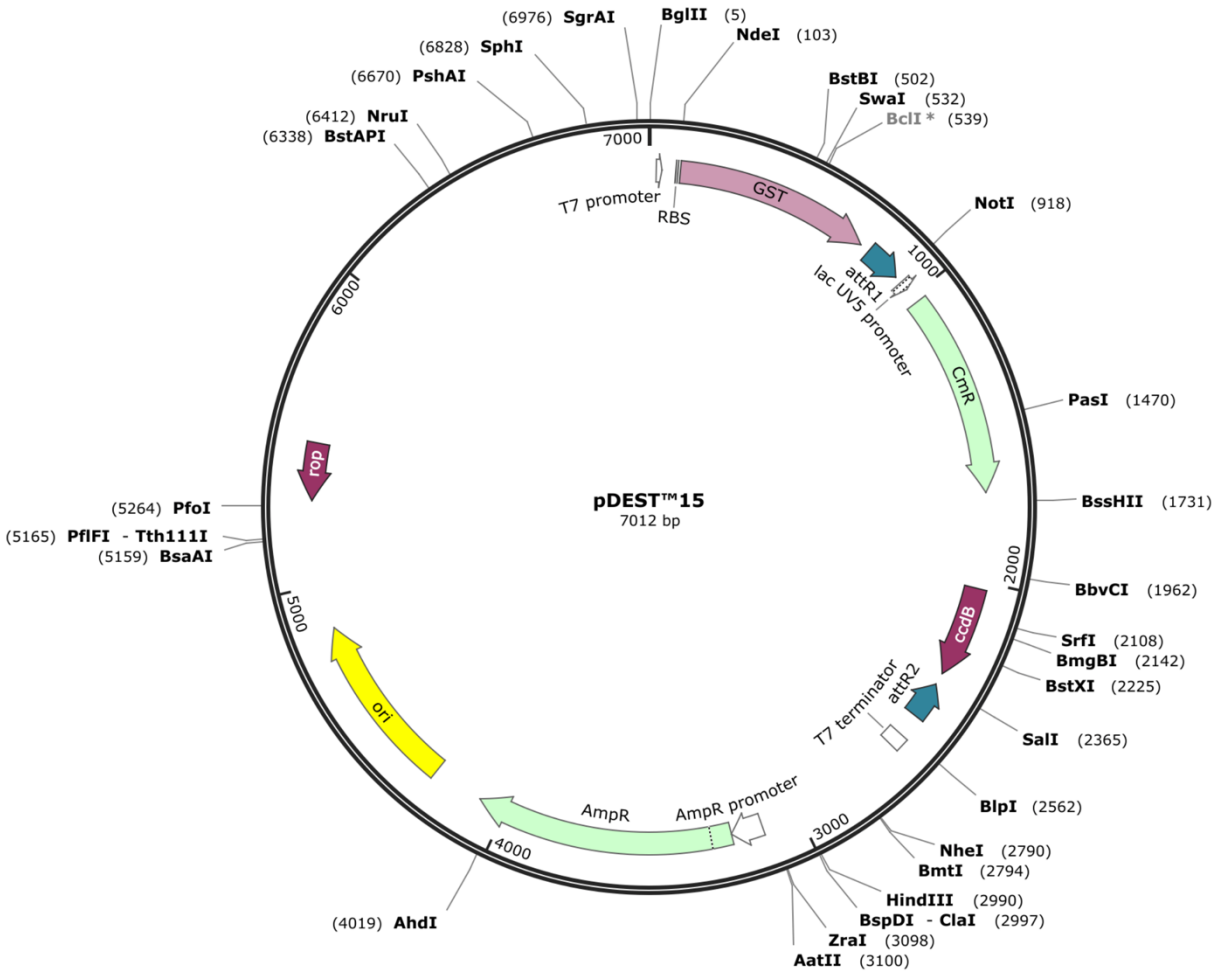

Venus1-C

length: 4,7 kb
origin: Clontech (pECFP-C1)

Cytomegalovirus immediate early gene enhancer/promotor
Flag-Tag
Venus1 (AS 1-154)
Kanamycin resistance gene

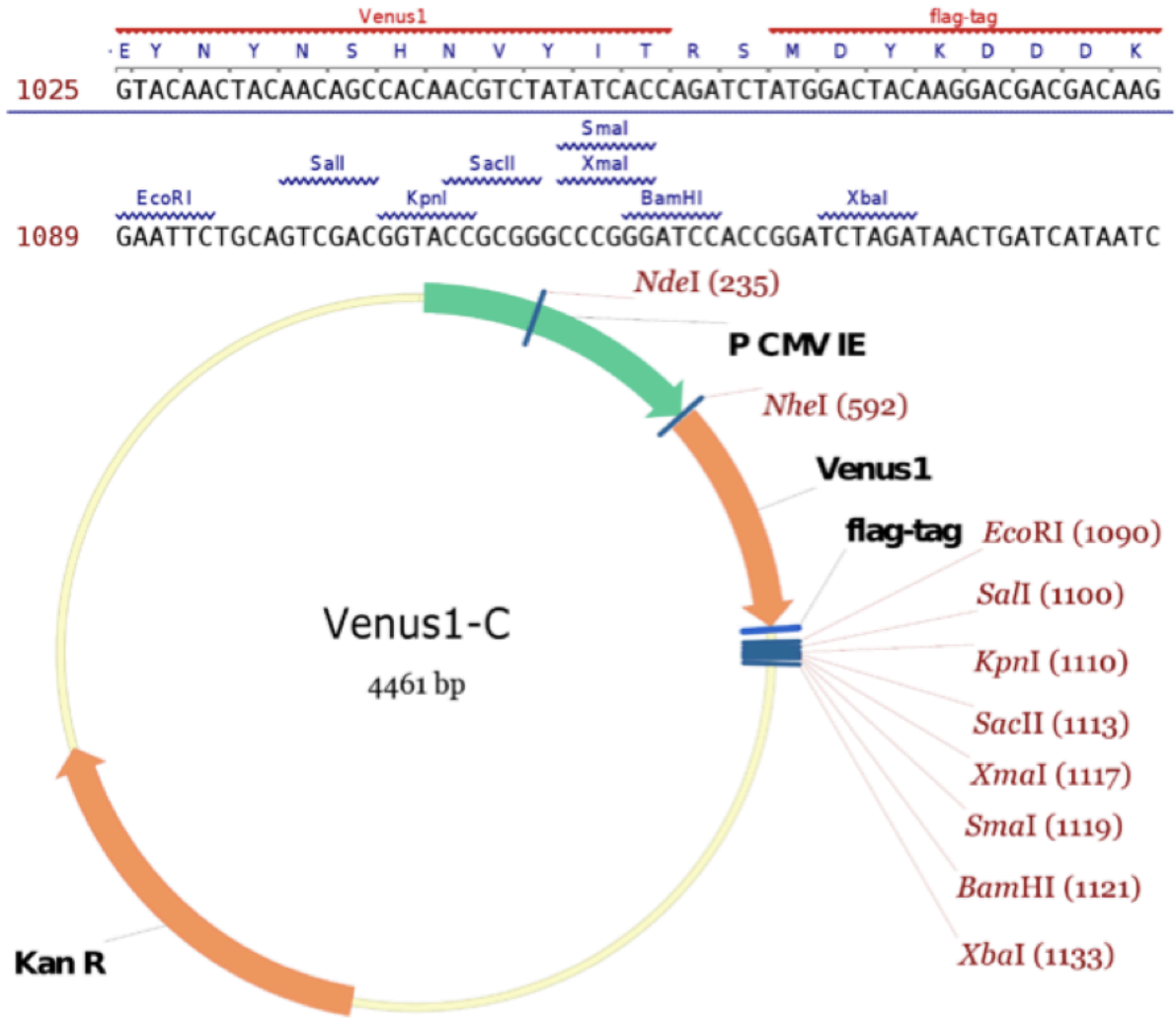

Venus2-C

length: 4,3 kb
origin: Clontech (pECFP-C1)

Cytomegalovirus immediate early gene enhancer/promotor
HA-Tag
Venus2 (AS 155-238)
Kanamycin resistance gene

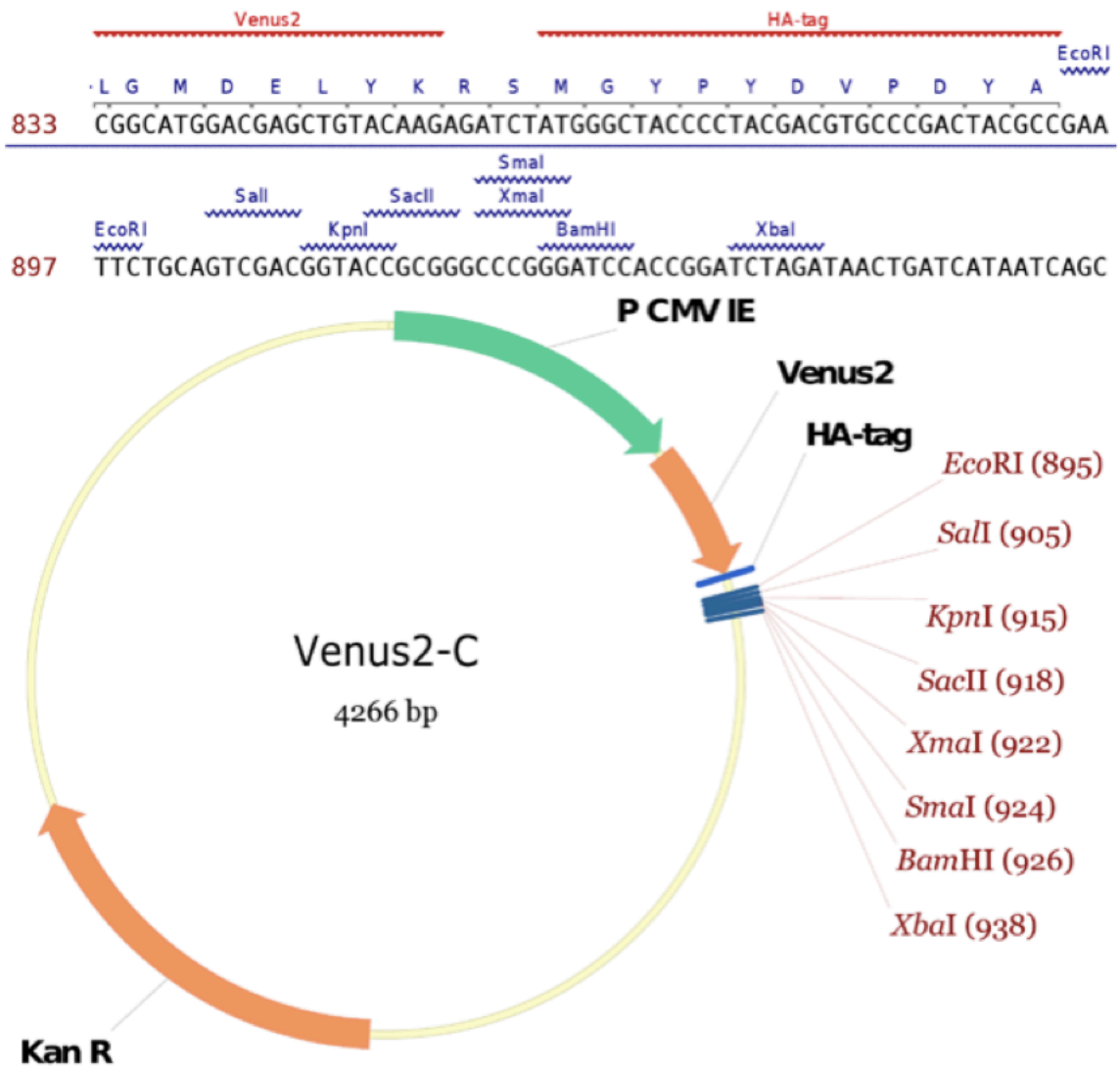

Venus1-N3

length: 4,5 kb
origin: Clontech (pECFP-C1/pEGFP-N3)

Cytomegalovirus immediate early gene enhancer/promotor
Flag-Tag
Venus1 (AS 1-154)
Kanamycin resistance gene

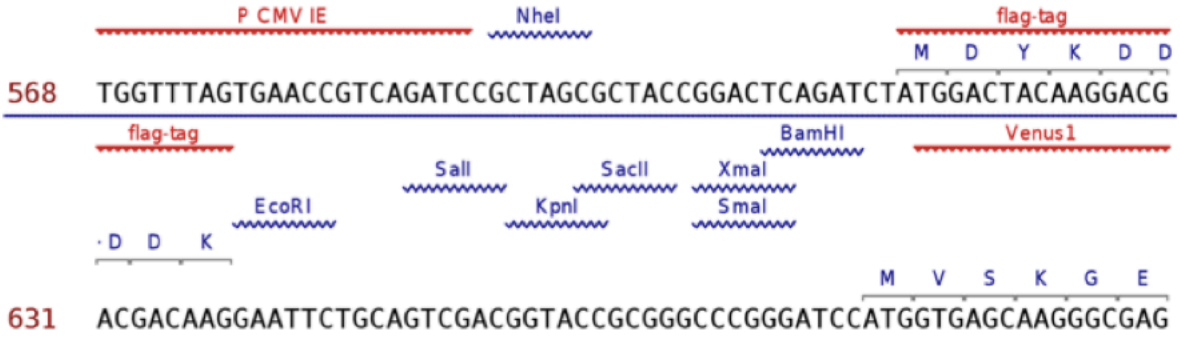

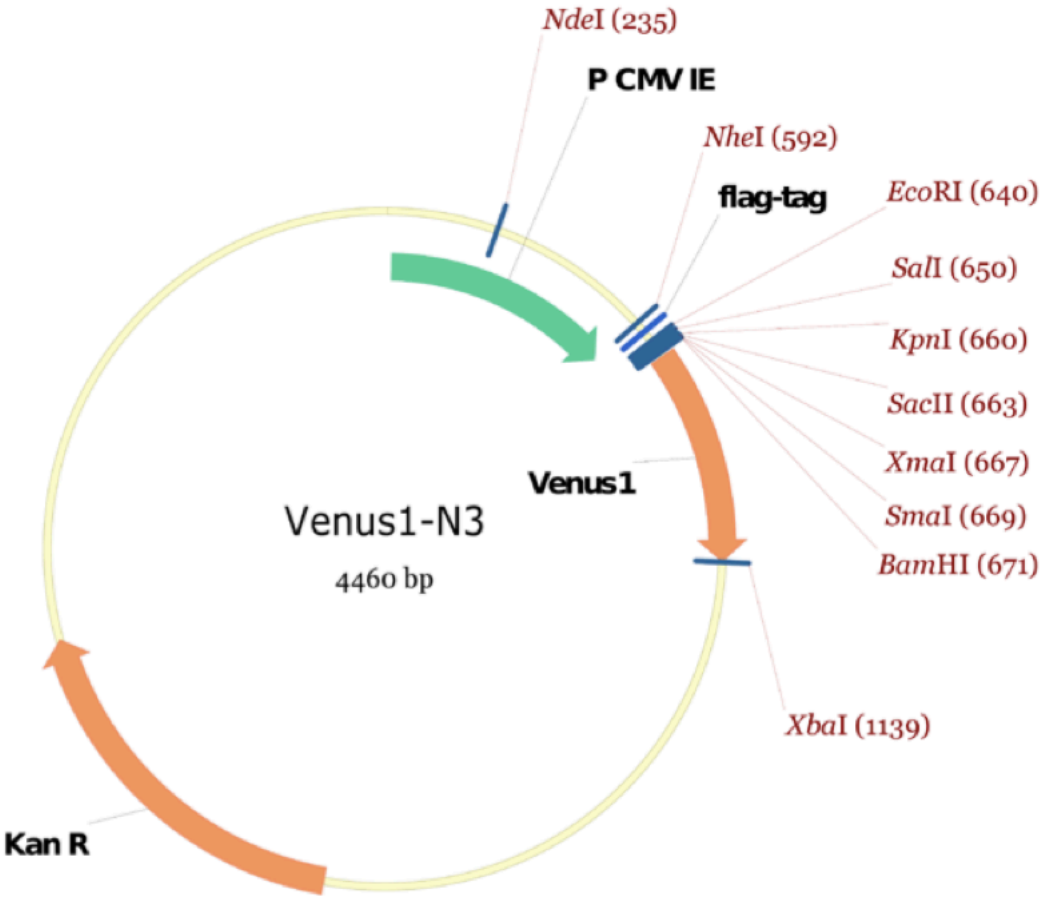

Venus2-N3

length: 4,3 kb
origin: Clontech (pECFP-N1/pEGFP-N3)

Cytomegalovirus immediate early gene enhancer/promotor
HA-Tag
Venus1 (AS 155-238)
Kanamycin resistance gene

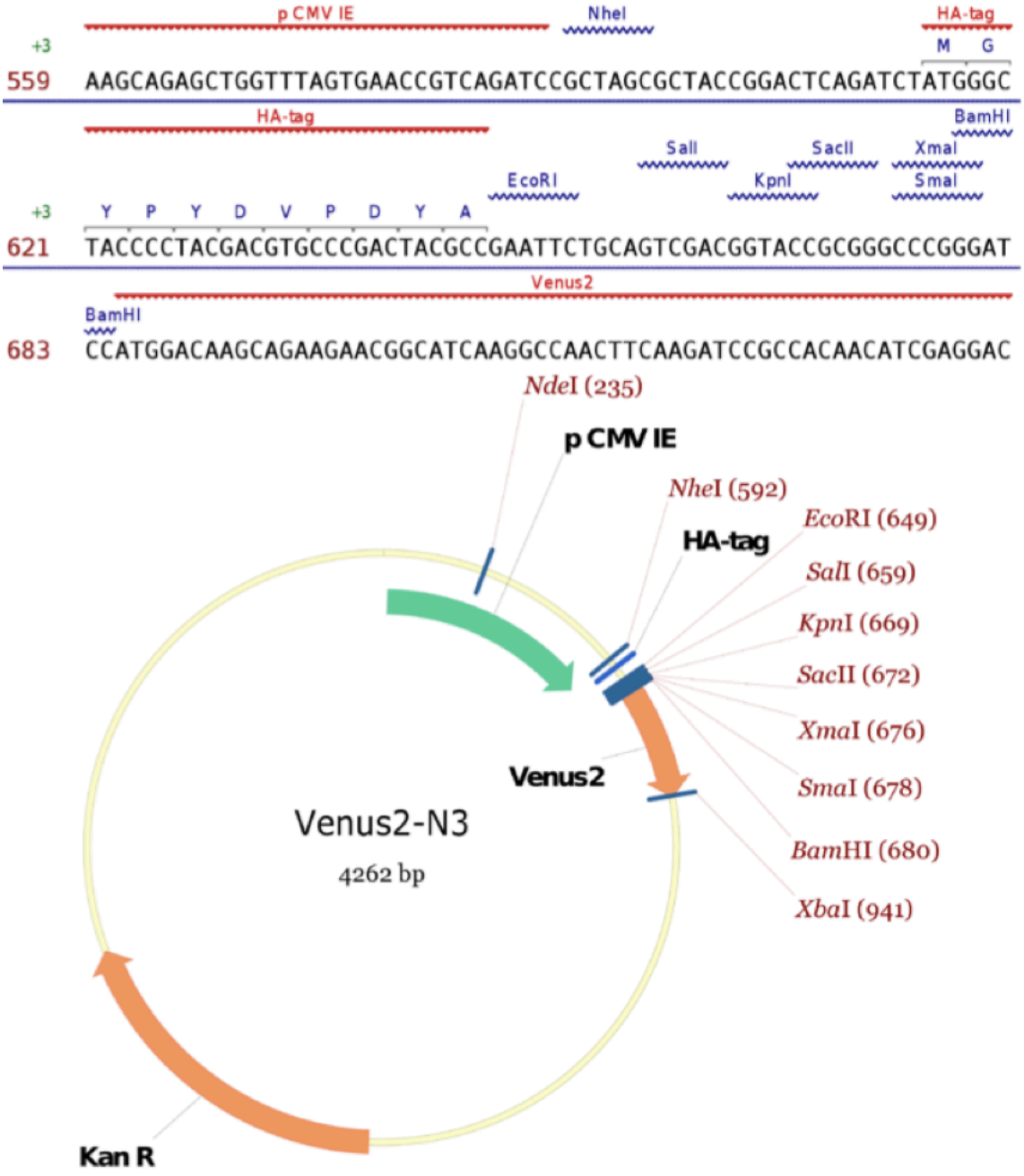

pEGFP-CPd

length: 4,7 kb
origin: Clontech

CMV-Promotor
GFP-Tag
Fl Origin
Kanamycin resistance gene

```
                          BamHI          SalI
      BglII       MluI          HindIII
GGACTCAGATCTCGAACGCGTGGATCCAAGCTTGTCGACCGATCCA
```

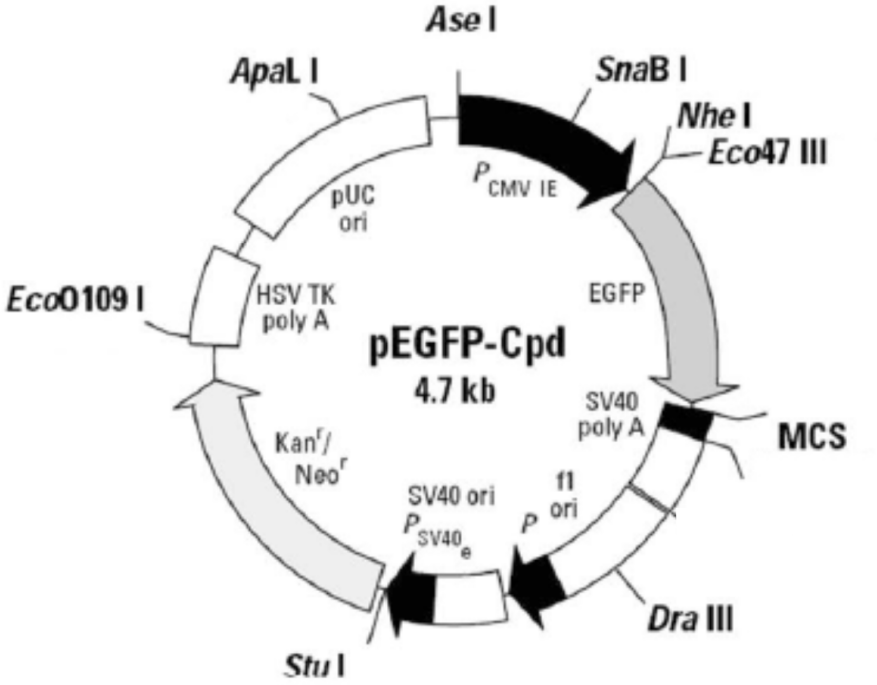

E. Synpo2 sequence

Synpo2b sequence

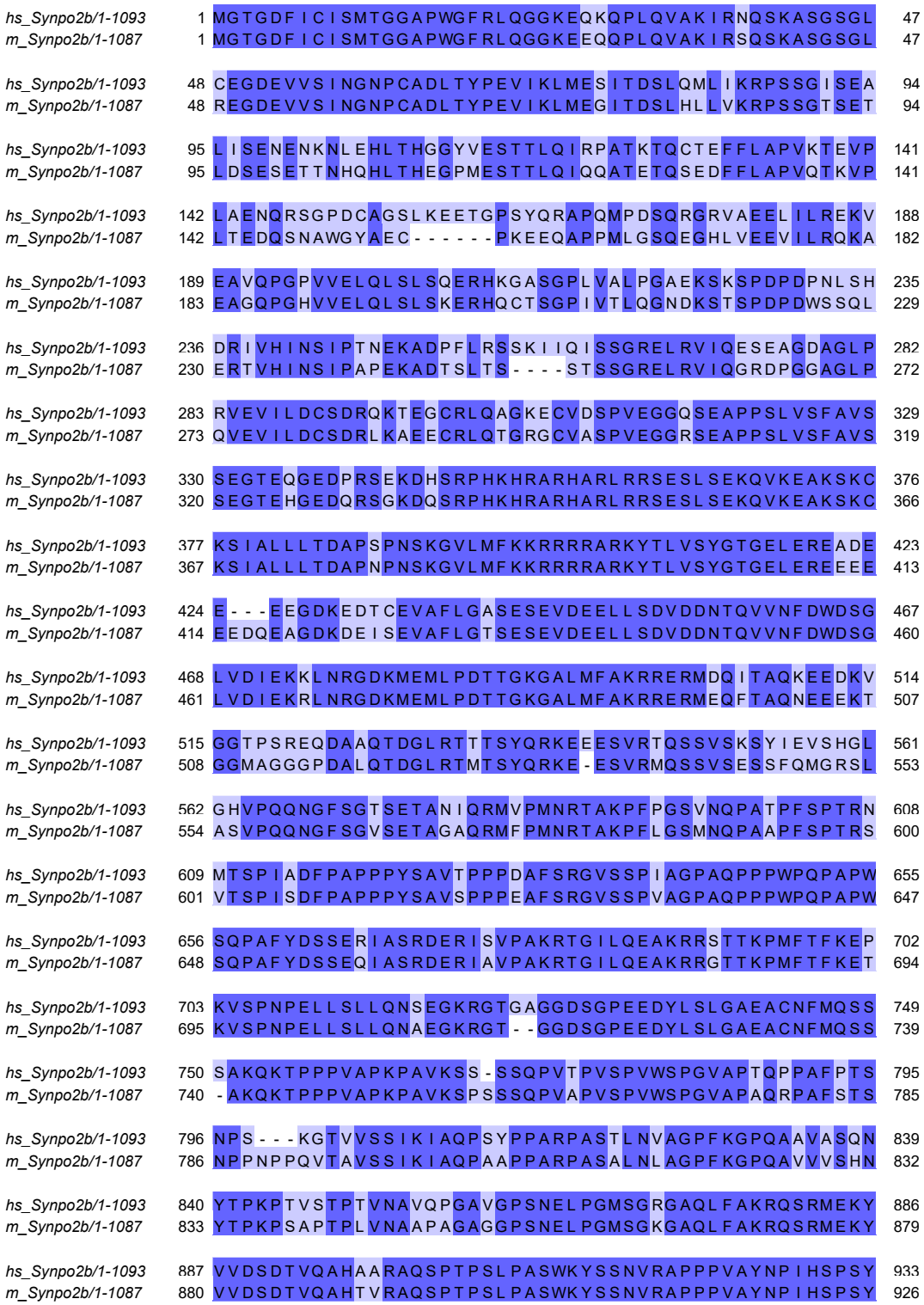

Figure A.1: Alignment of the human and mouse protein sequence of Synpo2b. Identical amino acids between Synpo2b human and mouse are marked dark blue (created with the Jalview software using the Clustal O Multiple Sequence Algorithm, Sievers *et al.*, 2011).

Synpo2e sequence

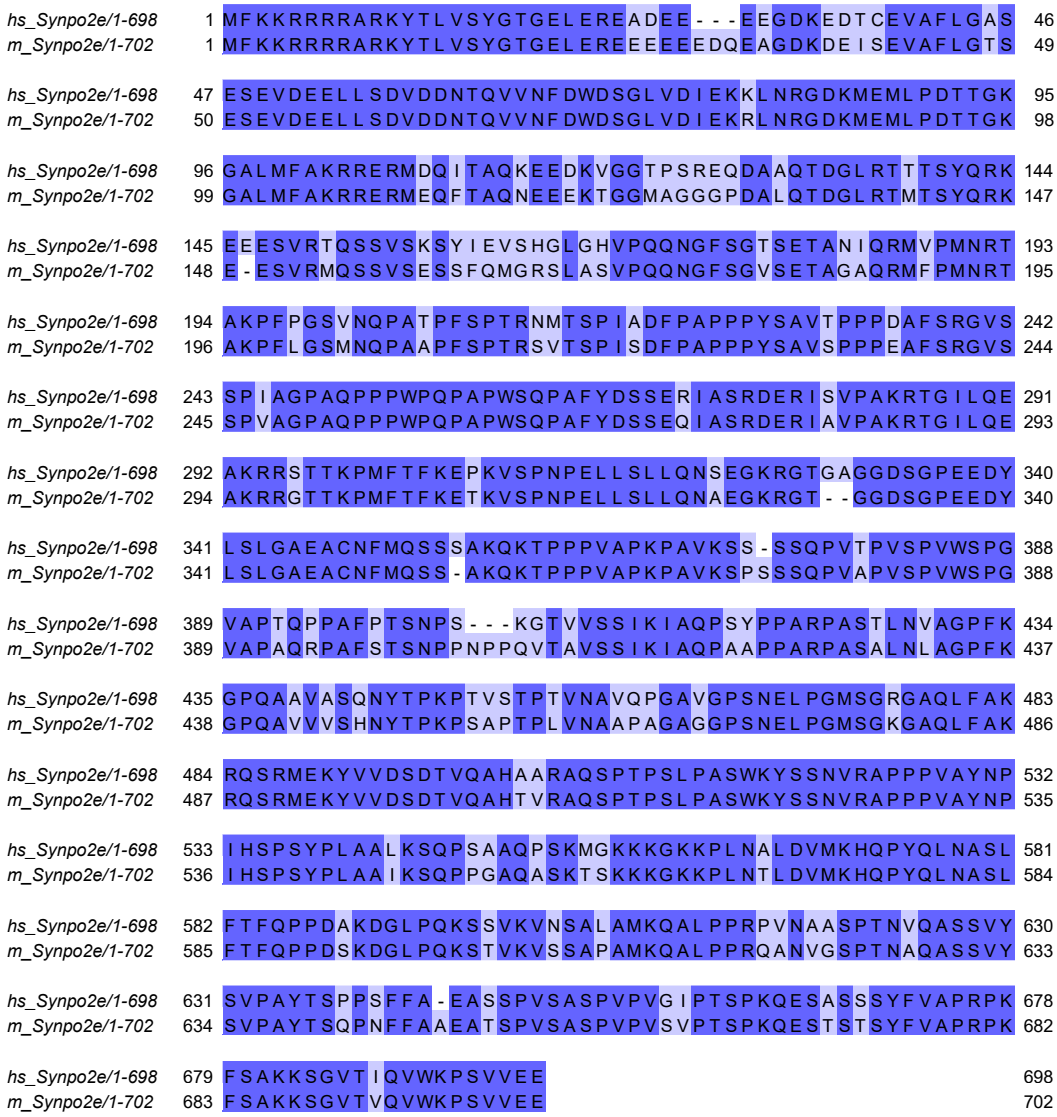

Figure A.1: Alignment of the human and mouse protein sequence of Synpo2e. Identical amino acids between Synpo2e human and mouse are marked dark blue (created with the Jalview software with the Clustal O Multiple Sequence Algorithm, Sievers *et al.*, 2011).

Acknowledgment

First, I would like to thank my supervisor Prof. Dr. Dieter O. Fürst for giving me the opportunity to work on this project, for a great supervision, and for fruitful discussions. He always gave very helpful suggestions, which were significant for the development of this work and always encouraged me to follow my own ideas.

I am greatly thankful to PD Dr. Gregor Kirfel for the takeover of the second referee position, the suggestions to improve this work, the constructive and critical annotations, his helpfulness, his encouragement, and his energetic support throughout the whole time.

Moreover, I would also like to thank Dr. Peter F. M. van der Ven for his ongoing support in all molecular biology questions and for the helpful tips and suggestions, which were very useful to push this work forward.

Next, I would like to acknowledge Prof. Dr. Bettina Warscheid for the provision of the phosphorylation data, Prof. Dr. Wachten for the provision of the mCherry-LC3B C2C12 cells and Prof. Dr. Frey for the provision of yeast-two-hybrid data.

Special thanks to Karin Bois, whose work and tireless diligence have contributed to this work. I would also like to take this opportunity to thank her for all the tips and assistance in the laboratory and above all for the very good and harmonious cooperation. Further on, I would like to thank all other technical assistants for the nice time together and for the support.

I would also like to thank my colleagues Lorena Heil and Marvin Aßent for the great time we had together and their open ear for all kinds of problems. Your friendship has made a significant contribution to a good time at the institute, but also beyond working hours in the everyday life. I would also like to thank Dr. Julia Kreuzberg for the good time together at the institute.

I thank all the staff from the Institute of Cell Biology, not mentioned by name, for the pleasant working atmosphere.

In the end I would like to thank my parents and my sister for always supporting me and for cheering me up in all situations in life and making it possible for me to complete my studies and doctorate. I am deeply grateful for your continuous encouragement and your strong faith in me.